

S. L. BRAUNSTEIN and H.-K. LO (eds.)

---

# SCALABLE QUANTUM COMPUTERS

PAVING THE WAY TO REALIZATION



 WILEY-VCH

Editors:

Prof. Dr. Samuel L. Braunstein, University of Wales, Bangor, UK

e-mail: schmuel@sees.bangor.ac.uk

Dr. Hoi-Kwong Lo, MagiQ Technologies, Inc., New York

e-mail: hoi\_kwong@magiqtech.com

Assistant Editor:

Pieter Kok, University of Wales, Bangor, UK

e-mail: pieter@sees.bangor.ac.uk

This book was carefully produced. Nevertheless, editors, authors and publisher do not warrant the information contained therein to be free of errors. Readers are advised to keep in mind that statements, data, illustrations, procedural details or other items may inadvertently be inaccurate.

1<sup>st</sup> edition, 2001

Cover Picture:

Photograph of a structured electronic device, showing an array of inter-connected microchannels, 1.6  $\mu\text{m}$  deep and 16  $\mu\text{m}$  wide. Surface-state electrons on superfluid helium in these channels is one of the novel systems under investigation for quantum computing.

(The device was fabricated on GaAs at the Niels Bohr Institute, Copenhagen. Image by Philip Glasson.)

Library of Congress Card No.: applied for

A catalogue record for this book is available from the British Library.

Die Deutsche Bibliothek - CIP Cataloguing-in-Publication-Data

A catalogue record for this publication is available from Die Deutsche Bibliothek

ISBN 3-527-40321-3

© WILEY-VCH Verlag Berlin GmbH, Berlin (Federal Republic of Germany), 2001

Printed on acid-free paper.

All rights reserved (including those of translation in other languages). No part of this book may be reproduced in any form - by photoprinting, microfilm, or any other means - nor transmitted or translated into machine language without written permission from the publishers. Registered names, trademarks, etc. used in this book, even when not specifically marked as such, are not to be considered unprotected by law.

Composition: Druckhaus „Thomas Müntzer“ GmbH, D-99947 Bad Langensalza. Printing: Strauss Offsetdruck GmbH, D-69509 Mörlenbach. Bookbinding: Wilhelm Osswald & Co., D-67433 Neustadt.

Printed in the Federal Republic of Germany.

WILEY-VCH Verlag Berlin GmbH

Bühningstraße 10

D-13086 Berlin

Federal Republic of Germany

..... 229

..... 235

..... 253

..... 273

..... 287

..... 305

..... 325

..... 339

..... 355

..... 363

**The Physical Implementation of Quantum Computation**

DAVID P. DiVINCENZO  
IBM T. J. Watson Research Center, Yorktown Heights, NY 10598 USA

**Abstract**

After a brief introduction to the principles and promise of quantum information processing, the requirements for the physical implementation of quantum computation are discussed. These five requirements, plus two relating to the communication of quantum information, are extensively explored and related to the many schemes in atomic physics, quantum optics, nuclear and electron magnetic resonance spectroscopy, superconducting electronics, and quantum-dot physics, for achieving quantum computing.

**1. Introduction**

The advent of quantum information processing, as an abstract concept, has given birth to a great deal of new thinking, of a very concrete form, about how to create physical computing devices that operate in the hitherto unexplored quantum mechanical regime. The efforts now underway to produce working laboratory devices that perform this profoundly new form of information processing are the subject of this book.

In this chapter I provide an overview of the common objectives of the investigations reported in the remainder of this special issue. The scope of the approaches, proposed and underway, to the implementation of quantum hardware is remarkable, emerging from specialties in atomic physics [1], in quantum optics [2], in nuclear [3] and electron [4] magnetic resonance spectroscopy, in superconducting device physics [5], in electron physics [6], and in mesoscopic and quantum dot research [7]. This amazing variety of approaches has arisen because, as we will see, the principles of quantum computing are posed using the most fundamental ideas of quantum mechanics, ones whose embodiment can be contemplated in virtually every branch of quantum physics.

The interdisciplinary spirit which has been fostered as a result is one of the most pleasant and remarkable features of this field. The excitement and freshness that has been produced bodes well for the prospect for discovery, invention, and innovation in this endeavor.

**2. Why *Quantum* Information Processing?**

The shortest of answers to this question would be, why not? The manipulation and transmission of information is today carried out by physical machines (computers, routers, scanners, etc.), in which the embodiment and transformations of this information can be described using the language of classical mechanics. But the final physical theory of the world is not Newtonian mechanics, and there is no reason to suppose that machines following the laws of quantum mechanics should have the same computational power as classical machines; indeed, since Newtonian mechanics emerges as a special limit of quantum mechanics, quantum machines can only have greater computational power than classical ones. The great pioneers and visionaries who pointed the way towards quantum computers, DEUTSCH [8], FEYNMAN [9], and others, were stimulated by such thoughts. Of course, by a

similar line of reasoning, it may well be asked whether machines embodying the principles of other refined descriptions of nature (perhaps general relativity or string theory) may have even more information processing capabilities; speculations exist about these more exotic possibilities, but they are beyond the scope of the present discussion.

But computing with quantum mechanics really deserves a lot more attention than worm-hole computing or quantum-gravity computing; quantum computing, while far in the future from the perspective of CMOS roadmaps and projections of chip fab advances, can certainly be seen as a real prospect from the perspective of research studies in quantum physics. It does not require science fiction to envision a quantum computer; the proposals discussed later in this issue paint a rather definite picture of what a real quantum computer will look like.

So, how much is gained by computing with quantum physics over computing with classical physics? We do not seem to be near to a final answer to this question, which is natural since even the ultimate computing power of classical machines remains unknown. But the answer as we know it today has an unexpected structure; it is not that quantum tools simply speed up all information processing tasks by a uniform amount. By a standard complexity measure (i.e., the way in which the number of computational steps required to complete a task grows with the "size"  $n$  of the task), some tasks are not sped up at all [10] by using quantum tools (e.g., obtaining the  $n$ th iterate of a function  $f(f(\dots f(x)\dots))$  [11]), some are sped up moderately (locating an entry in a database of  $n$  entries [12]), and some are apparently sped up exponentially (Shor's algorithm for factoring an  $n$ -digit number [13]).

In other types of information processing tasks, particularly those involving communication [14], both quantitative and qualitative improvements are seen [15]: for certain tasks (choosing a free day for an appointment between two parties from out of  $n$  days) there is a quadratic reduction of the amount of communicated data required, if quantum states rather than classical states are transmitted [16]. For some tasks (the "set disjointness problem", related to allocating non-overlapping segments of a shared memory in a distributed computation) the reduction of required communication is exponential [17]. Finally, there are tasks that are doable in the quantum world that have no counterpart classically: quantum cryptography provides an absolute secrecy of communication between parties that is impossible classically [18]. And for some games, winning strategies become possible with the use of quantum resources that are not available otherwise [19, 20].

This issue, and this chapter, are primarily concerned with the "hows" of quantum computing rather than the "whys," so we will leave behind the computer science after this extremely brief mention. There is no shortage of other places to obtain more information about these things; I recommend the recent articles by Aharonov [21] and by Cleve [22]; other general introductions [23] will give the reader pointers to the already vast specialized literature on this subject.

### 3. Realizing Quantum Computation

Let me proceed with the main topic: the physical realization of quantum information processing. As a guide to the remainder of the special issue, and as a means of reviewing the basic steps required to make quantum computation work, I can think of no better plan than to review a set of basic criteria that my coworkers and I have been discussing over the last few years [24] for the realization of quantum computation (and communication), and to discuss the application of these criteria to the multitude of physical implementations that are found below.

So, without further ado, here are the

## Five (plus two) requirements for the implementation of quantum computation

## 1. A scalable physical system with well characterized qubits

For a start, a physical system containing a collection of qubits is needed. A qubit (or, more precisely, the embodiment of a qubit) is [25] simply a quantum two-level system like the two spin states of a spin  $1/2$  particle, like the ground and excited states of an atom, or like the vertical and horizontal polarization of a single photon. The generic notation for a qubit state denotes one state as  $|0\rangle$  and the other as  $|1\rangle$ . The essential feature that distinguishes a qubit from a bit is that, according to the laws of quantum mechanics, the permitted states of a single qubit fills up a two-dimensional complex vector space; the general state is written  $a|0\rangle + b|1\rangle$ , where  $a$  and  $b$  are complex numbers, and a normalization convention  $|a|^2 + |b|^2 = 1$  is normally adopted. The general state of two qubits,  $a|00\rangle + b|01\rangle + c|10\rangle + d|11\rangle$ , is a four-dimensional vector, one dimension for each distinguishable state of the two systems. These states are generically *entangled*, meaning that they cannot be written as a product of the states of two individual qubits. The general state of  $n$  qubits is specified by a  $2^n$ -dimensional complex vector.

A qubit being "well characterized" means several different things. Its physical parameters should be accurately known, including the internal Hamiltonian of the qubit (which determines the energy eigenstates of the qubit, which are often, although not always, taken as the  $|0\rangle$  and  $|1\rangle$  states), the presence of and couplings to other states of the qubit, the interactions with other qubits, and the couplings to external fields that might be used to manipulate the state of the qubit. If the qubit has third, fourth, etc., levels, the computer's control apparatus should be designed so that the probability of the system ever going into these states is small. The smallness of this and other parameters will be determined by the capabilities of quantum error correction, which will be discussed under requirement 3.

Recognizing a qubit can be trickier than one might think. For example, we might consider a pair of one-electron quantum dots that share a single electron between them as a two-qubit system. It is certainly true that we can denote the presence or absence of an electron on each dot by  $|0\rangle$  and  $|1\rangle$ , and it is well known experimentally how to put this system into the "entangled" state  $1/\sqrt{2}(|01\rangle + |10\rangle)$  in which the electron is in a superposition of being on the left dot and the right dot. But it is fallacious to consider this as a two-qubit system; while the states  $|00\rangle$  and  $|11\rangle$  are other allowed physical states of the dots, superselection principles forbid the creation of entangled states involving different particle numbers such as  $1/\sqrt{2}(|00\rangle + |11\rangle)$ .

It is therefore false to consider this as a two-qubit system, and, since there are not two qubits, it is nonsense to say that there is entanglement in this system. It is correct to say that the electron is in a superposition of different quantum states living on the two different dots. It is also perfectly correct to consider this system to be the embodiment of a *single* qubit, spanned by the states (in the misleading notation above)  $|01\rangle$  ("electron on the right dot") and  $|10\rangle$  ("electron on the left dot"). Indeed, several of the viable proposals, including the ones by Schön, Averin, and Tanamoto in this special issue, use exactly this system as a qubit. However, false lines of reasoning like the one outlined here have sunk various proposals before they were properly launched (no such abortive proposals are represented in this book, but they can be found occasionally in the literature).

An amazing variety of realizations of the qubit are represented in this volume. There is a very well developed line of work that began with the proposal of CIRAC and ZOLLER [1] for an ion-trap quantum computer, in which, in its quiescent state, the computer holds the qubits in pairs of energy levels of ions held in a linear electromagnetic trap. Various pairs of energy levels (e.g., Zeeman-degenerate ground states, as are also used in the NMR approach [3] discussed by Cory) have been proposed and investigated experimentally. The many neutral-atom proposals (see chapters by KIMBLE [2], DEUTSCH [26], and BRIEGEL [27]) use similar atomic energy levels of neutral species. These atomic-physics based propos-

als use other auxiliary qubits such as the position of atoms in a trap or lattice, the presence or absence of a photon in an optical cavity, or the vibrational quanta of trapped electrons, ions or atoms (in the Platzman proposal below [6] this is the primary qubit). Many of the solid-state proposals exploit the fact that impurities or quantum dots have well characterized discrete energy level spectra; these include the spin states of quantum dots (see chapters by LOSS [7] and IMAMOGLU [2]), the spin states of donor impurities (see KANE [4]), and the orbital or charge states of quantum dots (see TANAMOTO [7]). Finally, there are a variety of interesting proposals which use the quantized states of superconducting devices, either ones involving the (Cooper-pair) charge (see SCHÖN, AVERIN, or the flux (see MOOI) [5].

*2. The ability to initialize the state of the qubits to a simple fiducial state, such as  $|000\dots\rangle$*

This arises first from the straightforward computing requirement that registers should be initialized to a known value before the start of computation. There is a second reason for this initialization requirement: quantum error correction (see requirement 3 below) requires a continuous, fresh supply of qubits in a low-entropy state (like the  $|0\rangle$  state). The need for a continuous supply of 0s, rather than just an initial supply, is a real headache for many proposed implementations. But since it is likely that a demonstration of a substantial degree of quantum error correction is still quite some time off, the problem of continuous initialization does not have to be solved very soon; still, experimentalists should be aware that the speed with which a qubit can be zeroed will eventually be a very important issue. If the time it takes to do this initialization is relatively long compared with gate-operation times (see requirement 4), then the quantum computer will have to be equipped with some kind of "qubit conveyor belt", on which qubits in need of initialization are carried away from the region in which active computation is taking place, initialized while on the "belt", then brought back to the active place after the initialization is finished. (A similar parade of qubits will be envisioned in requirement 5 for the case of low quantum-efficiency measurements [28].)

There are two main approaches to setting qubits to a standard state: the system can either be "naturally" cooled when the ground state of its Hamiltonian is the state of interest, or the standard state can be achieved by a measurement which projects the system either into the state desired or another state which can be rotated into it. These approaches are not fundamentally different from one another, since the projection procedure is a form of cooling; for instance, the laser cooling techniques used routinely now for the cooling of ion states to near their ground state in a trap [1] are closely connected to the fluorescence techniques used to measure the state of these ions. A more "natural" kind of cooling is advocated in many of the electron spin resonance based techniques (using quantum dots or impurities) [7, 4] in which the spins are placed in a strong magnetic field and allowed to align with it via interaction with their heat bath. In this kind of approach the time scale will be a problem. Since the natural thermalization times are never shorter than the decoherence time of the system, this procedure will be too slow for the needs of error correction and a "conveyor belt" scheme would be required. Cooling by projection, in which the Hamiltonian of the system and its environment are necessarily perturbed strongly, will have a time scale dependent on the details of the setup, but potentially much shorter than the natural relaxation times. One cannot say too much more at this point, as the schemes for measurement have in many cases not been fully implemented (see requirement 5). In the NMR quantum computer implementations to date (see Cory below), cooling of the initial state has been foregone altogether; it is acknowledged [3] that until some of the proposed cooling schemes are implemented (a nontrivial thing to do), NMR can never be a scalable scheme for quantum computing.

*3. Long relevant decoherence times, much longer than the gate operation time*

Decoherence times characterize the dynamics of a qubit (or any quantum system) in contact with its environment. The (somewhat overly) simplified definition of this time is that it is

ce, the presence  
apped electrons,  
t). Many of the  
all characterized  
see chapters by  
IE [4]), and the  
are a variety of  
ces, either ones  
ou) [5].

uch as  $|000\dots\rangle$   
sters should be  
ond reason for  
low) requires a

The need for a  
for many pro-  
antial degree of  
us initialization  
that the speed  
. If the time it  
tion times (see  
kind of "qubit  
m the region in  
n brought back  
qubits will be  
ents [28].)

stem can either  
of interest, or  
stem either into  
oaches are not  
a form of cool-  
cooling of ion  
ie fluorescence  
l of cooling is  
quantum dots or  
and allowed to  
time scale will  
he decoherence  
orrection and a  
h the Hamilto-  
ill have a time  
an the natural  
s for measure-  
.. In the NMR  
he initial state  
proposed cool-  
be a scalable

ime  
tem) in contact  
ne is that it is

the characteristic time for a generic qubit state  $|\psi\rangle = a|0\rangle + b|1\rangle$  to be transformed into the mixture  $\rho = |a|^2|0\rangle\langle 0| + |b|^2|1\rangle\langle 1|$ . A more proper characterization of decoherence, in which the decay can depend on the form of the initial state, in which the state amplitudes may change as well, and in which other quantum states of the qubit can play a role (in a special form of state decay called "leakage" in quantum computing [29, 30]), is rather more technical than I want to get here; but see Refs. [31] and [32] for a good general discussion of all these. Even the simplest discussion of decoherence that I have given here should also be extended to include the possibility that the decoherence of neighboring qubits is correlated. It seems safest to assume that they will be neither completely correlated nor completely uncorrelated, and the thinking about error correction has taken this into account.

Decoherence is very important for the fundamentals of quantum physics, as it is identified as the principal mechanism for the emergence of classical behavior. For the same reason, decoherence is very dangerous for quantum computing, since if it acts for very long, the capability of the quantum computer will not be so different from that of a classical machine. The decoherence time must be long enough that the uniquely quantum features of this style of computation have a chance to come into play. How long is "long enough" is also indicated by the results of quantum error correction, which I will summarize shortly.

I have indicated that the "relevant" decoherence times should be long enough. This emphasizes that a quantum particle can have many decoherence times pertaining to different degrees of freedom of that particle. But many of these can be irrelevant to the functioning of this particle as a qubit. For example, the rapid decoherence of an electron's position state in a solid state environment does not preclude its having a very long spin coherence time, and it can be arranged that this is the only time relevant for quantum computation. Which time is relevant is determined by the choice of the qubit basis states  $|0\rangle$  and  $|1\rangle$ ; for example, if these two states correspond to different spin states but identical orbital states, then orbital decoherence will be irrelevant.

One might worry that the decoherence time necessary to do a successful quantum computation will scale with the duration of the computation. This would place incredibly stringent requirements on the physical system implementing the computation. Fortunately, in one of the great discoveries of quantum information theory (in 1995–1996), it was found that error correction of quantum states is possible [33] and that this correction procedure can be successfully applied in quantum computation [34], putting much more reasonable (although still daunting) requirements on the needed decoherence times.

In brief, quantum error correction starts with coding; as in binary error correction codes, in which only a subset of all boolean strings are "legal" states, quantum error correction codes consist of legal states confined to a subspace of the vector space of a collection of qubits. Departure from this subspace is caused by decoherence. Codes can be chosen such that, with a suitable sequence of quantum computations and measurements of some ancillary qubits, the error caused by decoherence can be detected and corrected. As noted above, these ancillary qubits have to be continuously refreshed for use. I will not go much farther into the subject here, see [31] for more. It is known that quantum error correction can be made fully fault tolerant, meaning that error correction operations can be successfully intermingled with quantum computation operations, that errors occurring during the act of error correction, if they occur at a sufficiently small rate, do no harm, and that the act of quantum computation does not itself cause an unreasonable proliferation of errors.

These detailed analyses have indicated the magnitude of decoherence time scales that are acceptable for fault-tolerant quantum computation. The result is that, if the decoherence time is  $10^4$ – $10^5$  times the "clock time" of the quantum computer, that is, the time for the execution of an individual quantum gate (see requirement 4), then error correction can be successful. This is, to tell the truth, a rather stringent condition, quantum systems frequently do not have such long decoherence times. But sometimes they do, and our search for a successful physical implementation must turn towards these. At least this result says that

the required decoherence rate does not become ever smaller as the size and duration of the quantum computation grows. So, once the desired threshold is attainable, decoherence will not be an obstacle to scalable quantum computation.

Having said this, it must be admitted that it will be some time before it is even possible to subject quantum error correction to a reasonable test. Nearly all parts of requirements 1–5 must be in place before such a test is possible. And even the most limited application of quantum error correction has quite a large overhead: roughly 10 ancillary qubits must be added for each individual qubit of the computation. Fortunately, this overhead ratio grows only logarithmically as the size of the quantum computation is increased.

In the short run, it is at least possible to design and perform experiments which measure the decoherence times and other relevant properties (such as the correlation of decoherence of neighboring qubits) of candidate implementations of qubits. With such initial test experiments, caution must be exercised in interpreting the results, because decoherence is a very system-specific phenomenon, depending on the details of all the qubits' couplings to various environmental degrees of freedom. For example, the decoherence time of the spin of an impurity in the bulk of a perfect semiconductor may not be the same as its decoherence time when it is near the surface of the solid, in the immediate neighborhood of device structures designed to manipulate its quantum state. Test experiments should probe decoherence in as realistic a structure as is possible.

#### 4. A "universal" set of quantum gates

This requirement is of course at the heart of quantum computing. A quantum algorithm is typically specified [8] as a sequence of unitary transformations  $U_1, U_2, U_3, \dots$ , each acting on a small number of qubits, typically no more than three. The most straightforward transcription of this into a physical specification is to identify Hamiltonians which generate these unitary transformations, viz.,  $U_1 = e^{iH_1 t/\hbar}$ ,  $U_2 = e^{iH_2 t/\hbar}$ ,  $U_3 = e^{iH_3 t/\hbar}$ , etc.; then, the physical apparatus should be designed so that  $H_1$  can be turned on from time 0 to time  $t$ , then turned off and  $H_2$  turned on from time  $t$  to time  $2t$ , etc.

Would that life were so simple! In reality what can be done is much less, but much less can be sufficient. Understanding exactly how much less is still enough, is the main complication of this requirement. In all the physical implementations discussed in this volume, only particular sorts of Hamiltonians can be turned on and off; in most cases, for example, only two-body (two-qubit) interactions are considered. This immediately poses a problem for a quantum computation specified with three-qubit unitary transformations; fortunately, of course, these can always be re-expressed in terms of sequences of one- and two-body interactions [35], and the two-body interactions can be of just one type [36], the "quantum XOR" or "cNOT". There are some implementations in which multi-qubit gates can be implemented directly [37].

However, this still leaves a lot of work to do. In some systems, notably in NMR (see Cory), there are two-body interactions present which cannot be turned off, as well as others which are switchable. This would in general be fatal for quantum computation, but the particular form of the fixed interactions permit their effects to be annulled by particular "refocusing" sequences of the controllable interactions, and it has recently been discovered [38] that these refocusing sequences can be designed and implemented efficiently.

For many other systems, the two-body Hamiltonian needed to generate directly the cNOT unitary transformation is not available. For example, in the quantum-dot proposal described by Loss below [7], the only two-body interaction which should be easily achievable is the exchange interaction between neighboring spins,  $H \propto \vec{S}_i \cdot \vec{S}_{i+1}$ ; in the Imamoglu chapter [2], the attainable interaction is of the XY type, i.e.,  $H \propto S_{ix}S_{jx} + S_{iy}S_{jy}$ . An important observation is that with the appropriate sequence of exchange or XY interactions, in conjunction with particular one-body interactions (which are assumed to be more easily doable), the cNOT transformation can be synthesized [39]. It is incumbent on each implementation pro-



duration of the  
coherence will

is even possible  
of requirements  
ited application  
qubits must be  
ead ratio grows

which measure  
of decoherence  
initial test experi-  
ence is a very  
couplings to var-  
e of the spin of  
its decoherence  
hood of device  
i probe decoher-

um algorithm is  
..., each acting  
ghtforward tran-  
which generate  
, etc.; then, the  
ime 0 to time  $t$ ,

s, but much less  
he main compli-  
in this volume,  
es, for example,  
oses a problem  
ons; fortunately,  
- and two-body  
], the "quantum  
it gates can be

ly in NMR (see  
is well as others  
utation, but the  
ed by particular  
been discovered  
iently.

rectly the cNOT  
oposal described  
chievable is the  
oglu chapter [2],  
portant observa-  
, in conjunction  
sily doable), the  
ementation pro-

posals to exhibit such a sequence for producing the cNOT using the interactions that are naturally realizable.

Often there is also some sophisticated thinking required about the time profile of the two-qubit interaction. The naive description above uses a "square pulse" time profile, but often this is completely inappropriate; for instance, if the Hamiltonian can also couple the qubit to other, higher-lying levels of the quantum system, often the only way to get the desired transformation is to turn on and off the interaction smoothly and slowly enough that an adiabatic approximation is accurate [29, 30] (in a solid-state context, see also [40]). The actual duration of the pulse will have to be sufficiently long that any such adiabatic requirement is satisfied; then typically only the time integral  $\int dt H(t)$  is relevant for the quantum gate action. The overall time scale of the interaction pulse is also controlled by the attainable maximum size of the matrix elements of  $H(t)$ , which will be determined by various fundamental considerations, like the requirement that the system remains in the regime of validity of a linear approximation, and practical considerations, like the laser power that can be concentrated on a particular ion. Given these various constraints, the "clock time" of the quantum computer will be determined by the time interval needed such that two consecutive pulses have negligible overlap.

Another consideration, which does not seem to present a problem with any current implementation schemes, but which may be an issue in the future, is the classicality of the control apparatus. We say that the interaction Hamiltonian  $H(t)$  has a time profile which is controlled externally by some "classical" means, that is, by the intensity of a laser beam, the value of a gate voltage, or the current level in a wire. But each of these control devices is made up themselves of quantum mechanical parts. When we require that these behave classically, it means that their action should proceed without any entanglement developing between these control devices and the quantum computer. Estimates indicate that this entanglement can indeed be negligible, but this effect needs to be assessed for each individual case.

In many cases it is impossible to turn on the desired interaction between a pair of qubits; for instance, in the ion-trap scheme, no direct interaction is available between the ion-level qubits [1]. In this and in other cases, a special quantum subsystem (sometimes referred to as a "bus qubit") is used which can interact with each of the qubits in turn and mediate the desired interaction: for the ion trap, this is envisioned to be the vibrational state of the ion chain in the trap; in other cases it is a cavity photon whose wavefunction overlaps all the qubits. Unfortunately, this auxiliary quantum system introduces new channels for the environment to couple to the system and cause decoherence, and indeed the decoherence occurring during gate operation is of concern in the ion-trap and cavity-quantum electrodynamics schemes.

Some points about requirement 4 are important to note in relation to the implementation of error correction. Successful error correction requires fully parallel operation, meaning that gate operations involving a finite fraction of all the qubits must be doable simultaneously. This can present a problem with some of the proposals in which the single "bus qubit" is needed to mediate each interaction. On the other hand, the constraint that interactions are only among nearest neighbors in a lattice, as in many of the solid-state proposals, does allow for sufficient parallelism [41].

Quantum gates cannot be implemented perfectly; we must expect both systematic and random errors in the implementation of the necessary Hamiltonians. Both types of errors can be viewed as another source of decoherence and thus error correction techniques are effective for producing reliable computations from unreliable gates, if the unreliability is small enough. The tolerable unreliability due to random errors is in the same vicinity as the decoherence threshold, that is, the magnitude of random errors should be  $10^{-4}$ – $10^{-5}$  per gate operation or so. It might be hoped that systematic errors could be virtually eliminated by careful calibration; but this will surely not always be the case. It seems harder to give a

good rule for how much systematic error is tolerable, the conservative estimates give a very, very small number (the square of the above) [31], but on the other hand there seems to be some evidence that certain important quantum computations (e.g., the quantum Fourier transform) can tolerate a very high level of systematic error (over- or under-rotation). Some types of very large errors may be tolerable if their presence can be detected and accounted for on the fly (we are thinking, for example, about charge switching in semiconductors or superconductors).

Error correction requires that gate operations be done on coded qubits, and one might worry that such operations would require a new repertoire of elementary gate operations for the base-level qubits which make up the code. For the most important error correction techniques, using the so called "stabilizer" codes, this is not the case. The base-level toolkit is exactly the same as for the unencoded case: one-bit gates and cNOTs, or any gate repertoire that can produce these, are adequate. Sometimes the use of coding can actually *reduce* the gate repertoire required: in the work on decoherence free subspaces and subsystems, codes are introduced using blocks of three and four qubits for which two-qubit exchange interactions alone are enough to implement general quantum computation [42, 43]. This simplification could be very useful in the quantum-dot [7] or semiconductor-impurity [4] implementations.

#### 5. A qubit-specific measurement capability

Finally, the result of a computation must be read out, and this requires the ability to measure specific qubits. In an ideal measurement, if a qubit's density matrix is  $\rho = p|0\rangle\langle 0| + (1-p)|1\rangle\langle 1| + \alpha|0\rangle\langle 1| + \alpha^*|1\rangle\langle 0|$ , the measurement should give outcome "0" with probability  $p$  and "1" with probability  $1-p$  independent of  $\alpha$  and of any other parameters of the system, including the state of nearby qubits, and without changing the state of the rest of the quantum computer. If the measurement is "non-demolition", that is, if in addition to reporting outcome "0" the measurement leaves the qubit in state  $|0\rangle\langle 0|$ , then it can also be used for the state preparation of requirement 2; but requirement 2 can be fulfilled in other ways.

Such an ideal measurement as I have described is said to have 100% quantum efficiency; real measurements always have less. While the fidelity of a quantum measurement is not captured by a single number, the single quantum-efficiency parameter is often a very useful way to summarize it, just as the decoherence time is a useful if incomplete summary of the damage caused to a quantum state by the environment.

While quantum efficiency of 100% is desirable, much less is needed for quantum computation; there is, in fact, a tradeoff possible between quantum efficiency and other resources which results in reliable computation. As a simple example, if the quantum efficiency is 90%, then, in the absence of any other imperfections, a computation with a single-bit output (a so-called "decision problem", common in computer science) will have 90% reliability. If 97% reliability is needed, this can just be achieved by rerunning the calculation three times. Much better, actually, is to "copy" the single output qubit to three, by applying two cNOT gates involving the output qubit and two other qubits set to  $|0\rangle$ , and measuring those three. (Of course, qubits cannot be "copied", but their value in a particular basis can.) In general, if quantum efficiency  $q$  is available, then copying to somewhat more than  $1/q$  qubits and measuring all of these will result in a reliable outcome. So, a quantum efficiency of 1% would be usable for quantum computation, at the expense of hundreds of copies/remasures of the same output qubit. (This assumes that the measurement does not otherwise disturb the quantum computer. If it does, the possibilities are much more limited.)

Even quantum efficiencies much, much lower than 1% can be and are used for successful quantum computation: this is the "bulk" model of NMR (see Cory and [3]), where macroscopic numbers of copies of the same quantum computer (different molecules in solu-

tion) run simultaneously, with the final measurement done as an ensemble average over the whole sample. These kinds of weak measurements, in which each individual qubit is hardly disturbed, are quite common and well understood in condensed-matter physics.

If a measurement can be completed quickly, on the timescale of  $10^{-4}$  of the decoherence time, say, then its repeated application during the course of quantum computation is valuable for simplifying the process of quantum error correction. On the other hand, if this fast measurement capability is not available, quantum error correction is still possible, but it then requires a greater number of quantum gates to implement.

Other tradeoffs between the complexity and reliability of quantum measurement vs. those of quantum computation have recently been explored. It has been shown that if qubits can be initialized into pairs of maximally entangled states, and two-qubit measurements in the so-called Bell basis ( $\Psi^\pm = |01\rangle \pm |10\rangle$ ,  $\Phi^\pm = |00\rangle \pm |11\rangle$ ) are possible, then no two-qubit quantum gates are needed, one-bit gates alone suffice [44]. Now, often this tradeoff will not be useful, as in many schemes a Bell measurement would require two-bit quantum gates.

But the overall message, seen in many of our requirements, is that more and more, the theoretical study of quantum computation has offered a great variety of tradeoffs for the potential implementations: if X is very hard, it can be substituted with more of Y. Of course, in many cases both X and Y are beyond the present experimental state of the art; but a thorough knowledge of these tradeoffs should be very useful for devising a rational plan for the pursuit of future experiments.

#### 4. Desiderata for Quantum Communication

For computation alone, the five requirements above suffice. But the advantages of quantum information processing are not manifest solely, or perhaps even principally, for straightforward computation only. There are many kinds of information-processing tasks, reviewed briefly at the beginning, that involve more than just computation, and for which quantum tools provide a unique advantage.

The tasks we have in mind here all involve not only computation but also communication. The list of these tasks that have been considered in the light of quantum capabilities, and for which some advantage has been found in using quantum tools, is fairly long and diverse: it includes secret key distribution, multiparty function evaluation as in appointment scheduling, secret sharing, and game playing [14].

When we say communication we mean quantum communication: the transmission of intact qubits from place to place. This obviously adds more features that the physical apparatus must have to carry out this information processing. We formalize these by adding two more items to the list of requirements:

##### 6. The ability to interconvert stationary and flying qubits

##### 7. The ability to faithfully transmit flying qubits between specified locations

These two requirements are obviously closely related, but it is worthwhile to consider them separately, because some tasks need one but not the other. For instance, quantum cryptography [18] involves only requirement 7; it is sufficient to create and detect flying qubits directly.

I have used the jargon "flying qubits" [2], which has become current in the discussions of quantum communication. Using this term emphasizes that the optimal embodiment of qubits that are readily transmitted from place to place is likely to be very different from the optimal qubits for reliable local computation. Indeed, almost all proposals assume that photon states, with the qubit encoded either in the polarization or in the spatial wavefunction of the photon, will be the flying qubit of choice, and indeed, the well developed tech-

nology of light transmission through optical fibers provides a very promising system for the transmission of qubits. I would note, though, that my colleagues and I have raised the possibility that electrons traveling through solids could provide another realization of the flying qubit [14, 45].

Only a few completely developed proposals exist which incorporate requirements 6 and 7. Of course, there are a number of quite detailed studies of 7, in the sense that experiments on quantum cryptography have been very concerned with the preservation of the photon quantum state during transmission through optical fibers or through the atmosphere. However, these studies are rather disconnected from the other concerns of quantum computing. Requirement 6 is the really hard one; to date the only theoretical proposal sufficiently concrete that experiments addressing it have been planned is the scheme produced by Kimble and coworkers [46] for unloading a cavity photon into a traveling mode via atomic spectroscopy, and loading it by the time-reversed process. Other promising concepts, like the launching of electrons from quantum dots into quantum wires such that the spin coherence of the electrons is preserved, need to be worked out more fully.

## 5. Summary

So, what is the "winning" technology going to be? I don't think that any living mortal has an answer to this question, and at this point it may be counterproductive even to ask it. Even though we have lived with quantum mechanics for a century, our study of quantum effects in complex artificial systems like those we have in mind for quantum computing is in its infancy. No one can see how or whether all the requirements above can be fulfilled, or whether there are new tradeoffs, not envisioned in our present theoretical discussions but suggested by further experiments, that might take our investigations in an entirely new path.

Indeed, the above discussion, and the other chapters of this special issue, really do not cover all the foreseeable approaches. I will mention two of which I am aware: first, another computational paradigm, that of the cellular automaton, is potentially available for exploitation. This is distinguished from the above "general purpose" approach in that it assumes that every bit pattern throughout the computer will be subjected to the same evolution rule. It is known that general-purpose computation is performable, although with considerable overhead, by a cellular automaton. This is true as well for the quantum version of the cellular automaton, as LLOYD [47] indicated in his original work. New theoretical work by BENJAMIN [48] shows very explicitly how relatively simple local rules would permit the implementation of some quantum computations. This could point us perhaps towards some sort of polymer with a string of qubits on its backbone that can be addressed globally in a spectroscopic fashion. Experiments are not oriented towards this at the moment, but the tradeoffs are very different, and I don't believe it should be excluded in the future.

Second, even more speculative, but very elegant, is the proposal of KITAEV [49] to use quantum systems with particular kinds of topological excitations, for example nonabelian anyons, for quantum computing. It is hard to see at the moment how to turn this exciting proposal into an experimental program, as no known physical system is agreed to have the appropriate topological excitations. But further research in, for example, the quantum Hall effect might reveal such a system; more likely, perhaps, is that further understanding of this approach, and that of Freedman and his colleagues [50], will shed more light on doing quantum computing using the "standard" approach being considered in this book.

I am convinced of one thing: the ideas of quantum information theory will continue to exert a decisive influence on the further investigation of the fundamental quantum properties of complex quantum systems, and will stimulate many creative and exciting developments for many years to come.

## Acknowledgments

I gratefully acknowledge support from the Army Research Office under contract number DAAG55-98-C-0041. I thank Alec Maassen van den Brink for a careful reading of this manuscript.

## References

- [1] J. I. CIRAC and P. ZOLLER, Phys. Rev. Lett. **74**, 4091 (1995); T. PELLIZZARI, S. A. GARDINER, J. I. CIRAC, and P. ZOLLER, Phys. Rev. Lett. **75**, 3788 (1995); C. MONROE, D. M. MEEKHOF, B. E. KING, W. M. ITANO, and D. J. WINELAND, *Demonstration of a fundamental quantum logic gate*, Phys. Rev. Lett. **75**, 4714 (1995); A. SORENSEN and K. MOLMER, Phys. Rev. Lett. **82**, 1971 (1999); S. SCHNEIDER, D. F. V. JAMES, and G. J. MILBURN, *Method of quantum computation with 'hot' trapped ions*, quant-ph/9808012.
- [2] Q. A. TURCHETTE, C. J. HOOD, W. LANGE, H. MABUCHI, and H. J. KIMBLE, *Measurement of conditional phase shifts for quantum logic*, Phys. Rev. Lett. **75**, 4710 (1995); A. IMAMOGLU, D. D. AWSCHALOM, G. BURKARD, D. P. DIVINCENZO, D. LOSS, M. SHERWIN, and A. SMALL, Phys. Rev. Lett. **83**, 4204 (1999) (quant-ph/9904096).
- [3] N. GERSHENFELD and I. CHUANG, SCIENCE **275**, 350 (1997); D. CORY, A. FAHMY, and T. HAVEL, Proc. Nat. Acad. Sci. **94** (5), 1634 (1997).
- [4] B. KANE, NATURE **393**, 133 (1998); R. VRIJEN et al., *Electron spin resonance transistors for quantum computing in silicon-germanium heterostructures*, Phys. Rev. A, in press (quant-ph/9905096).
- [5] D. AVERIN, Solid State Commun. **105**, 659 (1998); A. SHNIRMAN, G. SCHÖN, and Z. HERMIN, Phys. Rev. Lett. **79**, 2371 (1997); J. E. MOOIJ, T. P. ORLANDO, L. LEVITOV, L. TIAN, C. H. VAN DER WAL, and S. LLOYD, Science **285**, 1036 (1999).
- [6] P. M. PLATZMAN and M. I. DYKMAN, SCIENCE **284**, 1967 (1999).
- [7] D. LOSS and D. P. DIVINCENZO, Phys. Rev. A **57**, 120 (1998) (cond-mat/9701055); M. SHERWIN, A. IMAMOGLU, and T. MONTROY, *Quantum computation with quantum dots and terahertz cavity quantum electrodynamics*, Phys. Rev. A **60**, 3508 (1999) (quant-ph/9903065); T. TANAMOTO, Phys. Rev. A **61**, 022305 (2000) (quant-ph/9902031).
- [8] D. DEUTSCH, Proc. R. Soc. London A **400**, 97 (1985); **425**, 73 (1989).
- [9] R. P. FEYNMAN, Int. J. Theor. Phys. **21**, 467 (1982); Found. Phys. **16**, 507 (1986). See also *Feynman Lectures on Computation*, eds. A. J. G. Hey and R. Allen (Perseus Press, 1996).
- [10] R. BEALS, H. BUHRMAN, R. CLEVE, M. MOSCA, and R. DE WOLF, *Quantum lower bounds by polynomials*, Proc. of the 39th Annual Symposium on the Foundations of Computer Science (IEEE Press, Los Alamitos, 1998), p. 352; quant-ph/9802049.
- [11] Y. OZHIGOV, *Quantum computer cannot speed up iterated applications of a black box*, quant-ph/9712051; B. Terhal, PhD Thesis, University of Amsterdam, 1999.
- [12] L. K. GROVER, *Quantum mechanics helps in searching for a needle in a haystack*, Phys. Rev. Lett. **79**, 325 (1997).
- [13] P. W. SHOR, *Polynomial time algorithms for prime factorization and discrete logarithms on a quantum computer*, SIAM J. Comput. **26**, 1484 (1997), and references therein.
- [14] D. P. DIVINCENZO and D. LOSS, *Quantum Computers and Quantum Coherence*, J. Magnetism Magn. Matl. **200**, 202–218 (1999).
- [15] R. CLEVE and H. BUHRMAN, Phys. Rev. A **56**, 1201 (1997).
- [16] H. BUHRMAN, R. CLEVE, and A. WIGDERSON, *Quantum vs. Classical Communication and Computation*, in *Proc. of the 30th Ann. ACM Symp. on the Theory of Computing* (ACM Press, 1998), p. 63; eprint quant-ph/9802040.
- [17] A. AMBAINIS, L. SCHULMAN, A. TA-SHMA, U. VAZIRANI, and A. WIGDERSON, *The quantum communication complexity of sampling*, in *Proc. of the 39th Annual Symposium on the Foundations of Computer Science* (IEEE Press, Los Alamitos, 1998); see <http://www.icsi.berkeley.edu/~amnon/Papers/qcc.ps>.
- [18] C. H. BENNETT and G. BRASSARD, *Quantum Cryptography: Public Key Distribution and Coin Tossing*, in *Proceedings of the IEEE International Conference on Computers, Systems and Signal Processing*, Bangalore, India (IEEE, New York, 1984), p. 175.

- [19] D. A. MEYER, *Quantum strategies*, Phys. Rev. Lett. **82**, 1052 (1999) (quant-ph/9804010); J. EISERT, M. WILKENS, and M. LEWENSTEIN, *Quantum games and quantum strategies*, Phys. Rev. Lett. **83**, 3077 (1999) (quant-ph/9806088); L. GOLDENBERG, L. VAIDMAN, and S. WIESNER, *Quantum gambling*, Phys. Rev. Lett. **82**, 3356 (1999) (quant-ph/9808001).
- [20] A. M. STEANE and W. VAN DAM, *Physicists Triumph at 'Guess my Number'*, Physics Today **53** (2), 35–39 (2000).
- [21] D. AHARONOV, *Quantum Computation in Annual Reviews of Computational Physics*, vol. VI (ed. Dietrich Stauffer, World Scientific, Singapore, 1998) (quant-ph/9812037).
- [22] R. CLEVE, *An Introduction to Quantum Complexity Theory*, to appear in *Collected Papers on Quantum Computation and Quantum Information Theory* (eds. C. Macchiavello, G. M. Palma, and A. Zeilinger, World Scientific, 2000) (quant-ph/9906111).
- [23] C. H. BENNETT, Physics Today **48** (10), 24 (1995); D. P. DiVINCENZO, Science **270**, 255 (1995); D. P. DiVINCENZO, Proc. R. Soc. London A **454**, 261 (1998) (and quant-ph/9705009); A. BARENCO, Contemp. Phys. **37**, 375 (1996); A. STEANE, Rep. Prog. Phys. **61**, 117 (1998); C. H. BENNETT and P. W. SHOR, IEEE Trans. Info. Theory **44**, 2724 (1998).
- [24] D. P. DiVINCENZO, in *Mesoscopic Electron Transport*, eds. L. Sohn, L. Kouwenhoven, and G. Schön (Vol. 345, NATO ASI Series E, Kluwer, 1997), p. 657 (cond-mat/9612126); D. P. DiVINCENZO and D. LOSS, *Superlattices and Microstructures* **23**, 419 (1998) (cond-mat/9710259); D. P. DiVINCENZO and D. LOSS, J. Magn. Mag. Matl. **200**, 202 (1999) (cond-mat/9901137).
- [25] B. SCHUMACHER, Phys. Rev. A **54**, 2614 (1996).
- [26] G. K. BRENNEN, C. M. CAVES, P. S. JESSEN, and I. H. DEUTSCH, Phys. Rev. Lett. **82**, 1060 (1999).
- [27] D. JAKSCH, H. J. BRIEGEL, I. J. CIRAC, C. GARDINER, and P. ZOLLER, Phys. Rev. Lett. **82**, 1975 (1999).
- [28] I am grateful to R. SCHOELKOPF and M. DEVORET for clarifying discussion on these points.
- [29] M. B. PLENIO and P. L. KNIGHT, Phys. Rev. A **53**, 2986 (1996).
- [30] M. B. PLENIO and P. L. KNIGHT, Proc. Roy. Soc. Lond. A **453**, 2017–2041 (1997).
- [31] J. PRESKILL, Proc. R. Soc. Lond. A **454**, 385 (1998) (quant-ph/9705031).
- [32] M. A. NIELSEN and I. L. CHUANG, *Quantum Computation and Quantum Information* (Cambridge University Press, 2000); see also M. A. NIELSEN, C. M. CAVES, B. SCHUMACHER, and H. BARNUM, Proc. R. Soc. Lond. A **454**, 277–304 (1998) (quant-ph/9706064).
- [33] P. SHOR, Phys. Rev. A **52**, 2493 (1995); A. M. STEANE, Phys. Rev. Lett. **77**, 793–797 (1996).
- [34] P. SHOR, in *Proceedings of the 37th Symposium on the Foundations of Computer Science* (IEEE Press, Los Alamitos, CA, 1996) (quant-ph/9605011); D. AHARONOV and M. BEN-OR, in *Proceedings of the 29th Annual ACM Symposium on the Theory of Computing* (ACM Press, New York, 1997) (quant-ph/9611025); E. KNILL, R. LAFLAMME, and W. ZUREK, Science **279**, 342 (1998). These results are reviewed in [31].
- [35] D. P. DiVINCENZO, *Two-bit gates are universal for quantum computation*, Phys. Rev. A **51**, 1015 (1995), cond-mat/9407022.
- [36] A. BARENCO, C. H. BENNETT, R. CLEVE, D. P. DiVINCENZO, N. MARGOLUS, P. SHOR, T. SLEATOR, J. A. SMOLIN, and H. WEINFURTER, *Elementary gates for quantum computation*, Phys. Rev. A **52**, 3457 (1995), quant-ph/9503016.
- [37] K. MOLMER and A. SORENSEN, Phys. Rev. Lett. **82**, 1835 (1999).
- [38] D. W. LEUNG, I. L. CHUANG, F. YAMAGUCHI, and Y. YAMAMOTO, *Efficient implementation of selective recoupling in heteronuclear spin systems using Hadamard matrices*, quant-ph/9904100.
- [39] G. BURKARD, D. LOSS, D. P. DiVINCENZO, and J. A. SMOLIN, Phys. Rev. B **60**, 11404 (1999); cond-mat/9905230.
- [40] G. BURKARD, D. LOSS, D. P. DiVINCENZO, Phys. Rev. B **59**, 2070 (1999); cond-mat/9808026.
- [41] D. GOTTESMAN, *Fault-Tolerant Quantum Computation with Local Gates*, J. Mod. Optics **47**, 333 (2000); quant-ph/9903099.
- [42] D. BACON, J. KEMPE, D. A. LIDAR, and K. B. WHALEY, *Universal fault-tolerant computation on decoherence-free subspaces*, quant-ph/9909058.
- [43] D. P. DiVINCENZO, G. BURKARD, D. LOSS, and E. V. SUKHORUKOV, *Quantum computation and spin electronics in Quantum Mesoscopic Phenomena and Mesoscopic Devices in Microelectronics*, eds. I. O. Kulik and R. Ellialtioglu (NATO Advanced Study Institute, Turkey, June 13–25, 1999), to be published; cond-mat/9911245.
- [44] D. GOTTESMAN and I. L. CHUANG, Nature **402**, 390 (1999).
- [45] D. LOSS and E. V. SUKHORUKOV, Phys. Rev. Lett. **84**, 1035 (2000).

04010); J. Eisner, Phys. Rev. Lett. **78**, 3221 (1997) (quant-ph/9611017).

ics Today **53**

s, vol. VI (ed.

ed Papers on  
G. M. Palma,

), 255 (1995);  
09); A. BARE-  
117 (1998);

oven, and G.  
mat/9612126);  
'8) (cond-mat/  
'9) (cond-mat/

1060 (1999).  
Lett. **82**, 1975

points.

n (Cambridge  
J H. BARNUM,

17 (1996).  
Science (IEEE  
R, in *Proceed-*  
ss, New York,  
, 342 (1998).

v. A **51**, 1015

., T. SLEATOR,  
s. Rev. A **52**,

ntation of se-  
/9904100.  
11404 (1999);

9808026.  
Optics **47**, 333

mputation on

mputation and  
Microelectro-  
June 13–25,

- [46] J. I. CIRAC, P. ZOLLER, H. J. KIMBLE, and H. MABUCHI, Phys. Rev. Lett. **78**, 3221 (1997) (quant-ph/9611017).
- [47] S. LLOYD, Science **261**, 1569 (1993); **263**, 695 (1994).
- [48] S. BENJAMIN, Phys. Rev. A **61**, 020301(R) (2000) (quant-ph/9909007).
- [49] A. YU. KITAEV, *Fault-tolerant quantum computation with anyons*, quant-ph/9707021; see also J. PRESKILL, in *Introduction to Quantum Computation and Information* (eds. H.-K. Lo, S. Popescu, and T. Spiller, World Scientific, Singapore, 1998) pp. 213–269 (quant-ph/9712048).
- [50] M. H. FREEDMAN, M. LARSEN, and Z. WANG, *A modular functor which is universal for quantum computation*, quant-ph/0001108; M. H. FREEDMAN, *Poly-locality in quantum computing*, quant-ph/0001077; M. H. FREEDMAN, A. YU. KITAEV, and Z. WANG, *Simulation of topological field theories by quantum computers*, quant-ph/0001071.



# Anomalous periodicity of the current-phase relationship of grain-boundary Josephson junctions in high- $T_c$ superconductors

E. Il'ichev, V. Zakosarenko, R. P. J. IJsselsteijn, H. E. Hoenig, V. Schultze, and H.-G. Meyer  
*Department of Cryoelectronics, Institute for Physical High Technology, P.O. Box 100239, D-07702 Jena, Germany*

M. Grajcar and R. Hlubina  
*Department of Solid State Physics, Comenius University, Mlynská Dolina F2, 842 15 Bratislava, Slovakia*  
 (Received 28 January 1999)

The current-phase relation (CPR) for asymmetric  $45^\circ$  Josephson junctions between two  $d$ -wave superconductors has been predicted to exhibit an anomalous periodicity. We have used the single-junction interferometer to investigate the CPR for these kinds of junctions in  $\text{YBa}_2\text{Cu}_3\text{O}_{7-x}$  thin films. A remarkable amplitude of the  $\pi$ -periodical component of the CPR has been experimentally found, providing an additional source of evidence for the  $d$ -wave symmetry of the pairing state of the cuprates. [S0163-1829(99)05629-5]

A number of experimental results confirm  $d_{x^2-y^2}$ -wave symmetry of the pairing state of high-temperature superconductors.<sup>1</sup> An unconventional pairing state requires the existence of zeros of the order parameter in certain directions in momentum space. Thermodynamic and spectroscopic measurements do indeed suggest their existence, but by themselves they do not exclude conventional  $s$ -wave pairing with nodes.<sup>1</sup> Direct evidence for the  $d$ -wave pairing state is provided by phase-sensitive experiments, which are based on the Josephson effect.<sup>2</sup> Quite generally, the current-phase relationship (CPR) of a Josephson junction,  $I(\varphi)$  is an odd periodic function of  $\varphi$  with a period  $2\pi$ .<sup>3</sup> Therefore  $I(\varphi)$  can be expanded in a Fourier series

$$I(\varphi) = I_1 \sin \varphi + I_2 \sin 2\varphi + \dots \quad (1)$$

In the tunnel limit we can restrict ourselves to the first two terms in Eq. (1). Since the order parameter is bound to the crystal lattice,  $I(\varphi)$  of a weak link depends on the orientation of the  $d$ -wave electrodes with respect to their boundary. The existing phase-sensitive experiments exploit possible sign changes of  $I_1$  between different geometries.<sup>2</sup> In this work we present a phase-sensitive experimental test of the pairing state symmetry of cuprates. Namely, in certain geometries, the  $I_1$  term should vanish by symmetry. In such cases, the CPR should exhibit an anomalous periodicity.

Let us analyze the angular dependence of  $I_{1,2}$  in a junction between two macroscopically tetragonal  $d$ -wave superconductors. As emphasized in Ref. 4, also heavily twinned orthorhombic materials such as  $\text{YBa}_2\text{Cu}_3\text{O}_{7-x}$  belong to this class, if the twin boundaries have odd symmetry. We consider an ideally flat interface between two superconducting electrodes. Let  $\theta_1$  ( $\theta_2$ ) denote the angle between the normal to the grain boundary and the  $a$  axis in electrode 1 (2), see Fig. 1. If we only keep the lowest-order angular harmonics, the symmetry of the problem dictates that<sup>4</sup>

$$I_1 = I_c \cos 2\theta_1 \cos 2\theta_2 + I_s \sin 2\theta_1 \sin 2\theta_2. \quad (2)$$

The coefficients  $I_c, I_s$  are functions of the barrier strength, temperature  $T$ , etc. The  $I_2$  term results from higher-order tunneling processes and we neglect its weak angular depen-

dence. It is seen from Eq. (2) that the criterion for the observation of an anomalous period of the CPR,  $I_1 = 0$ , is realized for an asymmetric  $45^\circ$  junction, i.e., a junction with  $\theta_1 = 45^\circ$  and  $\theta_2 = 0$ .

The  $I_2$  term is also present in weak links based on conventional  $s$ -wave superconductors but for all known types of weak links  $|I_2/I_1| < 1$ . For instance, for a tunnel junction  $|I_2/I_1| \ll 1$ . For a superconductor-normal-metal-superconductor (SNS) junction,  $I \propto \sin \varphi/2$  at  $T=0$ ,<sup>5</sup> and the Fourier expansion of Eq. (1) leads to  $I_2/I_1 = -2/5$ . Therefore a possible experimental observation of  $|I_2/I_1| \gg 1$  in an asymmetric  $45^\circ$  junction provides direct evidence of  $d$ -wave symmetry of the pairing state in the cuprates.

We have investigated the CPR of  $\text{YBa}_2\text{Cu}_3\text{O}_{7-x}$  thin-film bicrystals with asymmetric  $45^\circ$  [001]-tilt grain boundaries as sketched in Fig. 1, using a single-junction interferometer configuration in which the Josephson junction is inserted into a superconducting loop with a small inductance  $L$ . In a stationary state without fluctuations, the phase difference  $\varphi$  across the junction is controlled by applying an external magnetic flux  $\Phi_e$  penetrating the loop:  $\varphi = \varphi_e - \beta f(\varphi)$ . Here  $\varphi_e = 2\pi\Phi_e/\Phi_0$ ;  $\Phi_0 = 2.07 \times 10^{-15} \text{ Tm}^2$  is the flux quantum;  $f(\varphi) = I(\varphi)/I_0$  is the CPR normalized to the maximal Josephson current  $I_0$ , and  $\beta = 2\pi LI_0/\Phi_0$  is the normalized

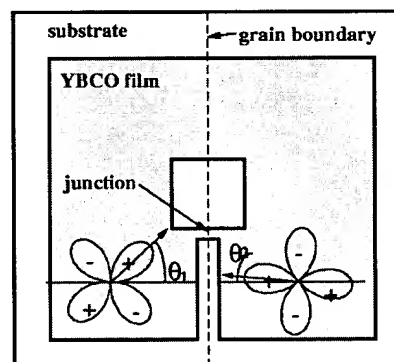


FIG. 1. Washer-shaped interferometer with one short Josephson junction (not in scale). Dimensions are given in the text.



critical current. In order to obtain the CPR for the complete phase range  $-\pi \leq \varphi \leq \pi$  the condition  $\beta < 1$  has to be fulfilled, because for  $\beta > 1$  the curve  $\varphi(\varphi_e)$  becomes multivalued. Following Ref. 3, we express the effective inductance of the interferometer using the derivative  $f'$  with respect to  $\varphi$  as  $L_{int} = L[1 + 1/\beta f'(\varphi)]$ . The inductance can be probed by coupling the interferometer to a tank circuit with inductance  $L_T$ , quality factor  $Q$ , and resonance frequency  $\omega_0$  through the mutual inductance  $M$ .<sup>8</sup> External flux in the interferometer is produced by a current  $I_{dc} + I_{rf}$  in the tank coil and can be expressed as  $\varphi_e = 2\pi(I_{dc} + I_{rf})M/\Phi_0 = \varphi_{dc} + \varphi_{rf}$ , where  $M^2 = k^2 L L_T$  with  $k$  a coupling coefficient. Taking into account the quasiparticle current in the presence of a voltage  $V$  across the junction the phase difference is given by the relation  $\varphi = \varphi_{dc} + \varphi_{rf} - \beta f(\varphi) - 2\pi\tau(\varphi)V/\Phi_0$ , where  $\tau(\varphi) = L/R_J(\varphi)$  with  $R_J(\varphi)$  the resistance of the junction. In the small-signal limit  $\varphi_{rf} \ll 1$  and in the adiabatic case  $\omega\tau \ll 1$ , keeping only the first-order terms, the effective inductance  $L_{eff}$  of the tank circuit-interferometer system is

$$L_{eff} = L_T \left( 1 - k^2 \frac{L}{L_{int}} \right) = L_T \left( 1 - \frac{k^2 \beta f'(\varphi)}{1 + \beta f'(\varphi)} \right).$$

Thus the phase angle  $\alpha$  between the driving current and the tank voltage  $U$  at the resonance frequency of the tank circuit  $\omega_0$  is

$$\tan \alpha(\varphi) = \frac{k^2 Q \beta f'(\varphi)}{1 + \beta f'(\varphi)}. \quad (3)$$

Using the relation  $[1 + \beta f'(\varphi)]d\varphi = d\varphi_{dc}$  which is valid for  $\varphi_{rf} \ll 1$  and  $\omega\tau \ll 1$ , one can find the CPR from Eq. (3) by numerical integration.

The advantage of the CPR measurement of an asymmetric  $45^\circ$  junction with respect to the by-now standard phase-sensitive tests of pairing symmetry based on the angular dependence of  $I_1$  is twofold. First, it avoids the complications of the analysis of experiments caused by the presence of the term  $I_s$ .<sup>4</sup> Second, flux trapped in the interferometer washer (see Fig. 1) does not invalidate the conclusions about the ratio  $|I_2/I_1|$  and hence about the pairing symmetry, which is not the case in standard phase-sensitive tests of the  $d$ -wave symmetry of the pairing state.<sup>9</sup>

The films of 100-nm thickness were fabricated using standard pulsed laser deposition on (001) oriented SrTiO<sub>3</sub> bicrystalline substrates with asymmetric [001] tilt misorientation angles of  $45^\circ \pm 1^\circ$ . The films were subsequently patterned by Ar ion-beam etching into  $4 \times 4$ -mm<sup>2</sup> square washer single-junction interferometer structures (Fig. 1). The widths of the junctions were 1–2  $\mu$ m. The square washer holes had a side length of 50  $\mu$ m. This geometry of the interferometer gives  $L \approx 80$  pH. The resistance of a similar single junction (without interferometer loop) was measured directly and  $R_J > 1$   $\Omega$  was found. Therefore the condition for the adiabatic limit  $\omega\tau \ll 1$  is satisfied. For measurements of  $\alpha(\varphi_{dc})$ , several tank circuits with inductances 0.2–0.8  $\mu$ H and resonance frequencies 16–35 MHz have been used. The unloaded quality factor of the tank circuits  $70 < Q < 150$  has been measured at various temperatures. The coupling factor  $k$  was determined from the period  $\Delta I_{dc}$  of  $\alpha(I_{dc})$  using  $M\Delta I_{dc} = \Phi_0$ . Its value varied between 0.03 and 0.09. The

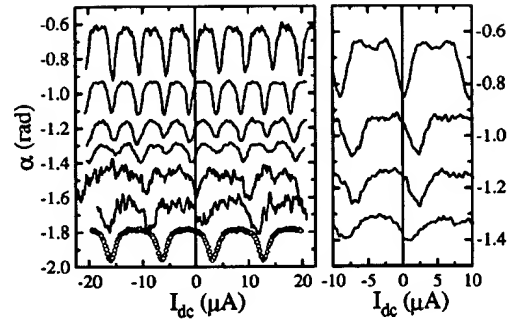


FIG. 2. Left panel: Phase angle between the driving current and the output voltage measured for sample No. 1 at different temperatures as a function of the dc current  $I_{dc}$ . The curves are shifted along the y axis and the data for  $T = 30$  and 40 K are multiplied by factor 4 for clarity. From top to bottom, the data correspond to  $T = 4.2, 10, 15, 20, 30$ , and 40 K. The data measured for  $36^\circ$  bicrystals ( $\theta_1 \approx 36^\circ, \theta_2 \approx 0$ ) at  $T = 40$  K in the same washer geometry are shown for comparison (open circles). Right panel: The same for sample No. 3. From top to bottom, the data correspond to  $T = 4.2, 10, 15$ , and 20 K.

amplitude of  $I_{rf}$  was set to produce a flux in the interferometer smaller than  $0.1 \Phi_0$  to ensure the small-signal limit.

The measurements have been performed in a gas-flow cryostat with a five-layer magnetic shielding in the temperature range  $4.2 \leq T < 90$  K. The experimental setup was calibrated by measuring interferometers of the same size with  $24^\circ$  and  $36^\circ$  grain boundaries. We have studied six samples, out of which for four samples the  $\pi$ -periodic component of  $I(\varphi)$  was experimentally observed. At low temperatures for two samples (Nos. 1 and 2) the value of  $I_2$  is larger than  $I_1$ . For sample Nos. 3 and 4  $I_2$  is approximately 10–20 % of  $I_1$  and for sample Nos. 5 and 6  $I_2$  is negligible. As an example we plot the phase angle  $\alpha$  as a function of the dc current  $I_{dc}$  for sample Nos. 1 and 3 (Fig. 2). The behavior of sample No. 1 at low temperatures is defined by the  $\pi$  periodic component of  $I(\varphi)$ . The curves for sample No. 3 are  $2\pi$ -periodic, nevertheless for the curve at  $T = 4.2$  K the local minima clearly show the presence of a  $\pi$ -periodic component.

In order to determine the CPR we assume that the period of  $\alpha(I_{dc})$  at  $T = 40$  K and  $\Delta I_{dc} = 9.6$   $\mu$ A, corresponds to  $\Delta \varphi_{dc} = 2\pi$ . We take  $\varphi_{dc} = 0$  at a maximum or minimum of  $\alpha$ . This is necessary in order to satisfy  $I(\varphi = 0) = 0$ , as required by general principles.<sup>3</sup> The experimentally observed shift of the first extreme of  $\alpha(I_{dc})$  from  $I_{dc} = 0$  (Fig. 2) can be due to flux trapped in the interferometer washer. Most probably, this flux resides in the long junction originated by the grain boundary crossing the washer of the interferometer. This long junction does not play an active role because the Josephson penetration depth is much smaller than the junction length, and external fields produced by  $I_{dc}$  are smaller than the first critical field. Nevertheless, the long junction sets the phase difference for  $I_{dc} = 0$  at the small junction.

In Fig. 3, we show the CPR determined from the data in Fig. 2. For all curves we have performed a minimal necessary shift consistent with  $I(\varphi = 0) = 0$ . Thus we have assumed that at  $\varphi_{dc} = 0$  a minimum of  $\alpha(\varphi_{dc})$  is realized. For an interferometer with a conventional  $s$ -wave weak link (and also for the  $36^\circ$  junction), at  $\varphi_{dc} = 0$  one gets a maximum of

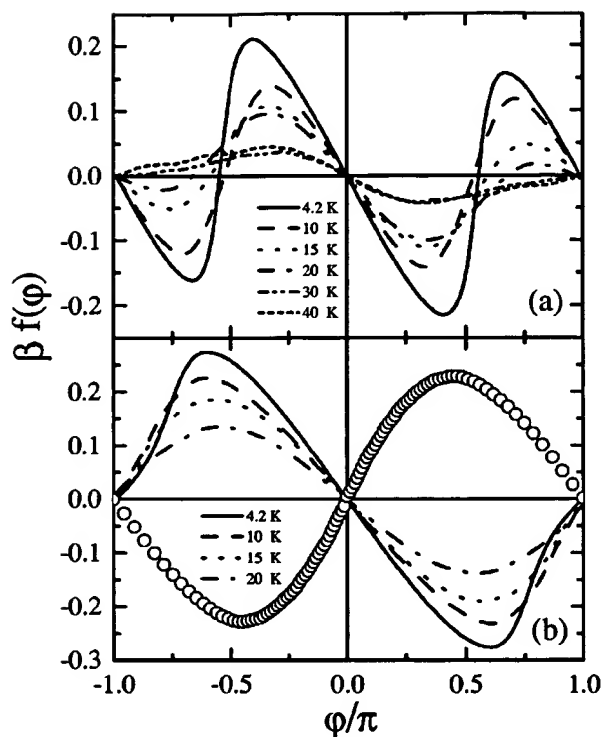


FIG. 3. (a) Josephson current through the junction for sample No. 1 as a function of the phase difference  $\varphi$ , determined from the data in Fig. 2. The scattering of  $\alpha(\varphi)$  values was reduced by folding the data back to the interval  $(0, \pi)$  and taking the average. Here, the symmetry  $\alpha(\varphi) = \alpha(-\varphi)$  was assumed. (b) The same for sample No. 3. The data for the asymmetric  $36^\circ$  bicrystal at  $T = 40$  K (open circles) are also shown.

$\alpha(\varphi_{dc})$ . Note that the minimum of  $\alpha(\varphi_{dc})$  at  $\varphi_{dc} = 0$  implies a paramagnetic response of the interferometer in the limit of small applied fields.

The amplitude of the  $\pi$ -periodic component of the CPR decreases drastically with increasing temperature, and at  $T = 40$  K its contribution is negligible for all samples. The temperature dependence of  $I_1$  and  $I_2$  could be determined with acceptable accuracy for sample No. 1 only. With decreasing  $T$ ,  $|I_2|$  grows monotonically down to  $T = 4.2$  K, while the  $I_1$  component exhibits only a weak temperature dependence (Fig. 4).

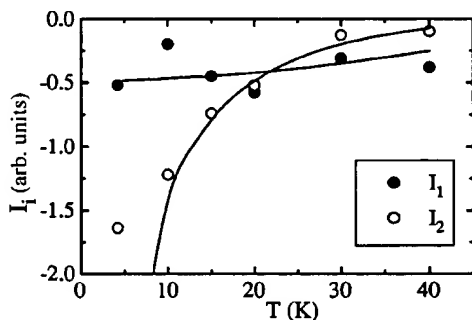


FIG. 4. Temperature dependence of the Fourier expansion coefficients  $I_{1,2}$  determined from the experimental data in Fig. 3(a). Solid lines are the Fourier expansion coefficients for the numerical data in Fig. 5.

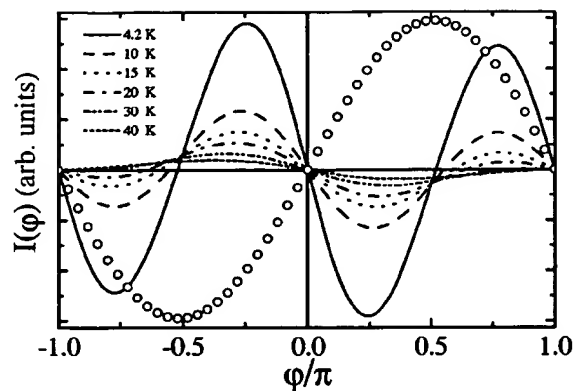


FIG. 5.  $I(\varphi)$  calculated according to Eq. (64) of Ref. 11 for a junction with  $\theta_1 = 45.5^\circ$ ,  $\theta_2 = 0$ ,  $\lambda d = 1.5$ ,  $\kappa = 0.5$ , and  $T_c = 60$  K.  $I(\varphi)$  at  $T = 40$  K for the  $36^\circ$  bicrystal (open circles) was calculated with the same parameters except for  $\theta_1 = 36^\circ$ .

Our experimental results can be understood as follows. It is well known that the microstructural properties of the grain boundaries, especially  $45^\circ$  boundaries, are defined by their faceted nature. Faceting is an intrinsic property of the grain boundaries,<sup>6,7</sup> and, due to  $d$ -wave symmetry of the order parameter, the properties of the junctions strongly depend on the particular distribution of the facets. Small deviations from the ideal geometry of the asymmetric  $45^\circ$  junction lead to a finite value of  $I_1$ . Thus for nearly ideal junctions  $|I_2/I_1| \gg 1$  at  $T \rightarrow 0$ . The region  $T \sim T_c$  can be analyzed quite generally within the Ginzburg-Landau theory. Let the electrodes be described by the (macroscopic) order parameters  $\Delta_{1,2} = |\Delta|e^{i\varphi_{1,2}}$ . Then the phase-dependent part of the energy of the junction is  $E = a[\Delta_1 \Delta_2^* + \text{H.c.}] + b[(\Delta_1 \Delta_2^*)^2 + \text{H.c.}] + \dots$  where  $a, b, \dots$  depend weakly on  $T$ .<sup>10</sup> Thus for  $T$  close to  $T_c$  we estimate  $I_1 \propto |\Delta|^2 \propto (T_c - T)$  and  $I_2 \propto |\Delta|^4 \propto (T_c - T)^2$ , leading to  $|I_2/I_1| \ll 1$ . With increasing deviations from ideal geometry  $|I_2/I_1|$  decreases. For large enough deviations, negligible values of  $|I_2|$  are expected. These expectations are qualitatively consistent with the experimental data (see also Fig. 4).

So far, our discussion was based solely on symmetry arguments. Let us attempt a more quantitative analysis of our data now. Two different microscopic pictures of asymmetric  $45^\circ$  Josephson junctions between  $d$ -wave superconductors have been considered in the literature. The first picture assumes a microscopically tetragonal material and an ideally flat interface.<sup>10-12</sup> Within this picture, only sample No. 1 can be analyzed. Sample No. 2 had  $I_0(T = 1.5 \text{ K}) \approx 10^{-2} \mu\text{A}$ . At this temperature only the  $\pi$ -periodic component of  $I(\varphi)$  was observed. At higher temperatures  $I_0$  was not measurable.  $I(\varphi)$  for sample No. 1 calculated according to the model of Ref. 11 is shown in Fig. 5. The experimental data can be fitted within a relatively broad range of barrier heights. However, if we require the  $I(\varphi)$  relation of the  $36^\circ$  junction to be fitted by the same (or smaller) barrier height as for the  $45^\circ$  junction, we conclude the barrier of the  $45^\circ$  junction to be rather low.<sup>14</sup> The dependence of  $I(\varphi)$  on  $T$  requires a choice of  $T_c \approx 60$  K in the non-self-consistent theory of Ref. 11. The reduction from the bulk  $T_c = 90$  K is probably due to a combined effect of surface degradation and order-parameter suppression at the sample surface. The temperature dependence

of the ratio of the  $\pi$  and  $2\pi$  periodic components in  $I(\varphi)$  is seen to be in qualitative agreement with experimental data in Fig. 3(a). This is explicitly demonstrated in Fig. 4 where we compare the experimentally obtained  $I_{1,2}$  with the results of the Fourier analysis of the curves in Fig. 5. The divergence of  $I_2$  as  $T \rightarrow 0$  is an artifact of the ideal junction geometry assumed in Ref. 11. If a finite roughness of the interface is taken into account, this divergence is cut off and the experimental data in Fig. 4 do indeed resemble theoretical predictions for a rough interface.<sup>12</sup> However, the non-self-consistent theory of Ref. 11 is unable to explain the experimentally observed steep CPR close to the minima of the junction energy [see Fig. 3(a)].

In a different approach a heavily meandering interface with  $\theta_i = \theta_i(x)$  is assumed. Now, the critical current density  $j_c(x)$  is a random function with a typical amplitude  $\langle |j_c(x)| \rangle \sim j_c$ . If the average critical current along the junction  $\langle j_c \rangle < j_c$ , a remarkable  $\pi$ -periodic component is present in the CPR. The relation  $|I_2/I_1|$  depends on the distribution of  $j_c(x)$  and can be much larger than one for  $\langle j_c \rangle \ll j_c$ .<sup>15,16</sup> This model qualitatively explains the obtained results for all samples, however for a quantitative comparison the actual microscopic distribution  $j_c(x)$  should be known. Note that

also within the picture of Refs. 15 and 16 the  $d$ -wave symmetry of the pairing state is crucial, otherwise the condition  $\langle j_c \rangle \ll j_c$  is difficult to satisfy.

Our present understanding of  $I(\varphi)$  in the asymmetric  $45^\circ$  junction is only qualitative. We cannot say whether the remarkable amplitude of the  $\pi$ -periodic component of  $I(\varphi)$  is dominated by the microscopically flat regions,<sup>13</sup> or due to the spatial inhomogeneity of the junction. This issue requires further study.

In conclusion, we have measured the magnetic-field response of a single-junction interferometer based on asymmetric  $45^\circ$  grain-boundary junctions in  $\text{YBa}_2\text{Cu}_3\text{O}_{7-x}$  thin films. A large  $\pi$ -periodic component of  $I(\varphi)$  has been experimentally found, which is in agreement with theoretical predictions for  $d_{x^2-y^2}$ -wave superconductors. Hence our results provide an additional source of evidence for the  $d$ -wave symmetry of the pairing state in the cuprates.

Financial support by the DFG (Ho 461/3-1) and partial support by INTAS (N 11459) are gratefully acknowledged. M. G. and R. H. were supported by the Slovak Grant Agency (Grant No. 1/4300/97) and the Comenius University (Grant No. UK/3927/98).

<sup>1</sup>For a review, see J. Annett, N. Goldenfeld, and A. J. Leggett, in *Physical Properties of High Temperature Superconductors*, edited by D. M. Ginsberg (World Scientific, New Jersey, 1996), Vol. V.

<sup>2</sup>See C. C. Tsuei *et al.*, *Science* **271**, 329 (1996), and references therein.

<sup>3</sup>A. Barone and G. Paterno, *Physics and Applications of the Josephson Effect* (Wiley, New York, 1982).

<sup>4</sup>M. B. Walker and J. Luettmann-Strathmann, *Phys. Rev. B* **54**, 588 (1996).

<sup>5</sup>I. O. Kulik and A. N. Omel'yanchuk, *Fiz. Nizk. Temp.* **4**, 296 (1978) [*Sov. J. Low Temp. Phys.* **4**, 142 (1978)].

<sup>6</sup>H. Hilgenkamp, J. Mannhart, and B. Mayer, *Phys. Rev. B* **53**, 14 586 (1996).

<sup>7</sup>J. Mannhart *et al.*, *Phys. Rev. Lett.* **77**, 2782 (1996).

<sup>8</sup>E. V. Il'ichev *et al.*, *J. Low Temp. Phys.* **106**, 503 (1997).

<sup>9</sup>R. A. Klemm, *Phys. Rev. Lett.* **73**, 1871 (1994).

<sup>10</sup>A. Huck, A. van Otterlo, and M. Sigrist, *Phys. Rev. B* **56**, 14 163 (1997).

<sup>11</sup>Y. Tanaka and S. Kashiwaya, *Phys. Rev. B* **56**, 892 (1997).

<sup>12</sup>Y. S. Barash, H. Burkhardt, and D. Rainer, *Phys. Rev. Lett.* **77**, 4070 (1996).

<sup>13</sup>C. R. Hu, *Phys. Rev. Lett.* **72**, 1526 (1994).

<sup>14</sup>This is consistent with the Fourier analysis of the data in Fig. 3 which results in a non-negligible  $I_n$  also for  $n \geq 3$ .

<sup>15</sup>A. J. Millis, *Phys. Rev. B* **49**, 15 408 (1994).

<sup>16</sup>R. G. Mints, *Phys. Rev. B* **57**, R3221 (1998).

## Nonsinusoidal Current-Phase Relationship of Grain Boundary Josephson Junctions in High- $T_c$ Superconductors

E. Il'ichev, V. Zakosarenko, R. P. J. IJsselsteijn, V. Schultze, H.-G. Meyer, and H. E. Hoenig

*Department of Cryoelectronics, Institute for Physical High Technology, P.O. Box 100239, D-07702 Jena, Germany*

H. Hilgenkamp and J. Mannhart

*Experimental Physics VI, Center for Electronic Correlations and Magnetism, Institute of Physics, Augsburg University, D-86135 Augsburg, Germany*

(Received 13 January 1998)

For various configurations of Josephson junctions incorporating superconductors with unconventional order parameter symmetry, such as most high- $T_c$  cuprates, deviations from the standard sinusoidal current-phase dependence have been predicted. To this point, these deviations have never been observed experimentally. We have measured the current-phase relation of high- $T_c$  Josephson junctions, namely,  $\text{YBa}_2\text{Cu}_3\text{O}_{7-x}$  thin film bicrystals, comprising symmetric  $45^\circ$  [001] tilt grain boundaries. The current-phase relations of all junctions investigated were found to be extremely nonharmonic, in agreement with a  $d_{x^2-y^2}$ -wave dominated symmetry of the order parameter. [S0031-9007(98)06674-5]

PACS numbers: 74.50.+r

The current-phase relation (CPR)  $f(\varphi)$  is a characteristic property of any weak link connecting two superconductors. It describes the dependence of the Cooper-pair current  $I_p$  on the phase difference  $\varphi$  of the order parameters of both superconducting electrodes. In a general form it is expressed as

$$I_p = I_c f(\varphi), \quad -1 \leq f(\varphi) \leq 1, \quad (1)$$

$I_c$  being the critical current of the weak link. It was shown by Josephson [1] that for ideal tunnel junctions between conventional superconductors the CPR is sinusoidal, i.e.,  $f(\varphi) = \sin(\varphi)$ . This sinusoidal dependence has been confirmed experimentally numerous times for standard tunnel junctions between conventional superconductors [2].

Recently, it has been revealed that the order parameter of most high- $T_c$  cuprates is unconventional, dominated by a  $d_{x^2-y^2}$  symmetry component [3–5]. Because of the sign change of the order parameter associated with this symmetry, strong deviations from the standard sinusoidal dependence have been predicted for the current-phase relations of various configurations of Josephson junctions employing such unconventional superconductors [6–9]. In particular, nonharmonic and double-periodic current-phase relations are expected for junctions oriented nominally perpendicular to the  $\langle 110 \rangle$  direction of one or of both electrodes, as well as for junctions for which the  $\langle 110 \rangle$  direction of one of the electrodes is aligned with the  $\langle 100 \rangle$  direction of the other, such as for  $45^\circ$  [001] tilt grain boundaries.

These predictions are highly unusual. Therefore, an experimental clarification of the CPR for high- $T_c$  junctions for which deviations from a standard harmonic behavior are expected is desirable. Such experiments will further

enhance the understanding of the influence of the order parameter symmetry on the properties of grain boundaries and high- $T_c$  Josephson junctions. In addition, they will provide valuable information for the design and use of Josephson junction-based circuits, of which many characteristics directly depend on the CPR. However, to our knowledge, such experiments have not been carried out. All available data refer to Josephson junctions for which nominally sinusoidal current-phase relations are expected. The CPR was measured for weak links prepared by ion irradiation [10], for step-edge junctions [11,12], and also for  $24^\circ$  bicrystal grain boundaries [12]. In nearly all of these cases sinusoidal current-phase relations were found. Deviations from a sinusoidal dependence have been observed only for one step-edge junction, measured at 77 K [12]. These deviations can be explained by the influence of thermal noise [13].

For these reasons we have investigated the CPR of  $\text{YBa}_2\text{Cu}_3\text{O}_{7-x}$  thin film bicrystals with symmetric  $45^\circ$  [001]-tilt grain boundaries, as sketched in Fig. 1(a). For these junctions, strong deviations from a sinusoidal CPR are anticipated.

Following a standard approach [14], the CPR was measured using a single-junction interferometer configuration in which the Josephson junction is part of a superconducting loop with a small inductance  $L$ . The phase difference  $\varphi$  across the junction is controlled by applying an external magnetic flux  $\Phi_e$  penetrating the loop:

$$\varphi = \varphi_e - \beta f(\varphi) + \varphi_n + 2\pi m. \quad (2)$$

Here,  $\varphi_e = 2\pi\Phi_e/\Phi_0$  is the external flux normalized to the flux quantum  $\Phi_0 (= 2.07 \times 10^{-15} \text{ Tm}^2)$ . The constant  $\beta = 2\pi LI_c/\Phi_0$  is the normalized critical current,  $\varphi_n$  is a term accounting for the effective noise, and  $m$  is

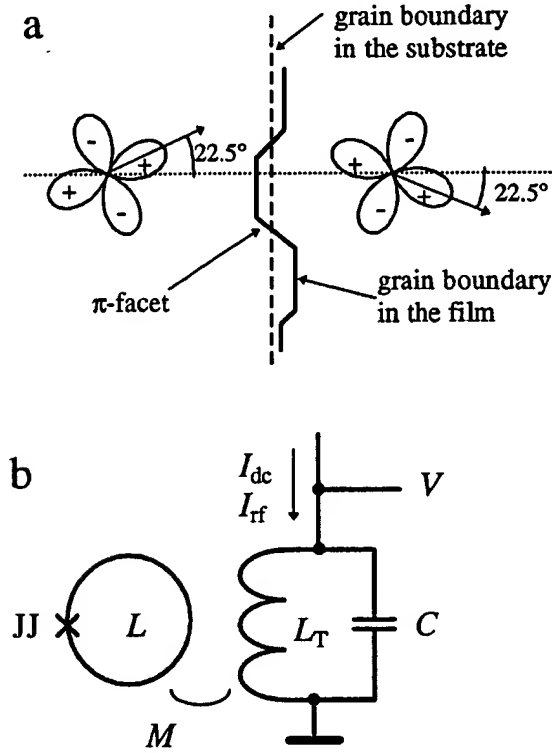


FIG. 1. (a) Schematic representation of a symmetric  $45^\circ$  [001]-tilt grain boundary junction in a  $d_{x^2-y^2}$  superconductor. The boundary in the superconducting thin film is meandering, leading to the occurrence of  $\pi$  facets. (b) Schematic of the measurement setup. The Josephson junction is denoted by JJ, and  $C$  indicates the capacitance of the tank circuit. The other denotations are explained in the text.

an integer. As capacitive contributions to the loop current are insignificant at the measurement frequencies, the junction capacitance has been neglected. The quasiparticle current is also negligible, for reasons discussed below.

The superconducting loop is inductively coupled to a tank circuit with inductance  $L_T$  [see Fig. 1(b)]. This tank circuit is driven with a current  $I_{rf}$  at a frequency  $\omega$  and a dc current  $I_{dc}$ . Thus,  $\varphi_e$  can be expressed as a sum of a dc and an rf component  $\varphi_e = \varphi_{dc} + \varphi_{rf}$ . In this arrangement, the effective impedance  $Z_{eff}(\omega)$  of the loop-tank circuit combination is a function of  $\varphi_e$ . As shown by Rifkin and Deaver [14], the CPR can be obtained from this dependence, provided that  $\varphi_{rf} \ll 1$ . To obtain the CPR for the complete phase range  $0 \leq \varphi \leq 2\pi$ , the condition  $\beta < 1$  has to be fulfilled in addition.

To enhance the accuracy of the measurement, we have adapted this common approach and retrieved the CPR from a measurement of the  $\varphi_{dc}$  dependence of the phase angle  $\alpha$  between the drive current  $I_{rf}$  and the tank voltage  $V$  at the resonant frequency of the tank circuit  $\omega_0$ . As described in Ref. [12], at  $\omega_0$ , the  $\alpha(\varphi_{dc})$  dependence is related to the derivative of the CPR  $f'(\varphi) \equiv df(\varphi)/d\varphi$  in the following way:

$$\tan \alpha(\varphi_{dc}) = \frac{k^2 Q \beta f'(\varphi(\varphi_{dc}))}{1 + \beta f'(\varphi(\varphi_{dc}))}. \quad (3)$$

Here  $k$  is the coupling factor between the tank inductance and the interferometer,  $k^2 = M^2/(LL_T)$ , where  $M$  is the mutual inductance [Fig. 1(b)]. Using Eq. (3), from the measured  $\alpha(\varphi_{dc})$  dependence  $f'(\varphi(\varphi_{dc}))$  is obtained. The CPR is restored by integrating  $f'(\varphi(\varphi_{dc}))$  numerically, using the  $d\varphi(\varphi_{dc})/d\varphi_{dc}$  dependence obtained from differentiating Eq. (2) with respect to  $\varphi_{dc}$ .

The samples investigated consisted of three bicrystalline  $\text{YBa}_2\text{Cu}_3\text{O}_{7-x}$  films with a  $T_c$  ( $R = 0$ ) of 88 K. The films, with thickness  $t = 100$  nm, were deposited by standard pulsed laser deposition on (001)-oriented  $\text{SrTiO}_3$  bicrystalline substrates [15] with symmetric [001]-tilt misorientation angles of  $45^\circ \pm 2^\circ$  and were subsequently patterned by Ar ion-beam etching into  $8 \times 8$  mm<sup>2</sup> or  $5 \times 5$  mm<sup>2</sup> square washer single-junction interferometer structures. The widths of the junctions were  $b \approx 2-3$   $\mu\text{m}$ . The washer holes had a side length of 50  $\mu\text{m}$ , leading to  $L \approx 80$  pH.

To minimize the influence of external noise, the samples were measured in superconducting and double magnetic shielding at a temperature of 4.2 K. The condition  $\beta < 1$  for the investigated interferometers was confirmed experimentally from the character of its response versus  $\varphi_{dc}$  [12].

$\text{YBa}_2\text{Cu}_3\text{O}_{7-x}$  grain boundaries with a symmetric [001] tilt angle of  $45^\circ$  typically have a normal-state interface-resistivity  $\rho_n > 1 \times 10^{-8}$   $\Omega \text{ cm}^2$ , which we also measured for boundaries fabricated under identical conditions as the junctions used in the present experiments. In the configuration used, this  $\rho_n$  corresponds to normal-state resistances  $R_n > 1$   $\Omega$ . Accordingly, the relaxation time of the interferometer  $\tau = L/R$  is short ( $\tau \ll 1/\omega_0$ ), and hence the quasiparticle current is negligible [12].

For the measurements of  $\alpha(\varphi_{dc})$ , two tank circuits with quality factor  $Q = 120$  and inductance  $L_T = 0.4$   $\mu\text{H}$ ,  $\omega_0 = 30$  MHz, and  $L_T = 0.73$   $\mu\text{H}$ ,  $\omega_0 = 23$  MHz, respectively, were employed. The phase angle was recorded as a function of  $I_{dc}$  after amplification of the tank voltage by a high-impedance amplifier. The coupling coefficient  $k$  was determined from the period of the  $\alpha(I_{dc})$  dependence. Values of  $k = 0.072$  and  $k = 0.054$  for the respective tank circuits are obtained. To ensure the validity of the small-signal limit, the measurements were carried out with  $\varphi_{rf} < 0.15$ .

A typical  $\alpha(I_{dc})$  dependence is shown in Fig. 2. The corresponding CPR, depicted in Fig. 3, is clearly deviating from the standard sinusoidal behavior. Samples fabricated on different substrates and measured with both tank coils followed closely the same behavior. It is emphasized that the experimental setup employed and the procedure followed are identical to those used to measure the current-phase relations of step-edge junctions and thin-film bicrystals with a symmetric [001] tilt of  $24^\circ$ . For

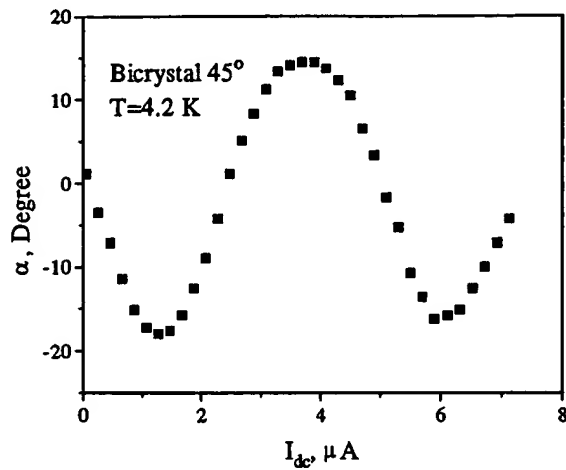


FIG. 2. Phase angle  $\alpha$  between the driving current and the output voltage measured at 4.2 K as a function of the dc current  $I_{dc}$ , for an  $\text{YBa}_2\text{Cu}_3\text{O}_{7-x}$  single junction interferometer circuit containing a symmetric  $45^\circ$  [001]-tilt grain boundary.

all of those samples nominally sinusoidal current-phase relations were observed, and all deviations of the apparent CPR from a sinusoidal one can be attributed to thermal noise [12,13].

The measured deviations from a sinusoidal dependence for the current-phase relations of these  $45^\circ$  bicrystals are startling. It is important to note that the effective Josephson penetration depth  $\Lambda_J = [\Phi_0/(4\pi\mu_0\langle j_c \rangle \lambda)]^{1/2} \approx 5 \mu\text{m}$  is larger than the width of the junction  $b$  (narrow-junction limit). Here  $\lambda$  is the London penetration depth. Although several mechanisms are known to cause nonsinusoidal current-phase relations for narrow junctions fabricated from conventional superconductors, all of these mechanisms fail to account for the anomalous dependencies presented.

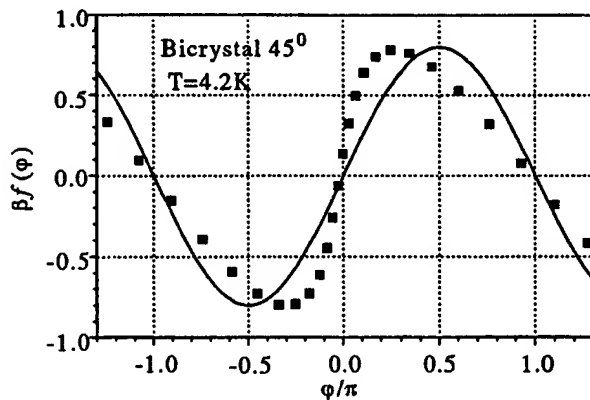


FIG. 3. The normalized current through the junction  $\beta f(\varphi)$  as a function of the phase difference  $\varphi$  restored from the measured  $\alpha(I_{dc})$  as shown in Fig. 2. For comparison, the function  $\beta \sin(\varphi)$  with  $\beta = 0.8$  is plotted as a solid line.

First, one potential source of such deviations is thermal noise. To evaluate its influence we consider a sinusoidal CPR and calculate with Eq. (3) the  $\alpha(\varphi_{dc})$  dependence, assuming a thermally induced Gaussian spread  $\rho(\varphi_n)$ . With this, the value of  $\tan \alpha(\varphi_{dc})$  is given by [12]

$$\tan \alpha(\varphi_{dc}) = k^2 Q \beta \times \int_{-\infty}^{\infty} \frac{\cos \varphi(\varphi_c, \varphi_n)}{1 + \beta \cos \varphi(\varphi_c, \varphi_n)} \rho(\varphi_n) d\varphi_n. \quad (4)$$

Using Eq. (4), minor deviations of the CPR from a standard sinusoidal behavior are well described quantitatively for  $24^\circ$  boundaries measured at 77 K [12]. However, no realistic set of  $\beta$  and  $\varphi_n$  exists to account for the large deviations of the CPR observed for the  $45^\circ$  boundaries.

Second, for weak links with a high current density, current-induced suppression of the order parameter in the electrodes close to the weak link can give rise to nonharmonic current-phase relations [16]. It is unrealistic that this effect is the cause for the deviations presented here, as the intragrain critical current density exceeds  $10^7 \text{ A/cm}^2$  at 4.2 K and is therefore much larger than the grain boundary  $\langle j_c \rangle < 4000 \text{ A/cm}^2$  at the same temperature.

Third, several additional mechanisms, described in [2], lead to deviations from a harmonic CPR. In all these cases, the slope of  $f(\varphi)$  at  $\varphi = 0$  is smaller than at  $\varphi = \pi$ , which is in contrast to our results. Therefore, these mechanisms cannot explain the current-phase relations observed either.

On the other hand, as will be pointed out in the following, the measured CPR can be accounted for by the unconventional order parameter symmetry of  $\text{YBa}_2\text{Cu}_3\text{O}_{7-x}$  and by the microstructural properties of the grain boundaries, in particular by their faceted nature [17,18]. Interestingly, due to the  $d_{x^2-y^2}$ -wave character of the order parameter, the faceting has a more significant influence on the electronic properties of boundaries with a misorientation close to  $45^\circ$  than on boundaries with considerably smaller misorientation angles [18]. This also concerns the CPR, as the  $45^\circ$  boundaries contain a higher density of facets that themselves show anomalous behavior. Two kinds of such anomalies, to be considered here, are described in the literature.

First, due to the sign difference of the adjacent lobes of the  $d_{x^2-y^2}$ -wave order parameter, many facets are biased with an additional  $\pi$  phase shift ( $\pi$  facets) [17–19]. These phase shifts give rise to unconventional junction properties, such as a spontaneous generation of magnetic flux in the grain boundary junction [19–21]. As described in Ref. [21], the local phase difference  $\varphi(x)$  along the grain boundary ( $0 < x < b$ ) can be written as

$$\varphi(x) = \xi(x) + \psi(x), \quad (5)$$

where  $\xi(x)$  is a rapidly alternating function accounting for the  $\pi$  phase shifts and for the spontaneously generated

magnetic flux in the junction, and  $\psi(x)$  is the remaining slowly varying phase difference reflecting the magnetic flux in the interferometer loop. For a narrow junction ( $b < \Lambda_J$ ),  $\psi$  is independent of  $x$ . With Eq. (5), the time-independent sine-Gordon equation, describing the spatial dependence of the local phase difference over the junction, becomes

$$\Lambda_J^2 \frac{\partial^2 \xi(x)}{\partial x^2} = \frac{j_c(x)}{\langle j_c \rangle} \sin[\psi + \xi(x)]. \quad (6)$$

The solution  $\xi(x)$  of this equation, and thus the pattern of self-generated flux, depends on  $\psi$ . The redistribution of this flux by a change of  $\psi$  is expected to lead to remarkable deviations from a harmonic dependence for the CPR measured for the entire junction, also if the local CPR is nominally sinusoidal.

Second, it has been proposed [7,8] that the CPR of facets formed by the (110) and by the (100) planes of the adjacent grains is periodic with  $\pi$  and thus has a double periodicity as compared to the standard case. Transmission electron microscopy has revealed that  $45^\circ$  [001] tilt grain boundaries in  $\text{YBa}_2\text{Cu}_3\text{O}_{7-x}$  tend to be composed for a considerable part of such facets [22]. For the whole junction, this leads to an anomalous CPR:

$$I = I_{c1} \sin \psi + I_{c2} \sin 2\psi, \quad (7)$$

by which the observed CPR can be described.

In summary, the current-phase relations of grain boundary junctions with a misorientation of  $45^\circ$  were measured with a modified Rifkin-Deaver method. The CPRs were deduced from measurements of the phase angle between the rf drive current and the rf tank voltage. The current-phase relations of the Josephson junctions showed pronounced deviations from a harmonic behavior, which cannot be accounted for by thermal noise or by other standard mechanisms, but are attributed to the  $d_{x^2-y^2}$ -wave symmetry of the order parameter and the faceting of the grain boundaries.

We are grateful to A. Golubov and M. Kupriyanov for fruitful discussions. Part of this work has been performed at the IBM Zürich Research Laboratory. Financial support by the DFG (Ho 461/1-1) and the BMBF (13N6519 and 13N6918/1) is gratefully acknowledged. One of us

(H. H.) thanks the Royal Dutch Academy of Sciences and the University of Twente for their support.

- [1] B.D. Josephson, Phys. Lett. **1**, 251 (1962); Rev. Mod. Phys. **36**, 216 (1964).
- [2] K.K. Likharev, Rev. Mod. Phys. **51**, 101 (1979).
- [3] C.C. Tsuei, J.R. Kirtley, C.C. Chi, Lock See Yu-Jahnes, A. Gupta, T. Shaw, J.Z. Sun, and M.B. Ketchen, Phys. Rev. Lett. **73**, 593 (1994).
- [4] D.J. Van Harlingen, Rev. Mod. Phys. **67**, 515 (1995).
- [5] D.J. Scalapino, Phys. Rep. **250**, 329 (1995).
- [6] Yu.S. Barash, A.V. Galaktionov, and A.D. Zaikin, Phys. Rev. B **52**, 665 (1995).
- [7] W. Zhang, Phys. Rev. B **52**, 3772 (1995).
- [8] Y. Tanaka and S. Kashiwaya, Phys. Rev. B **53**, R11957 (1996).
- [9] H. Burkhardt (to be published).
- [10] S.S. Tinchev, Physica (Amsterdam) **222C**, 173 (1994).
- [11] V. Polushkin, S. Uchaikin, S. Knappe, H. Koch, B. David, and D. Grundler, IEEE Trans. Appl. Supercond. **5**, 2790 (1995).
- [12] V. Zakosarenko, E.V. Il'ichev, R.P.J. IJsselsteijn, and V. Schultze, IEEE Trans. Appl. Supercond. **7**, 1057 (1997).
- [13] E.V. Il'ichev, V. Zakosarenko, V. Schultze, H.-G. Meyer, H.E. Hoenig, V.N. Glyantsev, and A. Golubov, Appl. Phys. Lett. **72**, 731 (1998).
- [14] R. Rifkin and B.S. Deaver, Phys. Rev. B **13**, 3894 (1976).
- [15] D. Dimos, P. Chaudhari, J. Mannhart, and F.K. LeGoues, Phys. Rev. Lett. **61**, 219 (1988).
- [16] M. Yu. Kupriyanov, Pis'ma Zh. Eksp. Teor. Fiz. **56**, 414 (1992) [JETP Lett. **56**, 399 (1992)].
- [17] C.A. Copetti, F. Rüders, B. Oelze, Ch. Buchal, B. Kabius, and J.W. Seo, Physica (Amsterdam) **253C**, 63 (1995).
- [18] H. Hilgenkamp, J. Mannhart, and B. Mayer, Phys. Rev. B **53**, 14586 (1996).
- [19] J. Mannhart, H. Hilgenkamp, B. Mayer, Ch. Gerber, J.R. Kirtley, K.A. Moler, and M. Sigrist, Phys. Rev. Lett. **77**, 2782 (1996).
- [20] R.G. Mints and V.G. Kogan, Phys. Rev. B **55**, R8681 (1997).
- [21] R.G. Mints (to be published).
- [22] J.A. Alarco, E. Olsson, Z.G. Ivanov, P.A. Nilsson, D. Winkler, E.A. Stepantsov, and A.Ya. Tzalenchuk, Ultramicroscopy **51**, 239 (1993).

# Dynamical Effects of an Unconventional Current-Phase Relation in YBCO dc SQUIDS

T. Lindström,<sup>1,\*</sup> S. A. Charlebois,<sup>1</sup> A. Ya. Tzalenchuk,<sup>2</sup> Z. Ivanov,<sup>1</sup> M. H. S. Amin,<sup>3</sup> and A. M. Zagorskin<sup>3,4</sup>

<sup>1</sup>*Department of Microelectronics and Nanoscience, Chalmers University of Technology and Göteborg University, SE-412 96 Göteborg, Sweden*

<sup>2</sup>*National Physical Laboratory, Teddington, Middlesex TW11 0LW, United Kingdom*

<sup>3</sup>*D-Wave Systems Inc., 320-1985 Broadway, Vancouver, British Columbia, Canada V6J 4Y3*

<sup>4</sup>*Physics and Astronomy Department, The University of British Columbia, 6224 Agricultural Road, Vancouver, Canada V6T 1Z1*  
(Received 20 December 2002; published 17 March 2003)

The predominant *d*-wave pairing symmetry in high-temperature superconductors allows for a variety of current-phase relations in Josephson junctions, which is to a certain degree fabrication controlled. In this Letter, we report on direct experimental observations of the effects of a non-sinusoidal current-phase dependence in YBCO dc SQUIDS, which agree with the theoretical description of the system.

DOI: 10.1103/PhysRevLett.90.117002

PACS numbers: 74.50.+r, 85.25.Dq

It is well established [1] that the wave function of a Cooper pair in most cuprate high-temperature superconductors (HTS) has a *d*-wave symmetry. Its qualitative distinction from, e.g., the anisotropic *s*-wave case is that the order parameter changes sign in certain directions, which can be interpreted as an *intrinsic* difference in the superconducting phase between the lobes equal to  $\pi$ .

The latter leads to a plethora of effects, such as formation of Andreev bound states at surfaces and interfaces in certain crystallographic orientations [2–4]. The current-phase dependence  $I_S(\phi)$  in Josephson junctions formed by *dd* junctions, as well as by *sd* junctions comprised of a cuprate and a conventional superconductor, depends both on the spatial orientation of the *d*-wave order parameter with respect to the interface, and on the quality of the latter [5–9]. Time-reversal symmetry can also be spontaneously violated and thus spontaneous currents generated [10–12]. Another effect can be doubling of the Josephson frequency [6,13,14].

In this Letter, we report on experimental observations of strong effects of an unconventional current-phase relation on the dynamics of two *dd* junctions integrated into a superconducting interference device (SQUID) configuration.

Since  $I_S(\phi)$  must be a  $2\pi$ -periodic odd function, it can be expanded in a Fourier series. In most cases, only the first two harmonics give a significant contribution to the current:

$$I_S(\phi) = I_c^I \sin \phi - I_c^{II} \sin 2\phi. \quad (1)$$

In Josephson systems of conventional superconductors, the second harmonic will usually be negligible [15] but in *dd* junctions the second harmonic may dominate. If  $I_c^{II} > I_c^I/2$ , the equilibrium state is no longer  $\phi = 0$  but becomes double degenerate at  $\phi = \pm \arccos(I_c^I/2I_c^{II}) \rightarrow \pm \pi/2$ . The system can then spontaneously break time-reversal symmetry by choosing either state. Spontaneous currents as well as fluxes can be generated in this state. The potential will have the shape of a double

well, and there are reasons to believe that it will be possible to observe quantum coherence in this system. The presence of a second harmonic in the current-phase relation (CPR) of a *dd* junction was confirmed by Il'ichev *et al.* [8].

A nonsinusoidal CPR of the junctions will change the dynamics of a dc SQUID [16]. Regarding the junctions as magnetically small, the supercurrent through the SQUID in the presence of an external flux  $\Phi_x \equiv \Phi_0 \cdot (\phi_x/2\pi)$  can be written as

$$I_s(\phi, \phi_x) = I_{c1}^I \sin \phi - I_{c1}^{II} \sin(2\phi) + I_{c2}^I \sin(\phi + \phi_x) - I_{c2}^{II} \sin 2(\phi + \phi_x). \quad (2)$$

The critical current through the SQUID is given by the usual expression  $I_c(\phi_x) = \max_{\phi} I_s(\phi, \phi_x)$ . The time-averaged voltage over the SQUID in the resistive regime is readily obtained in the resistively shunted junction approximation. By introducing  $\delta[\phi, \phi_x] = \phi_2 - \phi_1$  and applying the same method as in [17] with the necessary generalizations, we obtain the following for the average voltage over the SQUID:

$$\bar{V}^{-1} = \frac{G_1 + G_2}{2\pi} \int_{-\pi}^{\pi} d\phi \left[ I - (G_1 - G_2) \frac{\hbar}{2e} \frac{d\delta}{dt} - I_1 \left( \phi + \frac{\delta}{2} \right) - I_2 \left( \phi - \frac{\delta}{2} \right) \right]^{-1}. \quad (3)$$

Here  $G_{1,2}$  are the normal conductances of the junctions, and

$$\delta + \phi_x + \frac{\pi L}{\Phi_0} [I_2(\phi - \delta/2) - I_1(\phi + \delta/2)] = 0 \quad (4)$$

gives the difference,  $\delta$ , in phase drops across each junction. In deriving (3) and (4), we have assumed that the inductance  $L$  is equally divided between the SQUID arms. We have also neglected the spontaneous magnetic fluxes in the *dd* junctions, due to their small amplitude [11,18]. Though (4) is only explicitly solvable in the limit



$L \rightarrow 0$ , it always yields  $\delta[-\phi, -\phi_x] = -\delta[\phi, \phi_x]$ . This means that the usual inversion symmetry is retained.

The results of numerical calculations based on (2) and (3) are shown in Fig. 1. The cusps in the critical current correspond to the points at which the global maximum in (1) switches from one local maximum to another [16]. Note the quasi- $\Phi_0/2$  periodicity of the current isolines in the  $\bar{V} - \phi_x$  picture, reflecting the current-phase dependence (1), and their shift along the  $\Phi_x$  axis, which depends on the sign of the bias current (as it must to maintain the central symmetry with respect to the origin). The shift does not depend on the magnitude of the current since we neglect the self-inductance. For large biases, the  $\Phi_0$  periodicity is restored. Indeed, as the bias grows, one set of minima of the washboard potential,  $U = (h/2e)[-I^I \cos \phi + (I^{II}/2) \cos 2\phi - I\phi]$ , disappears first unless the first harmonic  $I^I$  is *exactly* zero.

We have fabricated and studied a large number of dc SQUIDs. The samples were fabricated from 250 nm thick YBCO films deposited on SrTiO<sub>3</sub> bicrystals. The grain-boundary junctions (GBJs) are of the asymmetric [001]-tilt type with the misorientation angle of 45° (0°–45° GBJ). For more information on GBJs see, for example, Ref. [19].

The pattern was defined using E-beam lithography and then transferred to a carbon mask employing a multistep process. Finally, the YBCO is etched through the mask using ion milling. This scheme allows us to fabricate

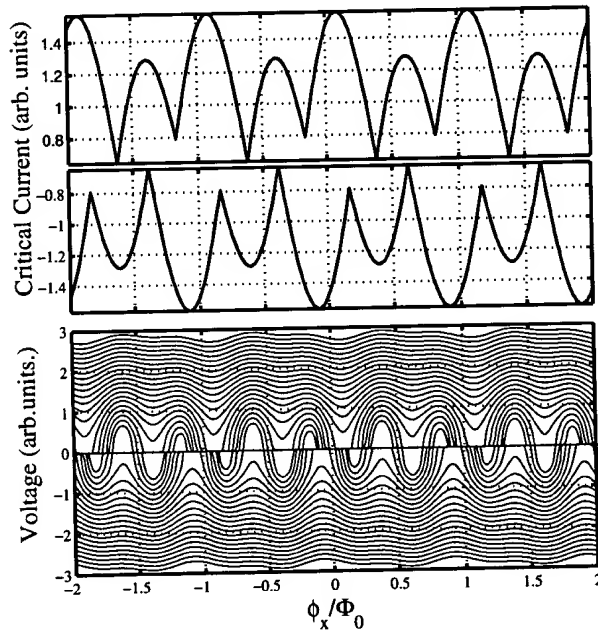


FIG. 1. The results of simulations of the  $I_c - \phi_x$  and  $\bar{V} - \phi_x$  dependence for a dc SQUID with  $I_{c1}^I = 1$ ,  $I_{c2}^I = 0.1$ ,  $I_{c1}^{II} = 0.2$  and  $I_{c2}^{II} = 0.4$  (arbitrary units). The different curves correspond to bias currents in the range  $I = I_{c1}^I$  to  $I = 5I_{c1}^I$ . We assume  $L = 0$  and  $G_1 = G_2$ .

high-quality bicrystal junctions as narrow as 0.2  $\mu\text{m}$ , as has been reported elsewhere [20]. In the SQUIDs under investigation, the junctions are nominally 2  $\mu\text{m}$  wide; hence, the fabrication-induced damage of the junctions is small.

The measurements were done in an EMC-protected environment using a magnetically shielded LHe cryostat. However, the magnetic shielding is imperfect, as is evident from the fact that the expected zero-field response of our SQUIDs is not exactly at zero. The measuring electronics is carefully filtered and battery powered whenever possible. In order to measure the dependence of the critical current on the applied field, we used a voltage discriminator combined with a sample-and-hold circuit. All measurements reported here were performed at 4.2 K.

The SQUID loops are  $(15 \times 15) \mu\text{m}^2$ . The numerically calculated inductance [21] is approximately 25 pH, yielding the factor  $\beta = 2\pi LI_c/\Phi_0$  between 0.5–2.

The SQUIDs were largely nonhysteretic with a resistance of about 2  $\Omega$ . The measured critical current varies from sample to sample but is in the range of tens of microamperes giving a current density of the order of  $J_c = 10^3 \text{ A/cm}^2$ . The estimated Josephson penetration length  $\lambda_J = \Phi_0/\sqrt{4\pi\mu_0 j_c \lambda_L}$  is approximately 2  $\mu\text{m}$  in all junctions, which means that the junctions are magnetically short. This is supported by the quasiperiod of the pattern in Fig. 2 being close to the expected value  $\phi_0/2\lambda_L w$  [17]. The differential conductance curves do not show any trace of a zero bias anomaly (ZBA), as is expected for 0°–45° GBJs. ZBAs have been observed by other groups in GBJs with other orientations [2].

The critical current is plotted as a function of applied magnetic field for two SQUIDs in Fig. 3. The result is in qualitative agreement with theory if we assume that the SQUID junctions have different ratios of the first and second harmonics of the critical current. This assumption

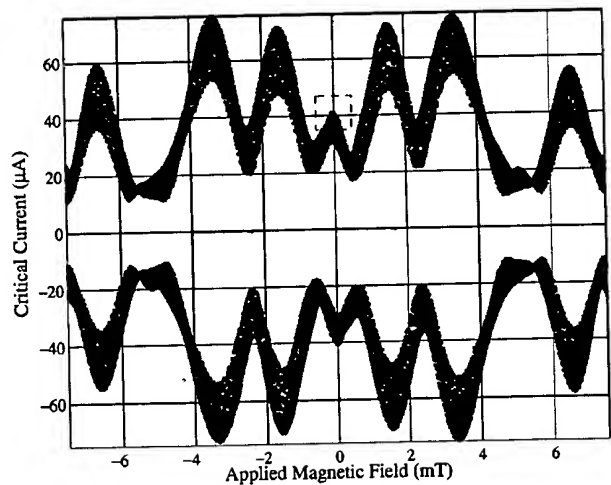


FIG. 2. Critical current as a function of magnetic field at 4.2 K. The dashed box indicates the area plotted in Fig. 3(a).

is supported by the fairly small modulation depth [it is easy to see from Eq. (2) that  $I_c$  would go exactly to zero in a SQUID with junctions of identical  $I_{c2}/I_{c1}$ ].

We can fit the data to Eq. (2), if we compensate for the residual background magnetic field and assume that we have a small excess current (of the order of a few  $\mu\text{A}$ ) in the junctions. The fitting parameters again confirm that there is a large asymmetry between the arms of the SQUIDs. Note that the model does not consider the flux penetration into the junctions,

The result for fields of the order of mT is presented in Fig. 2, which shows the  $I_c$  modulation of the SQUID enveloped by an anomalous Fraunhofer pattern quite similar to what has been reported by other groups [22,23] for  $0^\circ$ – $45^\circ$  GBJs. Note the inversion symmetry

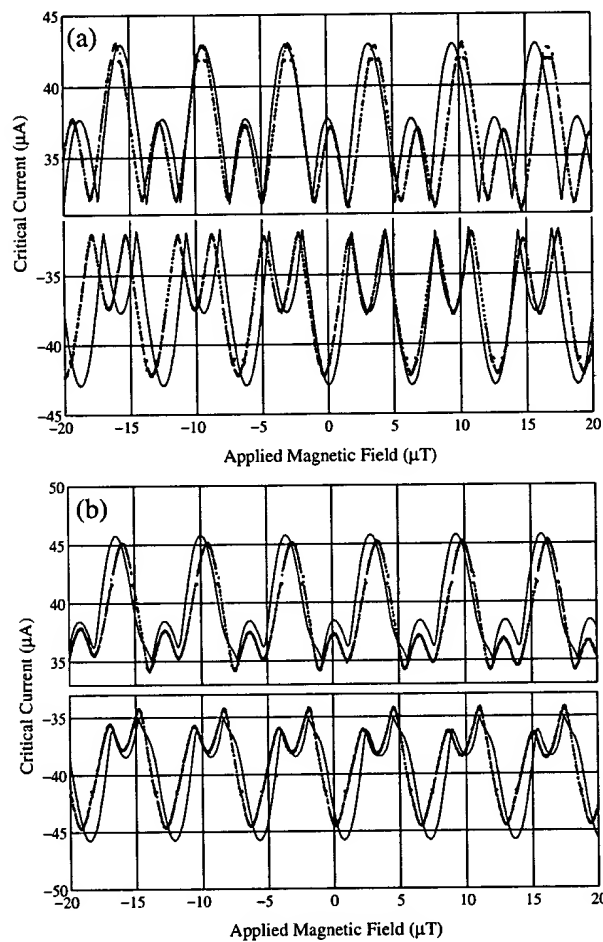


FIG. 3. Critical current as a function of applied magnetic field for two different SQUIDs that are nominally identical. The solid line represents the fitted expression. The fitting parameters are as follows: (a)  $I_{c1}^I = 9 \mu\text{A}$ ,  $I_{c2}^I = 0.3 \mu\text{A}$ ,  $I_{c1}^{II} = 3.7 \mu\text{A}$ , and  $I_{c2}^{II} = 22.7 \mu\text{A}$ ; (b)  $I_{c1}^I = 7.8 \mu\text{A}$ ,  $I_{c2}^I = 3.0 \mu\text{A}$ ,  $I_{c1}^{II} = 5.3 \mu\text{A}$ , and  $I_{c2}^{II} = 4.3 \mu\text{A}$ . In both cases, the fit has been adjusted with respect to the residual background field and the excess current of the junctions.

of the pattern with respect to the origin. That the global maximum is not in the center can be explained in several ways; it has been shown, for example, that this could be due to the presence of so-called  $\pi$  loops in the junction interface [24].

Figure 4 shows the  $V$ - $B$  dependence of one of the SQUIDs. The pattern is again field inversion symmetric. The overall structure is the same as in the model dependence of Fig. 1, but there is also an additional shift due to self-field effects, which depends on the magnitude of the bias current and corresponds (at maximum) to a flux  $\sim 0.1\Phi_0$ . In a beautiful experiment, a similar dependence was recently observed by Baselmans *et al.* in a Nb-Ag-Nb SNS junction where current injectors were used to change the occupation of current-carrying states in the normal region [25]. A deviation from the model occurs at  $\bar{V} = 100 \mu\text{V}$  where the minima and maxima switch. This is probably due to an LC resonance in the SQUID. Taking  $L = 25 \text{ pH}$ , this would require  $C = 0.8 \text{ pF}$ , which agrees with our measurements on single junctions

Remarkably, the observed offset of the  $V$ - $B$  characteristics with respect to the *direction* of the bias current appears to be a much more robust manifestation of the presence of a second harmonic of the Josephson current than the shape of the  $I_c - B$  curves itself. We observed the shift even in SQUIDs with the smallest junctions down to  $0.5 \mu\text{m}$  wide, where the deviations from the usual sinusoidal CPR were not obvious from the  $I_c - B$  dependence.

Generally, the nature of the transport through a GBJ will depend on its transmissivity  $D$ . Il'ichev *et al.* [8] have reported values of  $D$  as high as 0.3 in symmetric ( $22.5^\circ$ – $22.5^\circ$ )  $dd$  junctions as opposed to the usual estimate for a GBJ,  $D \sim 10^{-5}$ – $10^{-2}$ . Since usually  $I_c^{II}/I_c^I \propto D$ , a high-transmissivity GBJ is required in order

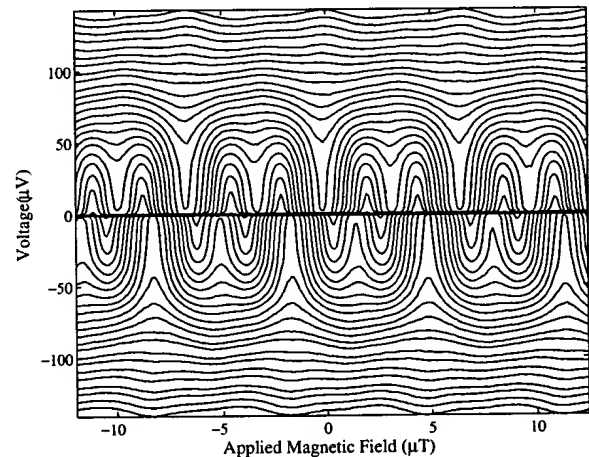


FIG. 4. Voltage modulation as a function of applied magnetic field for the SQUID whose  $I_c - B$  is shown in Fig. 3(a). The pattern is again inversion symmetric. Note the sign change at  $100 \mu\text{V}$ , which we believe is due to a LC resonance in the SQUID loop.

to observe effects of the second harmonic. An estimate of the *average* transmissivity of our junctions would be  $\rho_{ab}l/R_NA \sim 10^{-2}$  [26] assuming  $l$ , the mean-free path, to be equal to 10 nm and a resistivity in the  $a$ - $b$  plane  $\rho_{ab}$  equal to  $10^{-4} \Omega \text{ cm}$ . This is still too low to explain the strong second harmonic we observe. However, it is known from, e.g., TEM studies [19], that the grain-boundary is far from uniform; the properties can significantly vary depending on the local properties of the interface, effects such as oxygen diffusion out of the GB, etc., which are difficult to control. It is therefore reasonable to assume that there are many parallel transport channels through the GB [27,28]. Channels with high-transmissivity dominate the transport and might have  $D \sim 0.1$  even though the *average* transmissivity is much lower. This is also consistent with the fact that most of our SQUIDs seem to be highly asymmetrical which is to be expected if the distribution of channels is random. The ratios of  $I_c^I$  and  $I_c^{II}$  can vary as much as 10 times between two junctions in the same SQUID, even though the fluctuations of the *total*  $I_c$  from sample to sample are much smaller. It is also clear from general considerations that a high value of  $I_c^{II}$  *excludes* a high value of  $I_c^I$ , since the second harmonic usually dominates if the odd harmonics of the supercurrent are canceled by symmetry [29].

Recent studies of  $0^\circ$ – $45^\circ$  GBJs have demonstrated that the SQUID dynamics can be altered by the  $d$ -wave order parameter in YBCO [30]. It is, however, important to point out that our results *do not* directly relate to, e.g., tetracystal  $\pi$ -SQUID experiments; the latter crucially depend on having one  $\pi$  junction with negative critical current, but still only the first harmonic present in  $I_c(\phi)$ . Our SQUIDs have a conventional geometry, but unconventional current-phase relations.

One explanation for the pronounced effects of the second harmonic could be that relatively large sections of the interface are highly transparent and have a low degree of disorder. This in turn could be related to our fabrication scheme which seems to preserve the integrity of the barrier. This makes feasible their applicability in the quantum regime and supports our expectations that quantum coherence can be observed in this kind of structures.

In summary, we have observed a very pronounced second harmonic in the current-phase relation of a “conventional” YBCO dc SQUID with  $0^\circ$ – $45^\circ$  grain-boundary junctions. It has strongly influenced the SQUID dynamics. All details of the SQUID behavior were explained within a simple model of a  $dd$  junction with relatively high transparency. We believe that these effects are important for better understanding of HTS Josephson junction and SQUIDs.

Discussions with Evgeni Il'ichev, Alexander Golubov, Tord Claeson, and John Gallop are gratefully acknowledged. The work is in part supported by The Board for Strategic Research (SSF) via the “OXIDE” program, the Science Research Council, and the “Fonds québécois de la

recherche sur la nature et les technologies.” The processing work is done at the MC2 process laboratory at Chalmers University of Technology.

\*Electronic address: tobiasl@fy.chalmers.se

- [1] C. Tsuei and J. Kirtley, *Rev. Mod. Phys.* **72**, 969 (2000).
- [2] L. Alff *et al.*, *Phys. Rev. B* **58**, 11 197 (1998).
- [3] T. Löfwander, V. Shumeiko, and G. Wendin, *Supercond. Sci. Technol.* **14**, R53 (2001).
- [4] C.-R. Hu, *Phys. Rev. Lett.* **72**, 1526 (1994).
- [5] S. Yip, *Phys. Rev. B* **52**, 3087 (1994).
- [6] A. Zagorskin, *J. Phys. Condens. Matter* **9**, L419 (1997).
- [7] E. Il'ichev *et al.*, *Phys. Rev. B* **60**, 3096 (1999).
- [8] E. Il'ichev *et al.*, *Phys. Rev. Lett.* **86**, 5369 (2001).
- [9] P. Komissinski *et al.*, *Europhys. Lett.* **57**, 585 (2002).
- [10] A. Huck, A. van Otterlo, and M. Sigrist, *Phys. Rev. B* **56**, 14163 (1997).
- [11] M. H. S. Amin, A. N. Omelyanchouk, and A. M. Zagorskin, *Phys. Rev. B* **63**, 212502 (2001).
- [12] S. Östlund, *Phys. Rev. B* **58**, R14 757 (1998).
- [13] T. Löfwander, G. Johansson, M. Hurd, and G. Wendin, *Phys. Rev. B* **57**, R3225 (1998).
- [14] H. Arie *et al.*, *Phys. Rev. B* **62**, 11 864 (2000).
- [15] M. Keene, C. Gough, and A. Rae, *J. Phys. Condens. Matter* **3**, 6079 (1991).
- [16] M. H. S. Amin, M. Courty, and R. Rose, *IEEE Trans. Appl. Supercond.* **12**, 1877 (2002).
- [17] A. Barone and G. Paterno, *Physics and Applications of the Josephson Effect* (Wiley, New York, 1982).
- [18] M. H. S. Amin, S. N. Rashkeev, M. Courty, A. N. Omelyanchouk, and A. M. Zagorskin, *Phys. Rev. B* **66**, 174515 (2002).
- [19] H. Hilgenkamp and J. Mannhart, *Rev. Mod. Phys.* **74**, 297 (2002).
- [20] A. Tzalenchuk *et al.*, *Appl. Phys. Lett.* (to be published).
- [21] M. Khapaev, A. Kidiyarova-Shevchenko, P. Magnelind, and M. Kupriyanov, *IEEE Trans. Appl. Supercond.* **11**, 1090 (2001).
- [22] J. Mannhart, B. Mayer, and H. Hilgenkamp, *Z. Phys. B* **101**, 175 (1996).
- [23] W. Neils and D. van Harlingen, *Physica (Amsterdam)* **284B–288B**, 587 (2000).
- [24] H. Smilde *et al.*, *Phys. Rev. Lett.* **88**, 057004 (2002).
- [25] J. Baselmans, T. Heikkilä, B. van Wees, and T. Klapwijk, *Phys. Rev. Lett.* **89**, 207002 (2002); the pronounced second harmonic in this experiment appears due to nonequilibrium effects, see, e.g., J. C. Clarke, in *Nonequilibrium Superconductivity, Phonons and Kapitza Boundaries*, edited by K. E. Gray, NATO ASI Series (Plenum, New York, 1981), p. 353.
- [26] G. Blonder, M. Tinkham, and T. Klapwijk, *Phys. Rev. B* **25**, 4515 (1982).
- [27] Y. Naveh, D. Averin, and K. Likharev, *Phys. Rev. Lett.* **79**, 3482 (1997).
- [28] E. Sarnelli, G. Testa, and E. Esposito, *J. Supercond.* **7**, 387 (1994).
- [29] Y. Barash, *Phys. Rev. B* **61**, 678 (2000).
- [30] B. Chesca *et al.*, *Phys. Rev. Lett.* **88**, 177003 (2002).

# Feasibility of biepitaxial $\text{YBa}_2\text{Cu}_3\text{O}_{7-x}$ Josephson junctions for fundamental studies and potential circuit implementation

F. Tafuri

*Dipartimento di Ingegneria dell'Informazione, Seconda Università di Napoli, 81031 Aversa (CE) and  
INFN-Dipartimento Scienze Fisiche dell'Università di Napoli "Federico II", 80125 Napoli (ITALY)*

F. Carillo, F. Lombardi, F. Miletto Granozio, F. Ricci, U. Scotti di Uccio and A. Barone  
*INFN-Dipartimento Scienze Fisiche dell'Università di Napoli "Federico II", 80125 Napoli (ITALY)*

G. Testa and E. Sarnelli

*Istituto di Cibernetica del CNR, Via Toiano 6, Arco Felice (NA) (ITALY) also  
INFN*

J.R. Kirtley

*IBM T.J. Watson Research Center, P.O. Box 218, Yorktown Heights, NY 10598,  
USA  
(July 4, 2003)*

We present various concepts and experimental procedures to produce biepitaxial  $\text{YBa}_2\text{Cu}_3\text{O}_{7-x}$  grain boundary Josephson junctions. The device properties have an interesting phenomenology, related in part to the possible influence of " $\pi$ -loops". The performance of our junctions and Superconducting Quantum Interference Devices indicates significant improvement in the biepitaxial technique. Further, we propose methods for fabricating circuits in which "0-" and " $\pi$ -loops" are controllably located on the same chip.

## I. INTRODUCTION

The possibility of realizing electronic circuits in which the phase differences of selected Josephson junctions are biased by  $\pi$  in equilibrium is quite stimulating.<sup>1</sup> The concept of such  $\pi$ -phase shifts was originally developed in the "extrinsic" case for junctions with ferromagnetic barriers<sup>2</sup> and in the "intrinsic" case for junctions exploiting superconductors with unconventional order parameter symmetries.<sup>3</sup> As a result of the possible  $d_{x^2-y^2}$  order parameter symmetry of high critical temperature superconductors (HTS),<sup>4</sup> the presence of intrinsic  $\pi$  loops has also been considered for HTS systems.<sup>5</sup> This has been discussed recently in view of novel device concepts, and in particular for the implementation of a solid state qubit<sup>1,6-8</sup> and for Complementary Josephson junction electronics.<sup>9</sup> In this paper we discuss how  $\text{YBa}_2\text{Cu}_3\text{O}_{7-x}$  (YBCO) structures made by the biepitaxial technique<sup>10,11</sup> can be successfully employed to produce arbitrary circuit geometries in which both "0" and  $\pi$ -loops are present, and possibly to obtain a doubly degenerate state.<sup>1,6</sup> Of course, great caution should be used because of stringent requirements on junctions parameters for practical applications of such devices.

Josephson junctions based on artificially controlled grain boundaries have been widely employed for fundamental studies on the nature of HTS.<sup>4,7,8</sup> The lack of a

reliable technology based on the traditional trilayer configuration (i.e. a sandwich type junction with an insulator between the two superconducting electrodes) also enhanced interest in GB Josephson junctions for applications. Although the mechanism of high- $T_C$  superconductivity and the influence of grain boundaries on the transport properties are not completely determined, reproducible and good quality devices are routinely fabricated. YBCO GB junctions are usually classified as bicrystals,<sup>12</sup> biepitaxials,<sup>11</sup> and step-edges,<sup>13</sup> depending on the fabrication procedure. The bicrystal technique typically offers junctions with better performances and allows in principle the realization of all different types of GBs ranging from [001] and [100] tilt to [100] twist boundaries. GB junctions based on the step-edge and biepitaxial techniques offer the advantage, with respect to the bicrystal technology, of placing the junctions on the substrate without imposing any restrictions on the geometry. A comparison between the different GB techniques is far beyond the aim of this paper. Nevertheless we intend to show that significant improvements with respect to the original technique developed by Char et al.<sup>11</sup> are possible for biepitaxial junctions, and that the resulting devices have potential for applications. As a matter of fact, in traditional biepitaxial junctions, the seed layer used to modify the YBCO crystal orientation on part of the substrate produces an artificial  $45^\circ$  [001] tilt (c-axis

tilt) GB. The nature of such a GB seems to be an intrinsic limit for some real applications. A convincing explanation has been given in terms of the d-wave nature of the order parameter and more specifically by the presence of  $\pi$ -loops.<sup>14</sup> As demonstrated by studies on bicrystals, based on the same type of  $45^\circ$  [001] tilt GB, the presence of  $\pi$ -loops reduces the  $I_C R_N$  values (where  $I_C$  and  $R_N$  are the critical current and the high normal state resistance respectively), produces a dependence of the critical current  $I_C$  on the magnetic field  $H$  quite different from the Fraunhofer-like pattern, and generates unquantized flux noise at the grain boundary.<sup>14</sup>

We will show that the implementation of the biepitaxial technique<sup>10</sup> we developed to obtain  $45^\circ$  [100] tilt and twist (a-axis tilt and twist) GBs junctions makes such a technique interesting for both applications and fundamental studies. The phenomenology observed for the junctions based on these GBs and Scanning SQUID Microscopy investigations demonstrate the absence of  $\pi$ -loops, as we expect from their microstructure. As a consequence higher values of the  $I_C R_N$  values, a Fraunhofer like dependence of  $I_C$  on the magnetic field and lower values of the low frequency flux noise, when compared with  $45^\circ$  c-axis tilt GBs, have been measured. These features are important tests to employ junctions for applications. Scanning SQUID Microscopy investigations also gave evidence of “fractional” vortices in the presence of impurities. Finally, we extended the biepitaxial process to other types of GB by using different seed layers to obtain junction configurations where  $\pi$  loops can be controllably produced. We shall not dwell on conceptual principles and actual feasibility of qubit devices. Instead we discuss the importance of the biepitaxial technique in having “0” and “ $\pi$ ” loops on the same chip. This makes the biepitaxial technique more versatile and promising for circuit design.

## II. DEVICES: CONCEPTS AND FABRICATION PROCEDURE

As mentioned above, the biepitaxial technique allows the fabrication of various GBs by growing different seed layers and using substrates with different orientations. We have used MgO, CeO<sub>2</sub> and SrTiO<sub>3</sub> as seed layers. The MgO and CeO<sub>2</sub> layers are deposited on (110) SrTiO<sub>3</sub> substrates, while SrTiO<sub>3</sub> layers are deposited on (110) MgO substrates; in all these cases the seed layers grow along the [110] direction. Ion milling is used to define the required geometry of the seed layer and of the YBCO thin film respectively, by means of photoresist masks. YBCO films, typically 120nm in thickness, are deposited by inverted cylindrical magnetron sputtering at a temperature of 780° C. YBCO grows along the [001] direction on MgO (substrates or seed layers) and on the CeO<sub>2</sub> (seed layers), while it grows along the [103]/[013] direction on SrTiO<sub>3</sub> (substrates or seed layers). In order to select the [103] or [013] growth and to ensure a better structural uniformity

of the GB interface, we have also successfully employed vicinal substrates. However, most of the transport properties presented in this paper refer to samples not using vicinal substrates. Detailed structural investigations on these GBs, including Transmission Electron Microscopy (TEM) analyses, have been performed and the results have been presented elsewhere.<sup>10,16</sup>

Depending on the patterning of the seed layer and the YBCO thin film, different types of GBs ranging from the two ideal limiting cases of  $45^\circ$  a-axis tilt and  $45^\circ$  a-axis twist have been obtained (see Fig.1). The intermediate situation occurs when the junction interface is tilted at an angle  $\alpha$  different from 0 or  $\pi/2$  with respect to the a- or b-axis of the [001] YBCO thin film. In all cases, the order parameter orientations do not produce an additional  $\pi$  phase shift along our junction, in contrast with the  $45^\circ$  asymmetric [001] tilt junctions. As a consequence, no  $\pi$  loops should occur independently of the details of the interface orientation. In Fig. 1 we consider ideal interfaces and neglect meandering of the GBs or interface anomalies that will be considered below. The CeO<sub>2</sub> seed layer may produce a more complicated GB structure, in which a  $45^\circ$  c-axis tilt accompanies the  $45^\circ$  a-axis tilt or twist (see Fig.2a).<sup>15</sup> In this case, as shown in Fig.2b,  $\pi$  loops should occur in analogy with the traditional biepitaxial junctions based on  $45^\circ$  c-axis tilt GBs. In both Figs. 1 and 2 we display the possible  $d_{x^2-y^2}$ -wave order parameter symmetry in the junction configuration. Junctions were typically 4 microns wide. We also performed systematic measurements on SQUIDs based on the structure employing MgO as a seed layer and SrTiO<sub>3</sub> as a substrate. DC SQUIDs in different configurations and with loop inductance typically ranging from 10 to 100 pH have been investigated. The typical loop size leading to the 10(100) pH inductance is approximately  $10^2 \mu\text{m}^2$  ( $10^4 \mu\text{m}^2$ ).

## III. EXPERIMENTAL RESULTS

### A. Biepitaxial junctions employing MgO seed layers

In this section we attempt to cover most of the phenomenology of the transport properties of  $45^\circ$  a-axis tilt and twist biepitaxial junctions. In Fig. 3, current vs voltage (I-V) characteristics of a typical biepitaxial junction are given for various temperatures close to the critical temperature. In the inset the corresponding I-V characteristic at  $T = 4.2$  K is reported. They are closely described by the resistively-shunted-junction (RSJ) model and no excess current is observed. Nominal critical current densities  $J_C$  of  $5 \times 10^2 \text{ A/cm}^2$  at  $T = 77$  K, and of  $9 \times 10^3 \text{ A/cm}^2$  at  $T = 4.2$  K have been measured respectively. The  $R_N$  value ( $3.2 \Omega$ ) is roughly independent of the temperature for  $T < T_C$ , providing a normal state specific conductance  $\sigma_N = 70 (\mu\Omega\text{cm}^2)^{-1}$ . The maximum working temperature  $T_C$  of this device was 82 K. In this case

$I_C R_N$  is 1.3 mV at  $T = 4.2$  K. These values typically ranged from 1 mV to 2 mV at  $T = 4.2$  K. They are larger for the corresponding  $J_C$  values than those provided by conventional biepitaxials, and are of the same order of magnitude as in GB bicrystal and step edge junctions.<sup>10</sup> While the values of critical current density and normal state specific conductance in the tilt case are quite different from the twist case, the  $I_C R_N$  values are approximately the same for both. Moreover  $I_C R_N$  does not scale with the critical current density.<sup>10</sup> In the tilt cases  $J_C \approx 0.5\text{--}10 \times 10^3$  A/cm<sup>2</sup> and  $\sigma_N \approx 1\text{--}10$  ( $\mu\Omega\text{cm}^2$ )<sup>-1</sup> are measured at  $T = 4.2$  K respectively. Twist GBs junctions are typically characterized by higher values of  $J_C$  in the range  $0.1\text{--}4.0 \times 10^5$  A/cm<sup>2</sup> and of  $\sigma_N$  in the range  $20\text{--}120$  ( $\mu\Omega\text{cm}^2$ )<sup>-1</sup> (at  $T = 4.2$  K). For the twist case deviations from the RSJ model are more marked as a result of higher critical current densities. For high values of  $J_C$  GB junctions do not present any clear modulation of the critical current as a function of the magnetic field.

A demonstration of the possibility of tailoring the critical current density and of the different transport regimes occurring in the tilt and twist cases has been given by measuring the properties of junctions with different orientations of the GB barrier on the same chip. By patterning the seed layer as shown in Fig. 4a, we could measure the properties of a tilt junction and of junctions whose interface is tilted in plane by an angle  $\alpha = 30^\circ$ ,  $45^\circ$  and  $60^\circ$  with respect to the *a*- or *b*-axis of the [001] YBCO thin film respectively. In all cases the order parameter orientations do not produce an additional  $\pi$  phase shift along our junction, in contrast with the  $45^\circ$  [001] tilt junctions, and no  $\pi$  loops should occur. We measured the expected increase of the critical current density with increasing angle, which corresponds on average to an increase of the twist current component. The values measured at  $T = 4.2$  K are reported in Fig. 4a and range from the minimum value  $J_C = 3 \times 10^2$  A/cm<sup>2</sup> in the tilt case to the maximum  $J_C = 10^4$  A/cm<sup>2</sup> corresponding to an angle of  $60^\circ$ , for which the twist component is higher. The consistency of this result has been confirmed by the values of normal state resistances, which are higher in the tilt case and decrease with increasing  $\alpha$ . The  $I_C R_N$  values are about the same for all the junctions independently of the angle  $\alpha$ . In Fig. 4b the I-V characteristics measured at  $T = 4.2$  K, corresponding to the junctions of Fig. 4a, are shown for approximately the same voltage range. Deviations from RSJ behavior appear for higher values of the critical current density ( $\alpha = 60^\circ$ ). These results demonstrate that the grain boundary acts as a tunable barrier. This possibility of modifying the GB macroscopic interface plane by controlling the orientation of the seed layer's edge is somehow equivalent to the degree of freedom offered by bicrystal technology to create symmetric or asymmetric GBs, with the advantage of placing all the junctions on the same substrate. The  $45^\circ$  *a*-axis tilt and twist GBs and the intermediate situations can represent ideal structures to investigate the junction physics in a wide range of configurations. The anisotropy of the (103)

films and the possibility to select the orientation of the junction interface by suitably patterning the seed layer, and eventually the use of other seed layers which produce different YBCO in plane orientations, allow the fabrication of different types of junctions and the investigation of different aspects of HTS junction phenomenology. In particular we refer to the possibility of changing the tunneling matrix elements (by selecting the angle  $\alpha$ ) and to use the anisotropy of the layered structure of YBCO properties and of the order parameter symmetry.

The study of the junction properties in the presence of an external magnetic field  $H$  is a fundamental tool for the investigation of the Josephson effect in the various junctions, as well as a test of junction quality.<sup>17</sup> We observe modulations of the critical current  $I_C$  following the usual Fraunhofer-like dependence. The  $I_C(H)$  patterns are mostly symmetric around zero magnetic field, and in all samples the absolute maximum of  $I_C$  occurs at  $H=0$ . The presence of the current maximum at zero magnetic field is consistent with the fact that in our junction configuration the order parameter orientations do not produce an additional  $\pi$  phase shift, in contrast with the  $45^\circ$  [001] tilt GB junctions.<sup>14,10</sup> Some examples are given in Fig. 5, where the magnetic pattern relative to a SQUID and a single junction at  $T = 4.2$  K are shown respectively. In the former case we can also distinguish a smaller field modulation (with a period of 8 mG) which corresponds to the SQUID modulation (inset a). In the latter case the I-V characteristics are reported for different magnetic fields (inset b). Despite the Fraunhofer-like dependence, some deviations are evident, in agreement with most of the data available in literature.

For sake of completeness we also acknowledge some work we carried out by investigating Fiske steps as a function of  $H$  in other junctions, giving some evidence of a dielectric-like behavior<sup>18</sup> of some of the layers at the junction interface. We already reported about this work elsewhere.<sup>19</sup> The Fiske steps do not depend on the use of a particular substrate, since they have been observed in junctions based both on SrTiO<sub>3</sub> and MgO substrates. Typical values of the ratio between the barrier thickness  $t$  and the relative dielectric constant  $\epsilon_r$  range from 0.2 nm to 0.7 nm. Considerations on the dependence of  $I_C$  on the temperature ( $T$ ) can be also found in Ref.<sup>19</sup>. In junctions characterized by lower critical current densities,  $I_C$  tends to saturate at low temperatures, in contrast to those characterized by higher critical currents, for which there is a linear increase.<sup>10,20</sup>

## B. Scanning SQUID microscopy on biepitaxial junctions with MgO seed layer

Figure 6 is a scanning SQUID microscope<sup>21</sup> image of a  $200 \times 200 \mu\text{m}^2$  area along a grain boundary separating a (100) region from a (103) region (as labelled in the figure) of a thin YBCO biepitaxial film grown as described



above. The position of the grain boundary is indicated by the dashed line. The image was taken at 4.2 K in liquid helium with an octagonal SQUID pickup loop 4 microns in diameter after cooling the sample in a few tenths of a  $\mu$ T externally applied magnetic field normal to the plane of the sample. The grey-scaling in the image corresponds to a total variation of  $0.13\Phi_0$  of flux through the SQUID pickup loop. Visible in this image are elongated interlayer Josephson vortices in the (103) area to the right, and “fractional” vortices in the (100) area to the left, of the grain boundary. Fits to the interlayer vortices give a value for the  $c$ -axis penetration depth of about  $4\mu\text{m}$ . The “fractional” vortices are spontaneously generated in the (100) film, regardless of the value of external field applied.<sup>22</sup> Temperature dependent scanning SQUID microscope imaging shows that this spontaneous magnetization, which appears to be associated with defects in the film, arises when the film becomes superconducting.<sup>4,23</sup> Although it is difficult to assign precise values of total flux to the “fractional” vortices, since they are not well separated from each other, fits imply that they have less than  $\Phi_0$  of total flux in them, an indication of broken time-reversal symmetry. Although there is apparently some flux generated in the grain boundary region, the fact that these SQUIDs have relatively low noise seems to indicate that this flux is well pinned at the temperatures at which the noise measurements were made. These results are consistent with the absence of  $\pi$  loops along the grain boundary.

### C. Biepitaxial junctions employing $\text{CeO}_2$ seed layers

The  $\text{CeO}_2$  seed layer, as anticipated in section II, may produce an artificial GB that can be seen as a result of two rotations: a  $45^\circ$  [100] tilt or twist followed by a  $45^\circ$  [001] tilt around the  $c$ -axis of the (001) film. For this junction configuration a  $d$ -wave order parameter symmetry would produce  $\pi$ -loops, as shown in Fig. 2. We notice that such  $\pi$ -loops are structurally different from those usually obtained by the  $45^\circ$  [001] tilt GB junctions based on the traditional biepitaxial and bicrystal techniques. Due to the microstructure we expect especially in the [100] tilt case low critical current densities and high normal state resistances. We found that the deposition conditions to select the uniform growth of YBCO  $45^\circ$  tilted around the  $c$ -axis of the (001) film are critical. Preliminary measurements realized on tilt-type junctions with a  $\text{CeO}_2$  seed layer gave evidence of Josephson coupling in these GBs. The measured  $I_C R_N$  values are from  $200\mu\text{V}$  to  $750\mu\text{V}$  and are in the typical range of the GBs Josephson junctions.

### D. Biepitaxial SQUIDs employing $\text{MgO}$ seed layers

In this section we report on the characterization of dc-SQUIDs which are to our knowledge the first employing the GBs discussed above.<sup>24</sup> These SQUIDs exhibit very good properties, and noise levels which are among the lowest ever reported for biepitaxial junctions.<sup>24</sup> Apart from implications for applications, these performances are important for the study of the transport properties of HTS Josephson junctions. In Fig. 7 we show the magnetic field dependence of the voltage at 77 K for different values of the bias current for a dc-SQUID with an inductance of 13 pH. At this temperature  $I_C R_N$  is about  $20\mu\text{V}$ . The corresponding value of the screening parameter  $\beta = 2LI_C/\Phi_0$  is 0.03. In general low  $\beta$  values are mandatory to avoid the influence of asymmetric inductances in SQUID properties, and this has been crucial for experiments designed to study the order parameter symmetry.<sup>7</sup> The presented curves are quite typical. These SQUIDs usually work in a wide temperature range from low temperatures (4.2 K) up to temperatures above 77 K. The maximum working temperature was in this case 82 K. The achieved magnetic flux-to-voltage transfer functions  $V_\Phi = \partial V/\partial \Phi$ , where  $V$  and  $\Phi$  are the voltage across the device and the applied magnetic flux in the SQUID loop respectively, are suitable for applications. For instance at  $T = 77\text{ K}$  an experimental value of the SQUID amplitude voltage modulation  $\Delta V$  of 10.4 mV was measured, corresponding to  $V_\Phi = 36.9\mu\text{V}/\Phi_0$ .<sup>24</sup> Steps of different nature have been recurrently observed in the  $I$ - $V$  characteristics in the washer and hole configurations and characterized also in terms of the magnetic field dependence of the voltage at different values of the bias current.

The noise spectral densities of the same dc-SQUID have been measured at  $T = 4.2\text{ K}$  and  $T = 77\text{ K}$  using standard flux-locked-loop modulated electronics. The energy resolution  $\epsilon = S_\Phi/2L$  (with  $S_\Phi$  being the magnetic-flux-noise spectral density) at  $T = 4.2\text{ K}$  and  $T = 77\text{ K}$  is reported in Fig. 8. At  $T = 4.2\text{ K}$  and 10 kHz, a value of  $S_\Phi = 3\mu\Phi_0/\sqrt{\text{Hz}}$  has been measured, corresponding to an energy resolution  $\epsilon = 1.6 \times 10^{-30}\text{ J/Hz}$ . This value is the lowest reported in the literature for YBCO biepitaxial SQUIDs. Moreover, the low frequency  $1/f$  flux noise spectral density at 1 Hz is more than one order of magnitude lower than the one reported for traditional biepitaxials, as is also evident from the comparison with data at  $T = 4.2\text{ K}$  of Ref.<sup>25</sup>. The lower values of low frequency noise are consistent with the absence of  $\pi$ -loops on the scale of the faceting for these types of GBs, as clearly shown by Scanning SQUID Microscopy results. The  $\pi$ -loops produce some types of spontaneous magnetic flux in the GB region, which among other effects tends to degrade the SQUID's noise levels.<sup>14</sup>

#### IV. BIEPITAXIAL JUNCTIONS FOR EXPERIMENTS ON THE SYMMETRY OF THE ORDER PARAMETER AND FOR A DEVELOPMENT OF CONCEPTS FOR QUBITS

The particular junction configurations investigated in this work allow some consideration of the possible impact of these types of junctions on the study of the Josephson effect and the order parameter symmetry in YBCO and on the development of concepts for devices.<sup>1,6,9,7</sup> We first recall that the biepitaxial technique can provide circuits composed completely of junctions without any  $\pi$ -loops (see Fig. 9a). By varying the interface orientation with respect to the [103] electrode orientation, the junction properties can be adjusted. On the other hand the traditional biepitaxial technique,<sup>11</sup> producing 45° [001] tilt GBs (see Fig. 9b) or the types of junctions described in the previous section by using CeO<sub>2</sub> (see Fig. 9c), can controllably generate  $\pi$ -loops on macroscopic scales. In these schemes we use a corner geometry with a 90° angle. This angle  $\alpha$  can be obviously tuned to enhance the effects related to the phase shift (see dashed line in Fig. 9b) and this change is particularly easy to realize by using the biepitaxial technique.

In this section we focus our attention mainly on the feasibility of the biepitaxial junctions to obtain the doubly degenerate state required for a qubit. In Ref.<sup>1a</sup> the design is based on quenching the lowest order coupling by arranging a junction with its normal aligned with the node of the d-wave order parameter, thus producing a double periodic current-phase relation. It has been shown that the use of  $\pi$  phase shifts in a superconducting phase qubit provides a naturally bistable device and does not require external bias currents and magnetic fields.<sup>1b</sup> The direct consequence is the quietness of the device over other designs. A  $\pi$  junction provides the required doubly degenerate fundamental state, which also manifests itself in a doubly periodic function of the critical current density as a function of the phase.<sup>8</sup> The same principle has been used in small inductance five junction loop frustrated by a  $\pi$ -phase shift.<sup>1b</sup> This design provides a perfectly degenerate two-level system and offers some advantages in terms of fabrication ease and performance. HTS may represent a natural solution for the realization of the required  $\pi$ -phase shift due to the pairing symmetry of the order parameter and, therefore, due to the possibility of producing  $\pi$  phase shifts. Experimental evidence of YBCO  $\pi$ -SQUIDS has been given by employing the bicrystal technique on special tetracrystal substrates.<sup>7</sup> The biepitaxial technique, beyond providing junctions with opportune properties, would guarantee the versatility necessary for the implementation of a real device, as shown below. As a matter of fact, we notice that our technique allows the realization of circuits where  $\pi$ -loops can be controllably located in part of the substrate and separated from the rest of the circuit based on “0”-loops, i.e. junctions where no additional  $\pi$  phase

shifts arise. This can be easily made by depositing the MgO and CeO<sub>2</sub> seed layers on different parts of the substrate, which will be also partly not covered by any seed layer.

As a test to show how the biepitaxial junctions could be considered for preliminary tests and device implementation for quantum computing without the topological restriction imposed by the bicrystal technique, we refer to the structures proposed in Ref.<sup>1</sup> as exemplary circuits.

The former is composed by a s-wave (S)- d-wave (D)- s-wave (S') double junction connected with a capacitor and an ordinary “0” Josephson junction based on s-wave superconductors (the S-D'-S junction generates the doubly degenerate state). The latter consists of a five junction loop with a  $\pi$  junction. Our technique would combine the possibility of placing the ordinary “0” junctions corresponding to the MgO seed layer and to exploit the possible doubly degenerate state of asymmetric 45° GB junctions corresponding to the CeO<sub>2</sub> seed layer to replace the S-D-S' system or the  $\pi$  junction respectively. Our structure would be obviously composed only of HTS. In Figs. 10a and 10b we show how devices for instance such as those proposed in Ref.<sup>1</sup> could be obtained by employing the biepitaxial technique respectively. The application to the five junction loop is straightforward (Fig. 10b) and the advantages of this structure have been already discussed in Ref.<sup>1b</sup>. The biepitaxial technique can offer possible alternatives for the realization of the structures above. In particular the double junctions of the original S-D-S' system can be also replaced by a D'-D-D" structure (Fig. 10c) by exploiting our technique, in contrast to the bicrystal technology which could not give this possibility. Such a configuration could offer some advantages, if we consider that asymmetric 45° bicrystal GB Josephson junctions did not give systematic evidence of the doubly degenerate state. The doubly degenerate state seems to occur only in high quality low transparency GB junctions<sup>8,26</sup> and it is known that S-I-D junctions do not have double periodicity of the critical current as a function of the phase.<sup>26</sup> A consequence of a possible nodeless order parameter<sup>4,23</sup> at the D-D' GB interface could be a closer similarity with a S-I-D junction with loss of the doubly degenerate state. If this is the case, we speculate that the double junctions structure for symmetry reasons would produce a leading term in the Josephson coupling energy of the form  $E_d \cos 2\theta$  (double periodic) and that the possible dipolar component of the magnetic field would be almost completely compensated in this configuration.<sup>1b</sup> This can be considered as an attempt to construct a “microscopic”  $2\theta$ -junction. We finally notice that the topological advantages offered by the biepitaxial junctions would therefore be crucial in both the cases considered for the realization of the structure in Fig. 10, and important to reduce de-coherence effects. Bicrystal substrates would in fact impose on the circuit additional junctions required by the circuit design and, as a consequence, generate additional noise and de-coherence in the device.



## V. CONCLUSIONS

The performance of the presented junctions and SQUIDs demonstrates that significant improvements in the biepitaxial technique are possible, and the resulting devices have potential for applications. We have presented a phenomenology that is consistent with the expected absence of  $\pi$ -loops in  $45^\circ$  [100] tilt and twist grain boundaries junctions. The use of a  $\text{CeO}_2$  rather than a  $\text{MgO}$  seed layer can produce  $\pi$ -loops in the same junction configurations. The versatility of the biepitaxial technique has been recently used to obtain different types of grain boundaries. The advantage of placing junctions in arbitrary locations on the substrate without imposing any restrictions on the geometry, and the ease of obtaining different device configurations by suitably patterning the seed layer, make the biepitaxial technique competitive for the testing of new concept devices, such as those based on  $\pi$ -loops. Some simple examples of situations in which  $\pi$ -loops can be suitably produced in specific locations of a more complicated circuit have also been discussed.

## ACKNOWLEDGMENTS

This work has been partially supported by the projects PRA-INFM "HTS Devices" and SUD-INFM "Analisi non distruttive con correnti parassite tramite dispositivi superconduttori" and by a MURST COFIN98 program (Italy). The authors would like to thank Dr. E. Ilichev and A. Golubov for interesting discussions on the topic.

- <sup>1</sup> L.B. Ioffe, V.B. Geshkenbein, M.V. Feigel'man, A.L. Fauchere and G. Blatter, *Nature* **398**, 679 (1999); G. Blatter, V. B. Geshkenbein and L. B. Ioffe, *Cond. Mat.* 9912163 (1999)
- <sup>2</sup> L.N. Bulaevskii, V.V. Kuzii and A.A. Sobyenin, *JETP Lett.* **25**, 290 (1977)
- <sup>3</sup> V.B. Geshkenbein, A.I. Larkin and A. Barone, *Phys. Rev. B* **36**, 235 (1986)
- <sup>4</sup> C.C. Tsuei and J.R. Kirtley, to be published in *Review of Modern Physics* (1999); C.C. Tsuei, J.R. Kirtley, C.C. Chi, L.S. Yu-Jahnes, A. Gupta, T. Shaw, J.Z. Sun and M.B. Ketchen, *Phys. Rev. Lett.* **73**, 593 (1994); J.R. Kirtley, C.C. Tsuei, J.Z. Sun, C.C. Chi, L.S. Yu-Jahnes, A. Gupta, M. Rupp and M.B. Ketchen, *Nature* **373**, 225 (1995); D.A. Wollman, D.J. Van Harlingen, J. Giapintzakis, D.M. Ginsberg, *Phys. Rev. Lett.* **74**, 797 (1995); D.A. Wollman, D.J. Van Harlingen and A.J. Leggett, *Phys. Rev. Lett.* **73**, 1872 (1994)
- <sup>5</sup> M. Sigrist and T.M. Rice, *J. Phys. Soc. Jap.* **61**, 4283 (1992)
- <sup>6</sup> A.M. Zagorskin, *Cond. Mat.* 9903170 (1999)
- <sup>7</sup> R. Schulz, B. Chesca, B. Goetz, C.W. Schneider, A. Shmehl, H. Bielefeldt, H. Hilgenkamp and J. Mannhart, *Appl. Phys. Lett.* **76**, 912 (2000)
- <sup>8</sup> E. Il'ichev, V. Zakosarenko, R.P.J. Ijsselstein, H.E. Honig, V. Schultze, H.G. Meyer, M. Grajcar and R. Hlubina, *Phys. Rev. B* **60**, 3096 (1999)
- <sup>9</sup> E. Terzioglu and M.R. Beasley, *IEEE Trans. Appl. Supercond.* **8**, 48 (1998)
- <sup>10</sup> F. Tafuri, F. Miletto Granozio, F. Carillo, A. Di Chiara, K. Verbist and G. Van Tendeloo, *Phys. Rev. B* **59**, 11523 (1999)
- <sup>11</sup> K. Char, M.S. Colclough, S.M. Garrison, N. Newman and G. Zaharchuk, *Appl. Phys. Lett.* **59**, 773 (1991)
- <sup>12</sup> D. Dimos, P. Chaudari, J. Mannhart and F.K. LeGoues, *Phys. Rev. Lett.* **61**, 219 (1988)
- <sup>13</sup> R. W. Simon, J.F. Burch, K.P. Daly, W.D. Dozier, R. Hu, A.E. Lee, J.A. Luine, H.M. Manasevit, C.E. Platt, S.M. Schwarzbein, D.St. John, M.S. Wire and M.J. Zani, in "Science and Technology of Thin Films Superconductors 2", R.D. McConnel and R. Noufi Eds. (Plenum, New York, 1990), p. 549
- <sup>14</sup> J. Mannhart, H. Hilgenkamp, B. Mayer, Ch. Gerber, J.R. Kirtley, K.A. Moler and M. Sigrist, *Phys. Rev. Lett.* **77**, 2782 (1996)
- <sup>15</sup> U. Scotti di Uccio, F. Lombardi, F. Ricci, E. Manzillo, F. Miletto Granozio, F. Carillo and F. Tafuri unpublished (2000)
- <sup>16</sup> K. Verbist, O. Lebedev, G. Van Tendeloo, F. Tafuri, F. Miletto Granozio and A. Di Chiara, *Appl. Phys. Lett.* **74**, 1024 (1999)
- <sup>17</sup> A. Barone and G. Paterno, *Physics and Applications of the Josephson Effect*, (J. Wiley, New York, 1982)
- <sup>18</sup> J. Mannhart, R. Gross, K. Hipler, R.P. Huebner, C.C. Tsuei, D. Dimos and P. Chaudari, *Science* **245**, 839 (1989)
- <sup>19</sup> F. Tafuri, B. Nadgorny, S. Shokhor, M. Gurvitch, F. Lombardi, F. Carillo, A. Di Chiara and E. Sarnelli, *Phys. Rev. B* **57**, R14076 (1998)
- <sup>20</sup> F. Tafuri, S. Shokhor, B. Nadgorny, M. Gurvitch, F. Lombardi and A. Di Chiara, *Appl. Phys. Lett.* **71**, 125 (1997)
- <sup>21</sup> J.R. Kirtley *et al.*, *Appl. Phys. Lett.* **66**, 1138 (1995)
- <sup>22</sup> F. Tafuri and J.R. Kirtley, *cond-mat /0003106*.
- <sup>23</sup> D.B. Bailey, M. Sigrist and R.B. Laughlin, *Phys. Rev. B* **55**, 15239 (1997); M. Sigrist, *Progr. Theor. Physics* **99**, 899 (1998).
- <sup>24</sup> G. Testa, E. Sarnelli, F. Carillo and F. Tafuri, *Appl. Phys. Lett.* **75**, 3542 (1999)
- <sup>25</sup> A.H. Miklich, J. Clarke, M.S. Colclough, and K. Char, *Appl. Phys. Lett.* **60**, 1989 (1992)
- <sup>26</sup> Y. Tanaka and S. Kashiwaya, *Phys. Rev. B* **56**, 893 (1997)

FIG. 1. A schematic representation of the artificial grain boundary structure. The boundary is obtained at the interface between the [001] oriented YBCO film grown on the [110]  $\text{MgO}$  seed layer and the [103] YBCO film grown on the bare [110] STO substrate. In contrast with the  $45^\circ$  [001] tilt bicrystal junctions, in this case the order parameter orientations do not produce an additional  $\pi$  phase shift.

FIG. 2. The  $\text{CeO}_2$  seed layer produces an artificial GB that can be seen as a result of two rotations: a  $45^\circ$  [100] tilt or twist followed by a  $45^\circ$  tilt around the c-axis of the (001) film. For this junction configuration a d-wave order parameter symmetry would produce  $\pi$ -loops.

FIG. 3. Current vs voltage (I-V) characteristics of the biepitaxial junction for temperature close to the critical temperature. In the inset the I-V curve at  $T = 4.2$  K is shown.

FIG. 4. a) Scheme of the seed layer patterning, which allows the measurement on the same chip of the properties of a tilt junction and of junctions whose interface is tilted in plane of an angle  $\alpha = 30^\circ, 45^\circ$  and  $60^\circ$  with respect the a- or b-axis of the (001) YBCO thin film respectively. b) The I-V characteristics (measured at  $T = 4.2$  K) of the microbridges reported in Fig. 4a.

FIG. 5. Magnetic-field dependence of the critical current of a [100] tilt biepitaxial dc-SQUID. The absolute maximum is observed for zero field. A double-period modulation is observed. The longer period modulation is the diffraction pattern due to the magnetic field sensed by a single junction, while the shorter period SQUID modulation is shown more clearly in the inset (a). In the inset (b) I-V curves are shown as a function of an externally applied magnetic field at  $T = 4.2$  K. A typical Fraunhofer-like dependence is evident.

FIG. 6. Scanning SQUID microscope image of a  $200 \times 200 \mu\text{m}^2$  area along a grain boundary separating a (100) region from a (103) region of a thin YBCO biepitaxial film grown. The position of the grain boundary is indicated by the dashed line.

FIG. 7. Magnetic field dependence of the voltage of a [100] tilt biepitaxial dc-SQUID at 77 K for different values of the bias current.

FIG. 8. Magnetic flux noise spectral densities of a [100] tilt biepitaxial SQUID at  $T=77$  K and  $T=4.2$  K. The SQUID, with an inductance  $L=13$  pH, was modulated with a standard flux-locked-loop electronics. The right axis shows the energy resolution. Data at  $T = 4.2$  K are compared with results on SQUIDs based on [001] tilt biepitaxial junctions from Ref. 25.

FIG. 9. a) 3-dimensional view of a SQUID based on  $45^\circ$  [100] tilt and twist GBs; no  $\pi$ -loops should occur. b) Top view of  $\pi$ -SQUID based on  $45^\circ$  [001] tilt GBs. c) 3-dimensional view of a  $\pi$ -SQUID based on GBs resulting from two rotations: a  $45^\circ$  [100] tilt or twist followed by a  $45^\circ$  [001] tilt

FIG. 10. Scheme of the qubit structure proposed in Ref.1 designed using the biepitaxial grain boundaries proposed in the paper. The double junctions of the original S-D-S' system can be also replaced by D'-D-D''.

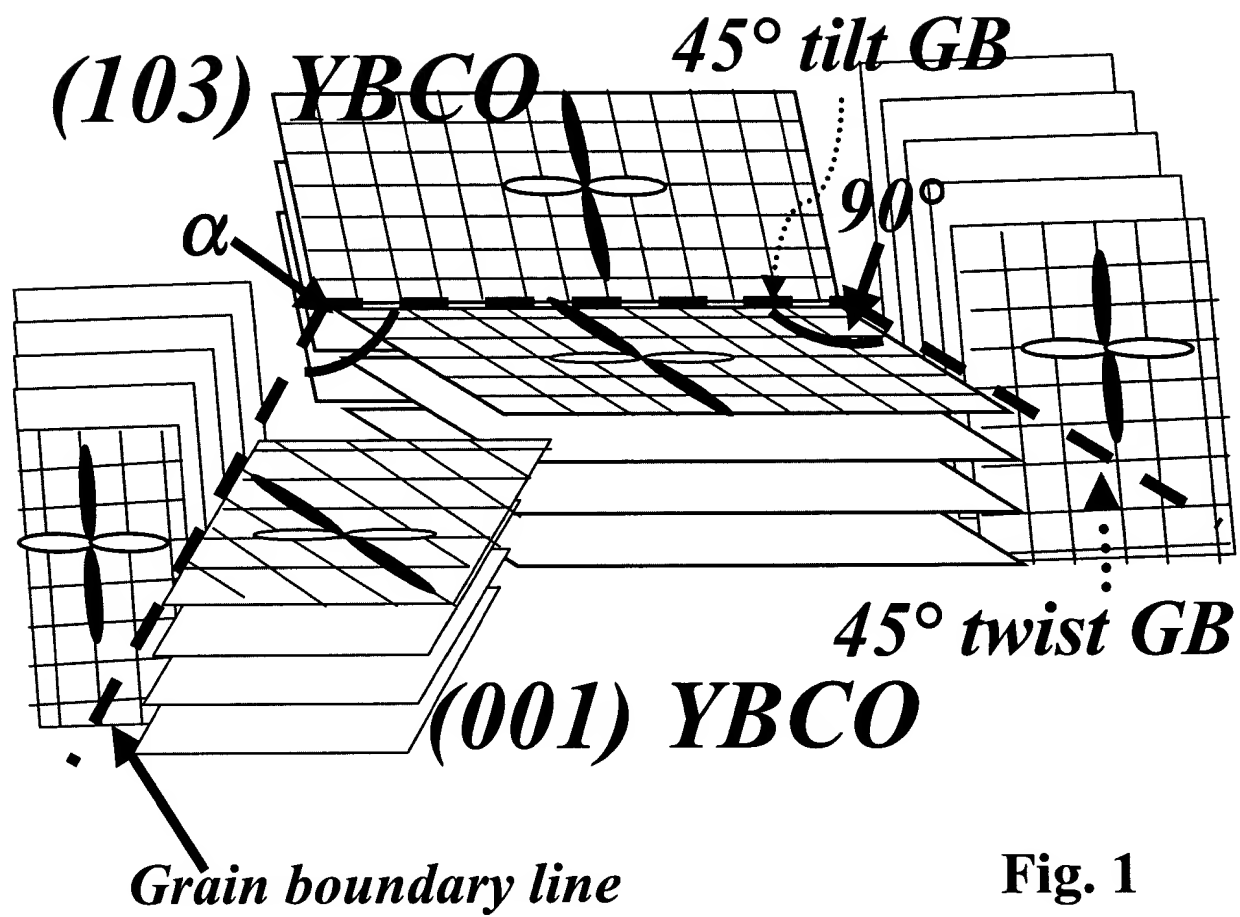
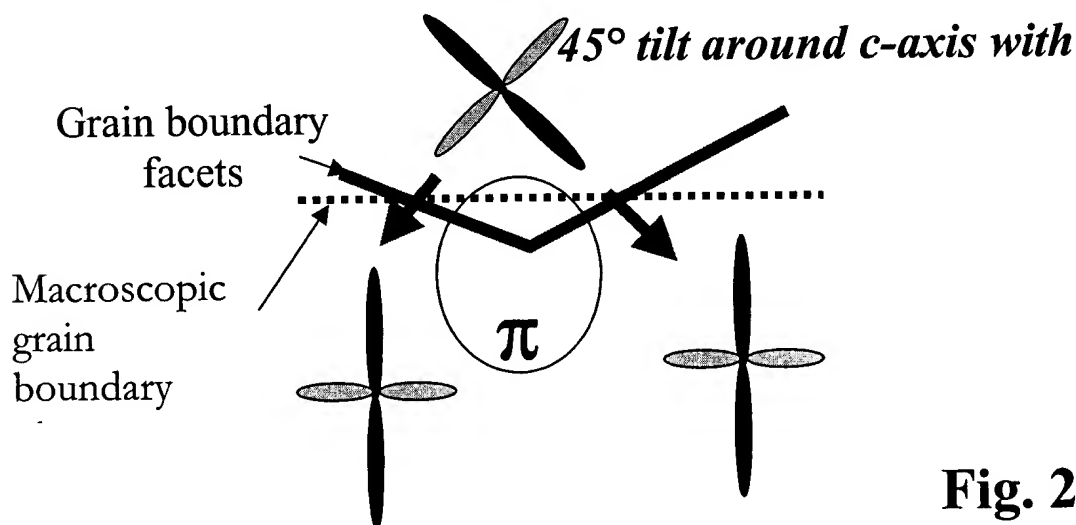
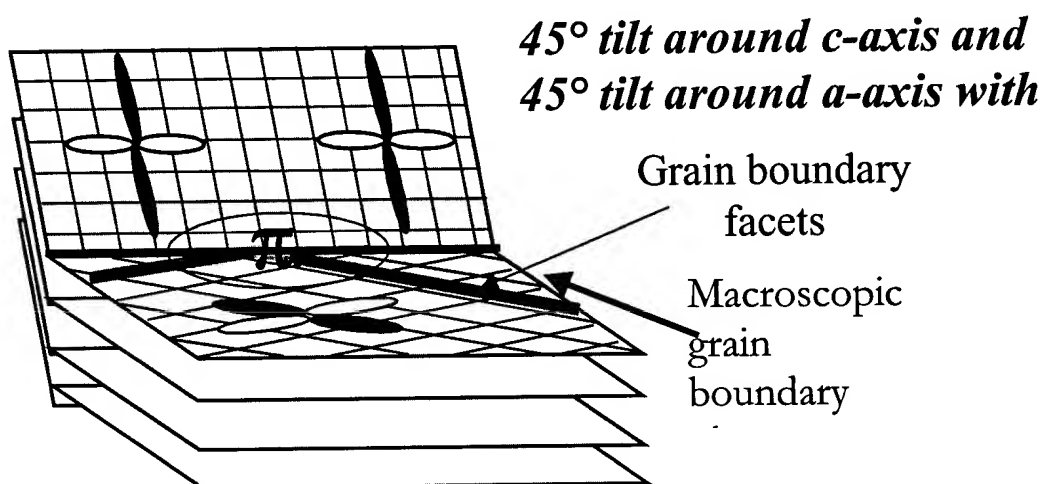
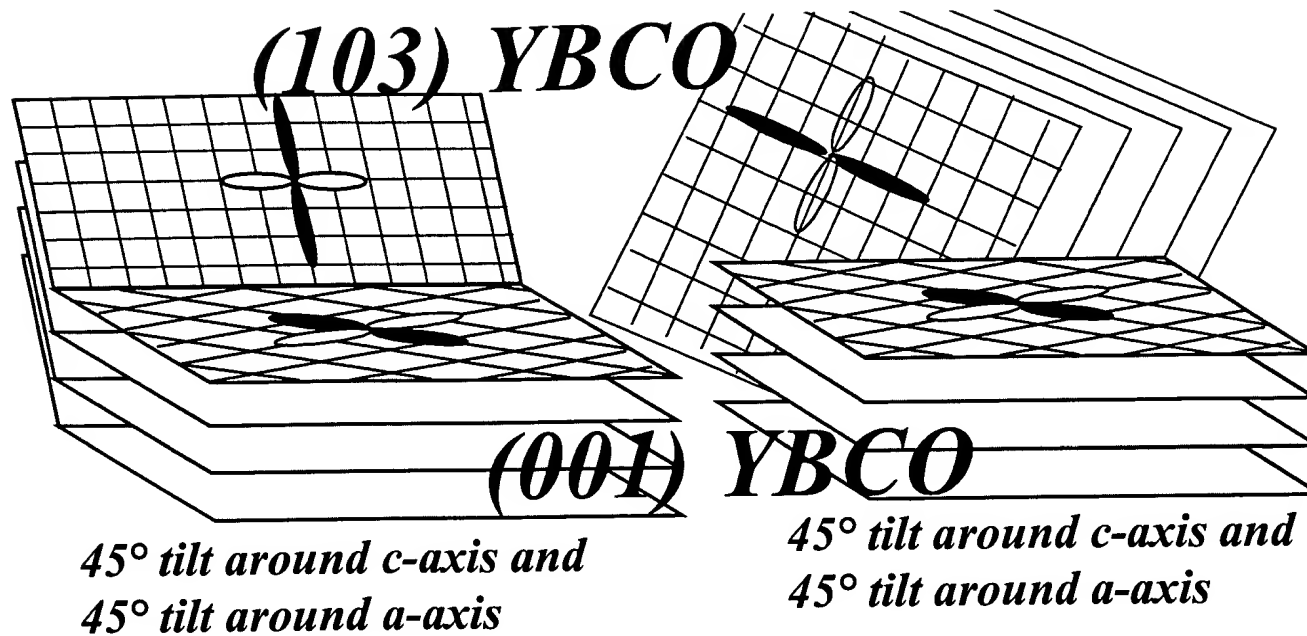


Fig. 1



**Fig. 2**

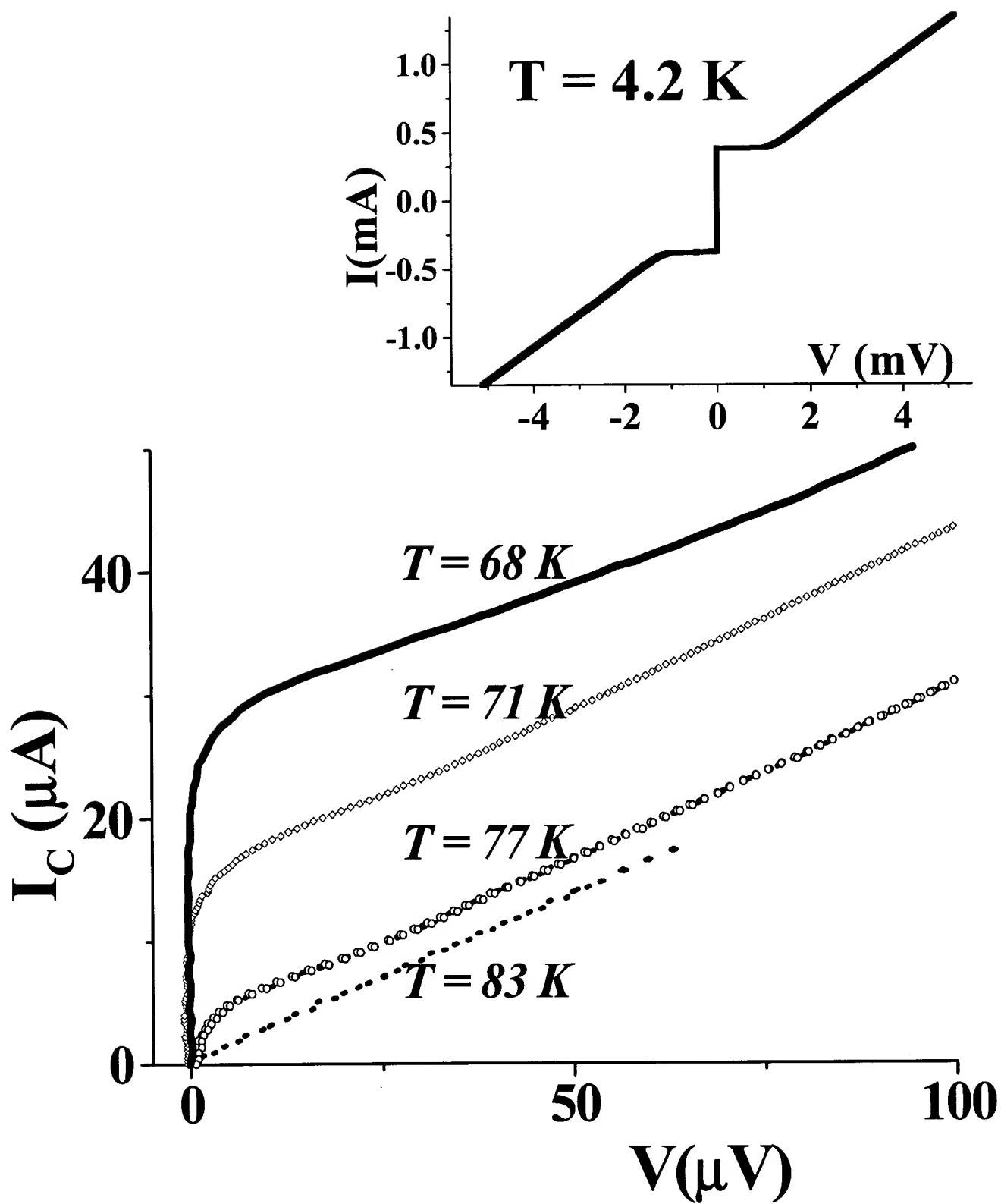
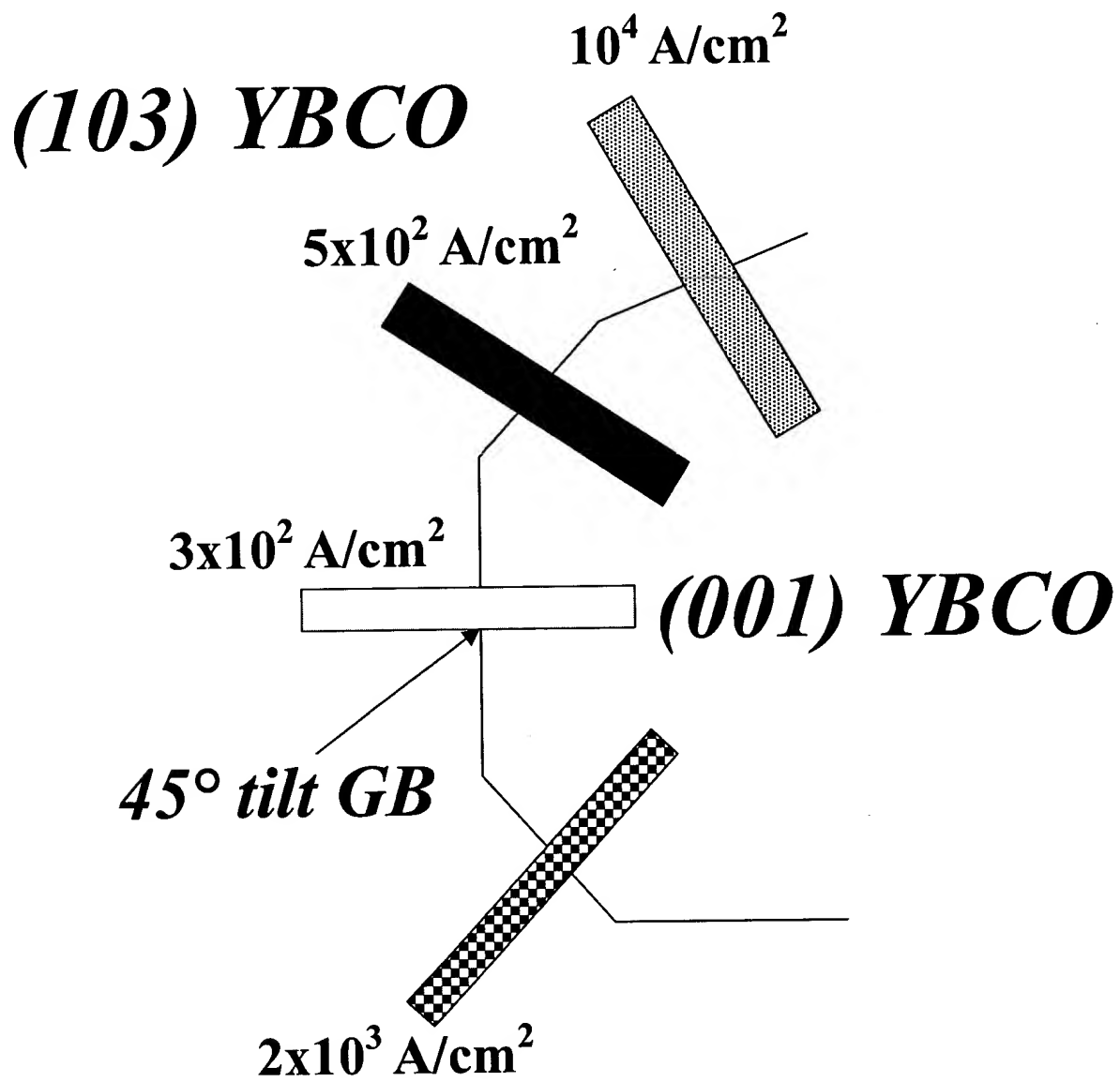
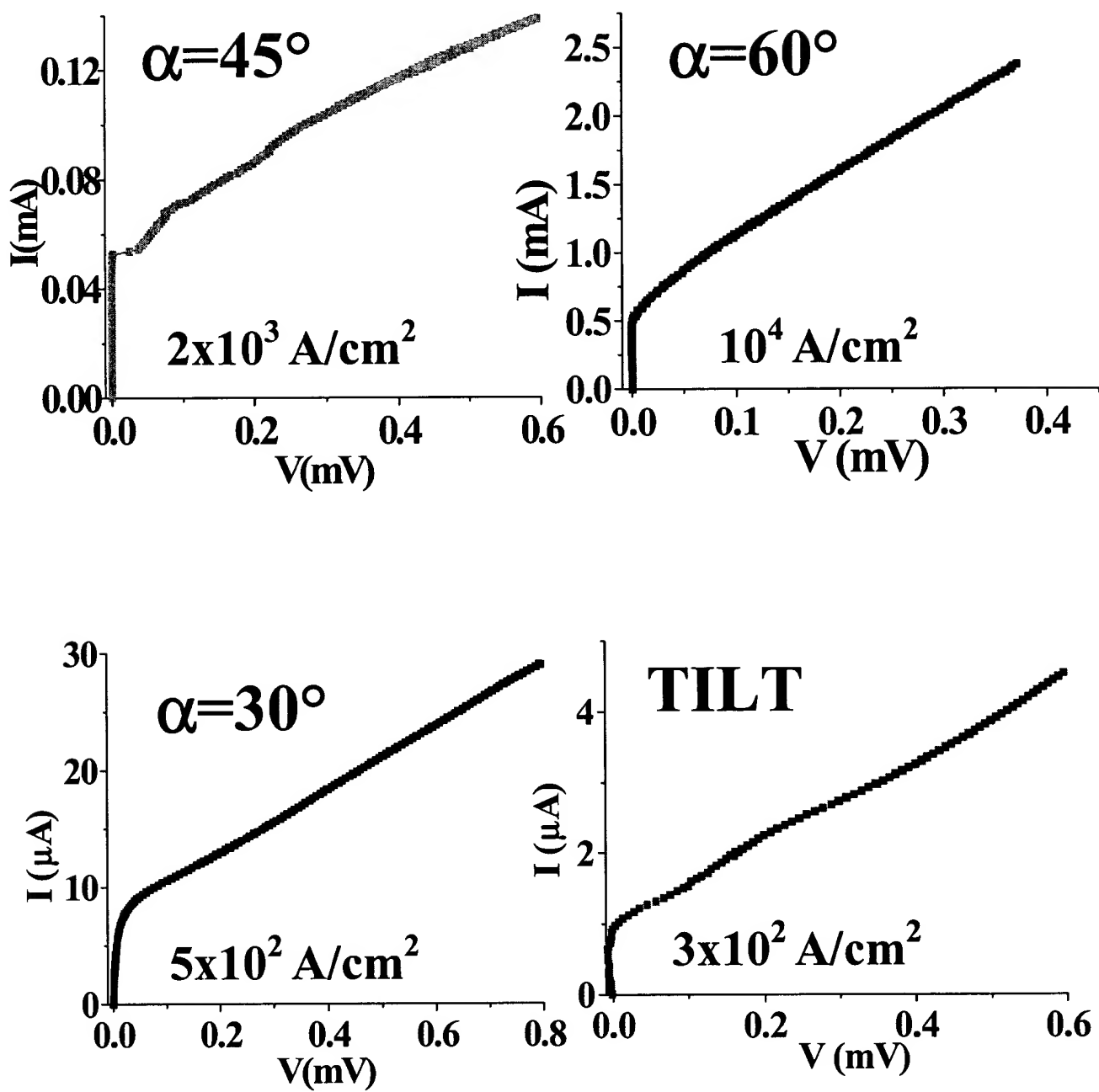


Fig. 3

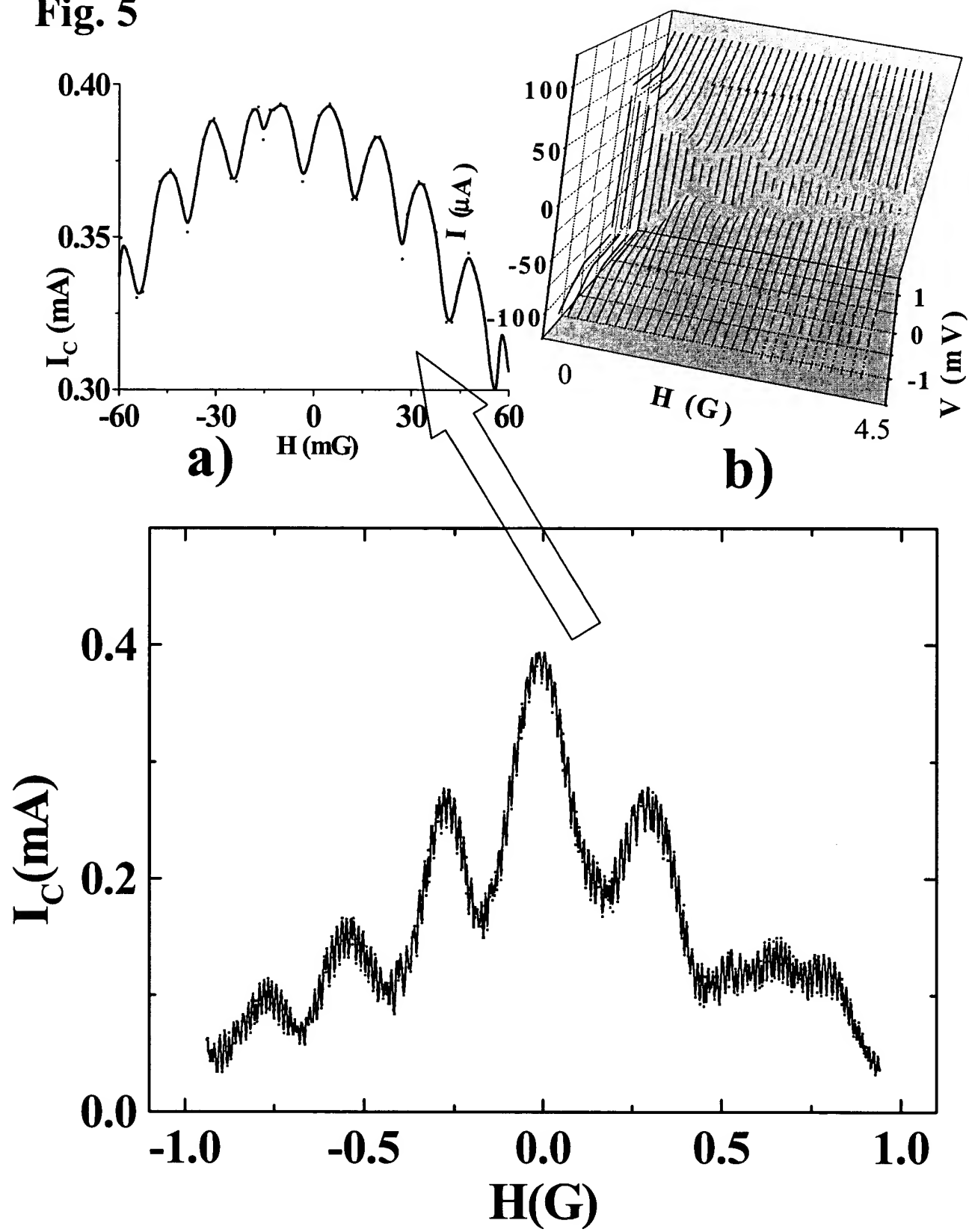


**Fig. 4a**

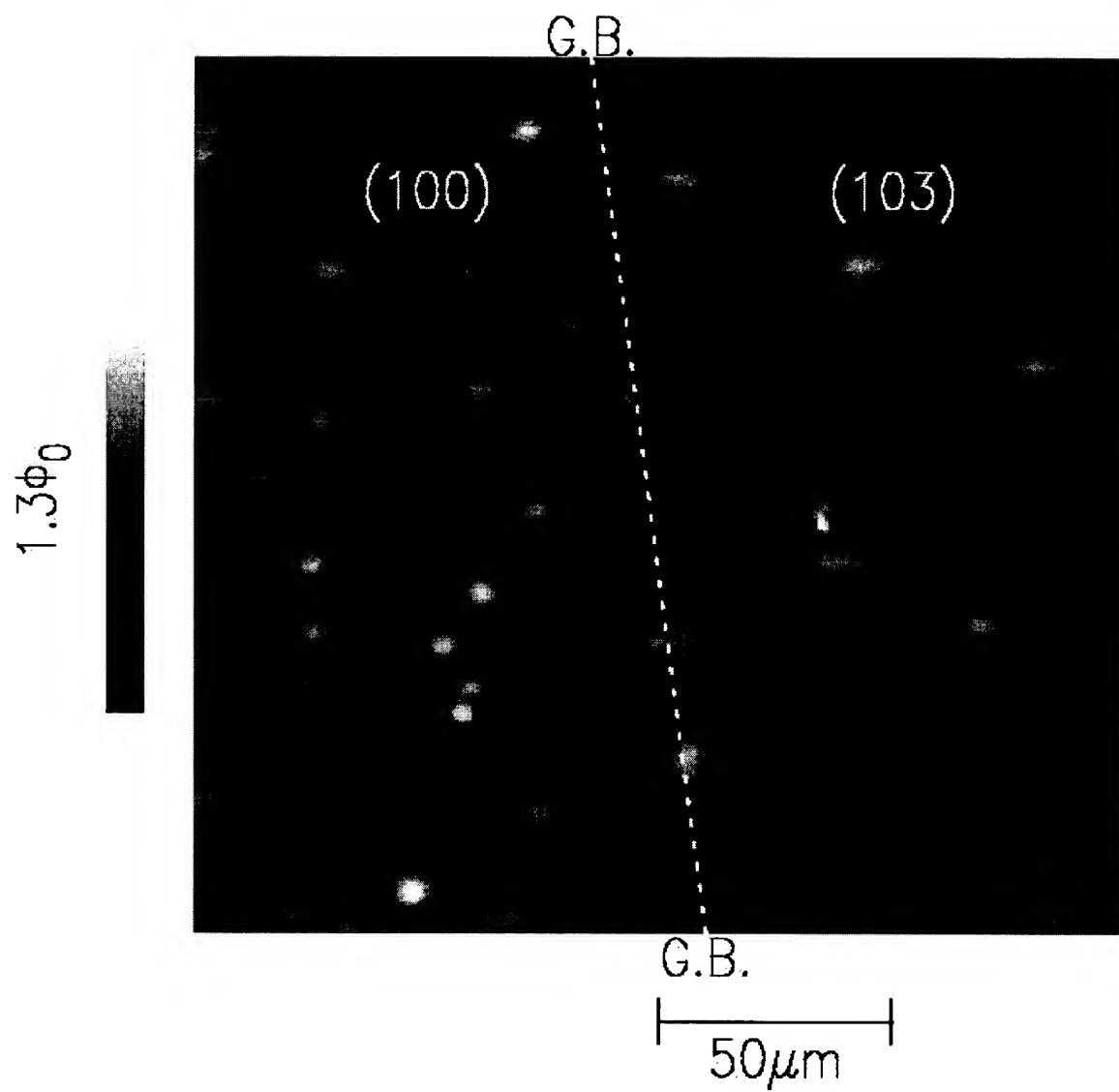
**Fig. 4b**



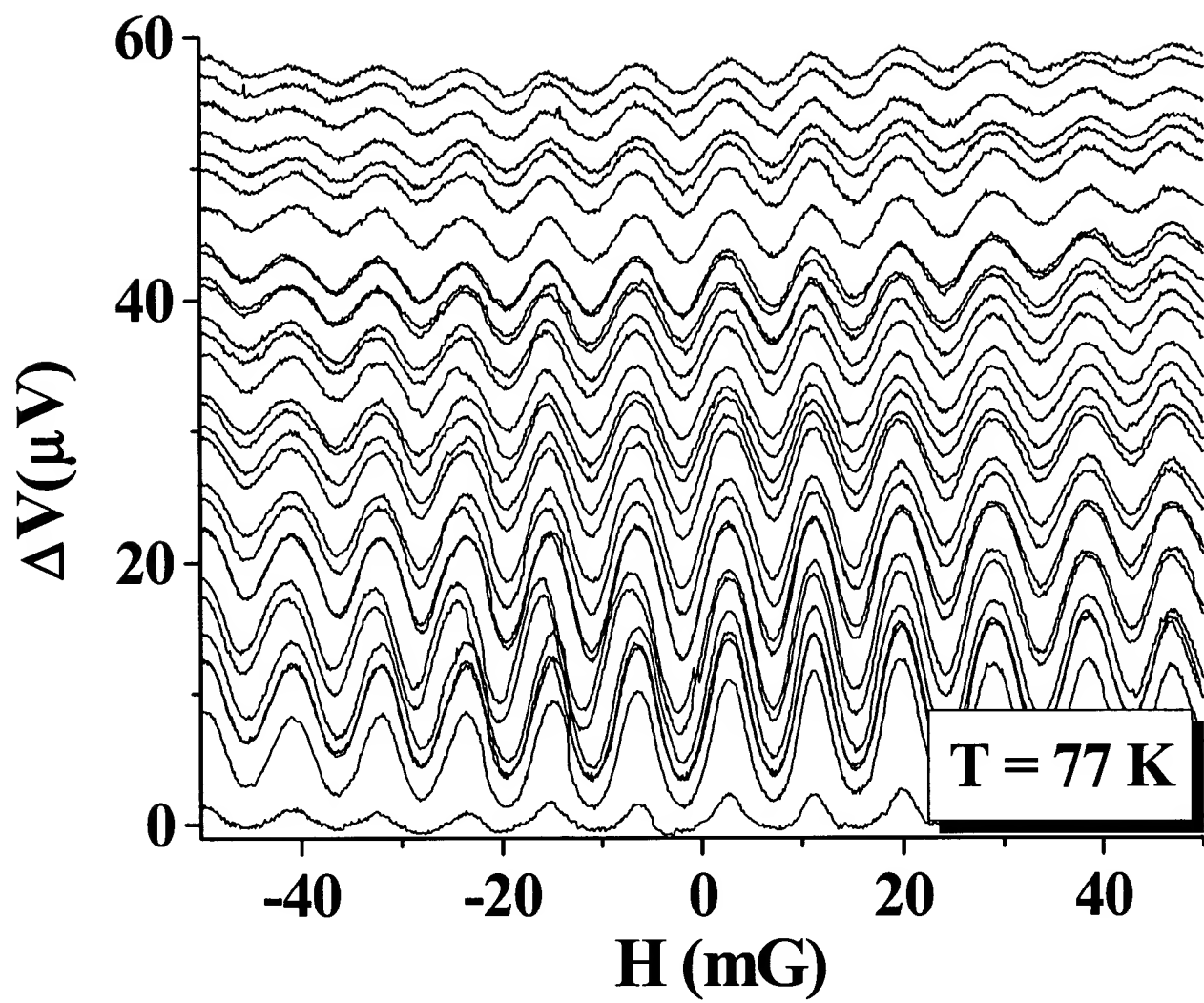
**Fig. 5**





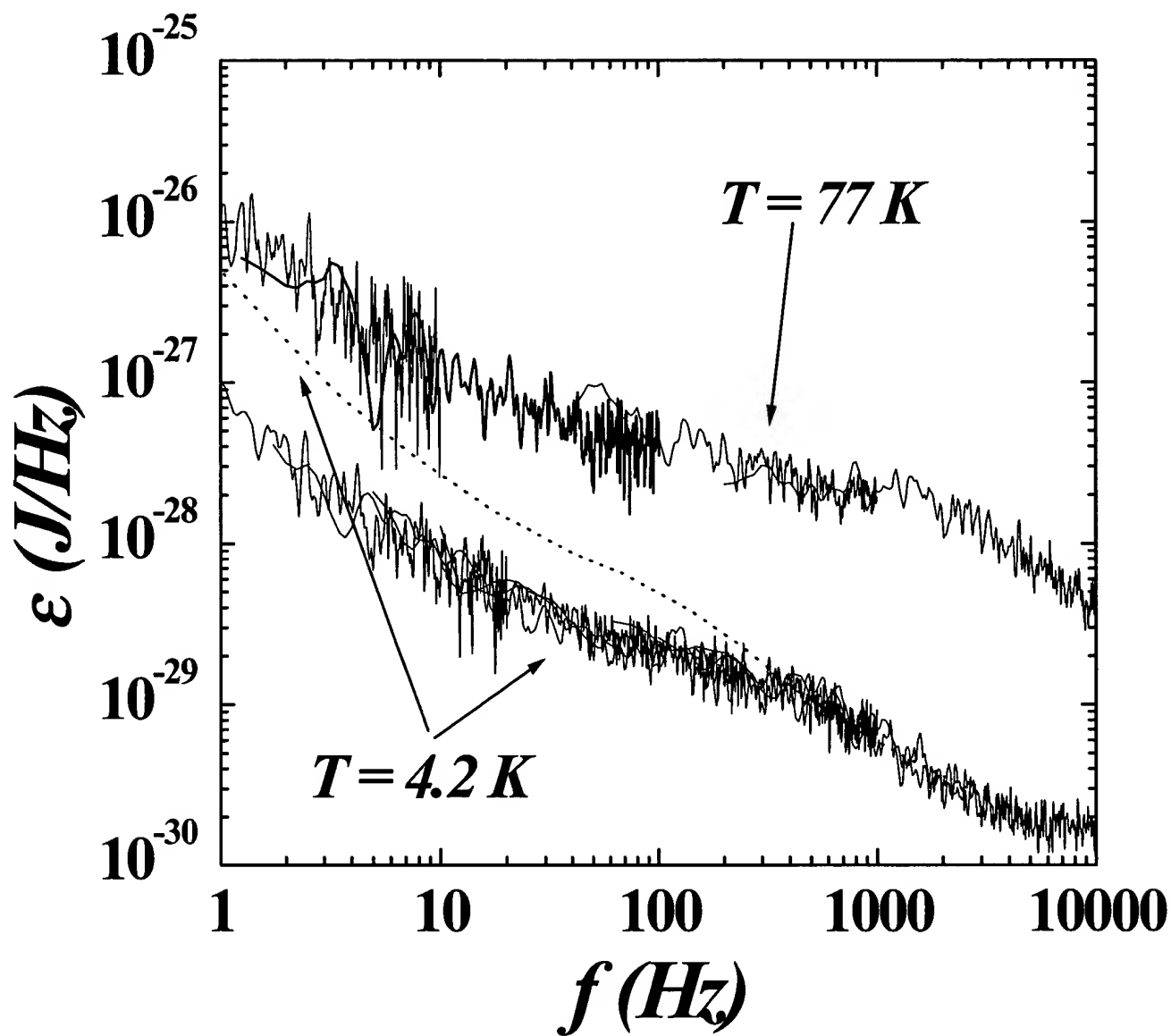


**Fig. 6**



**Fig. 7**

**Fig. 8**



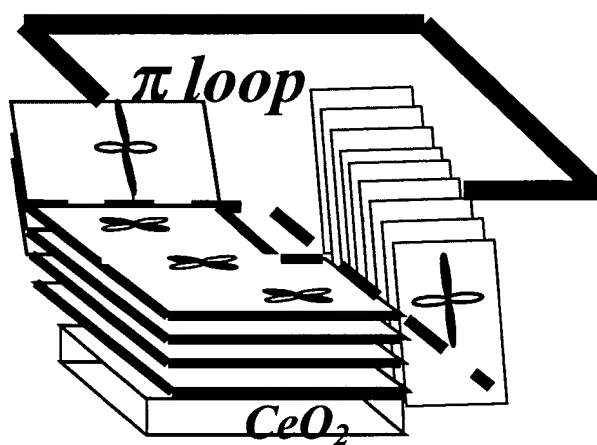
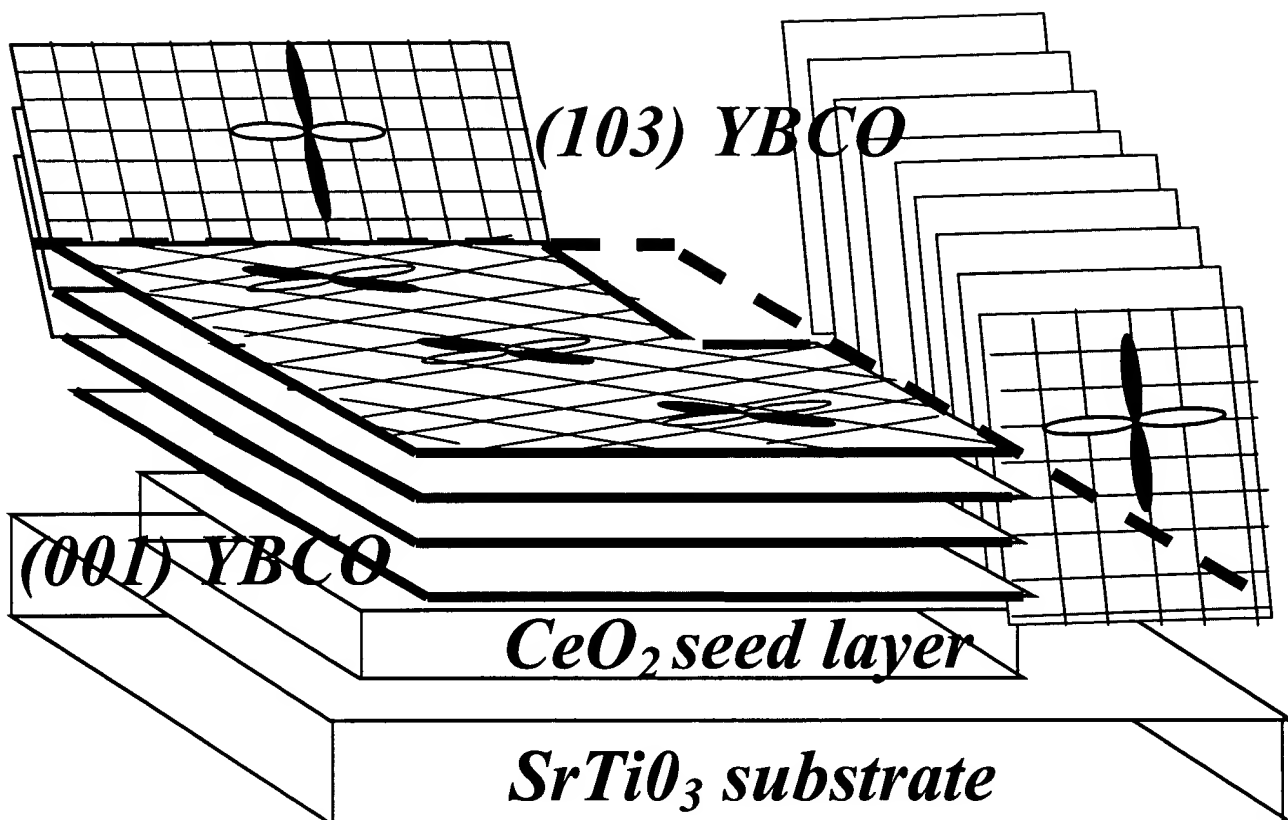


**Fig. 9a**

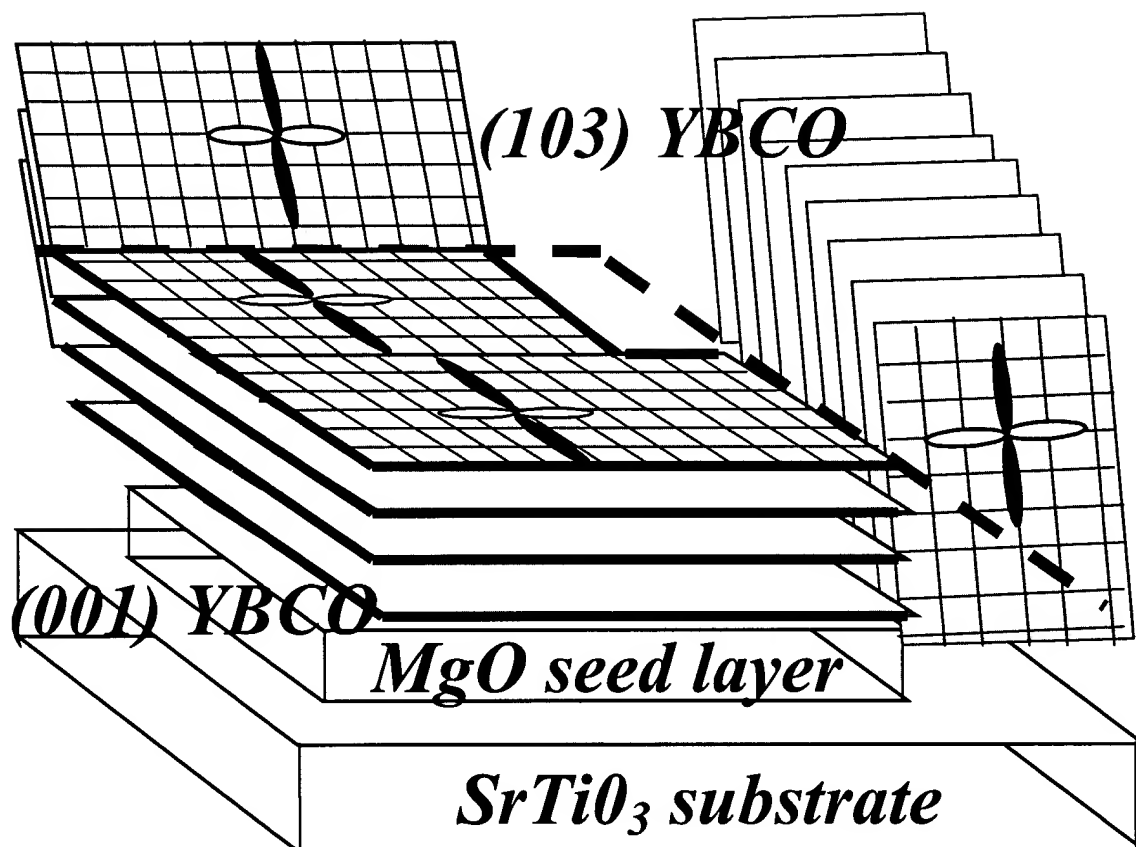
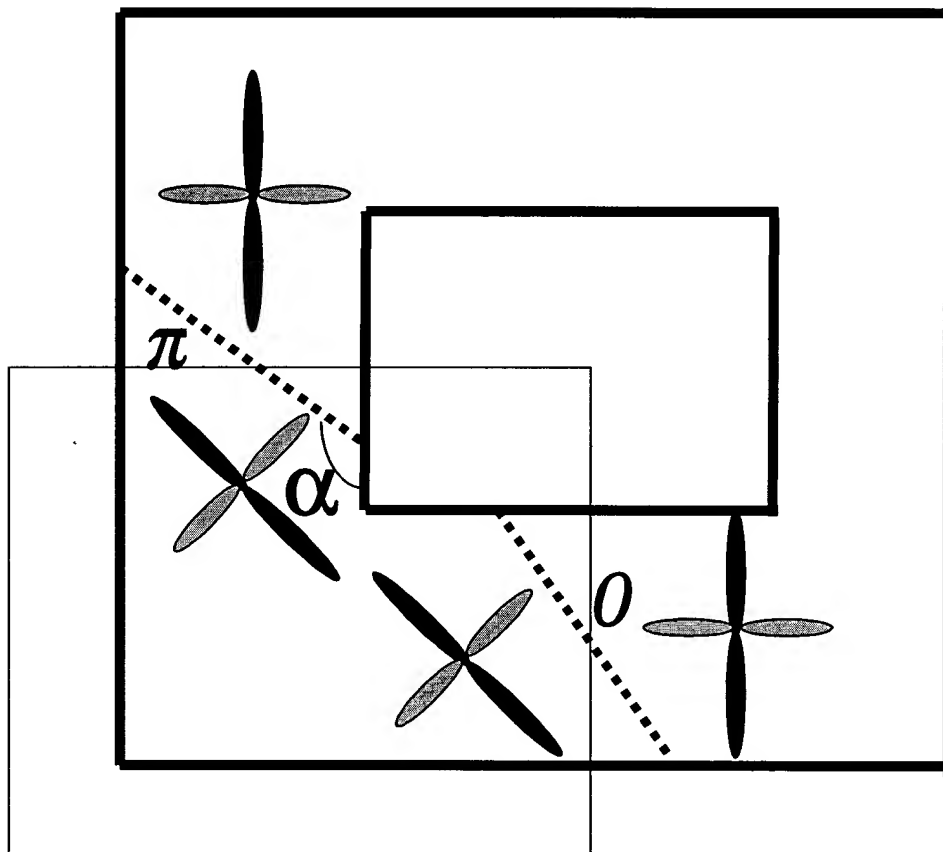
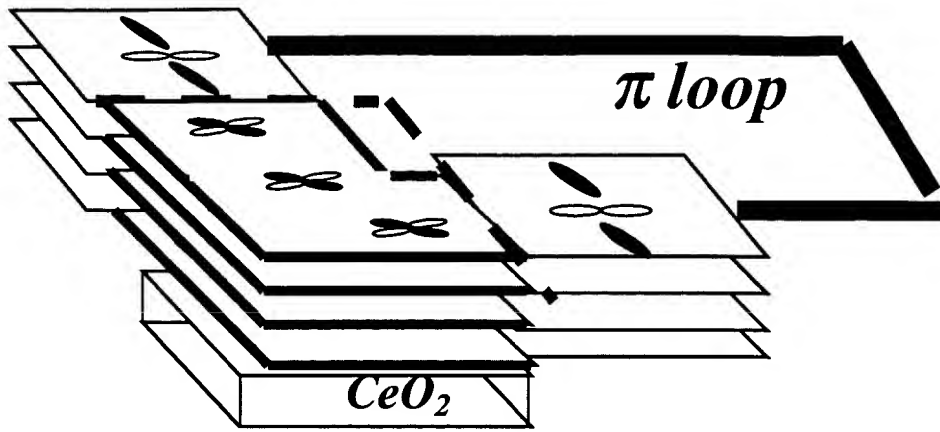


**Fig. 9b**

Fig. 9c



*a)*

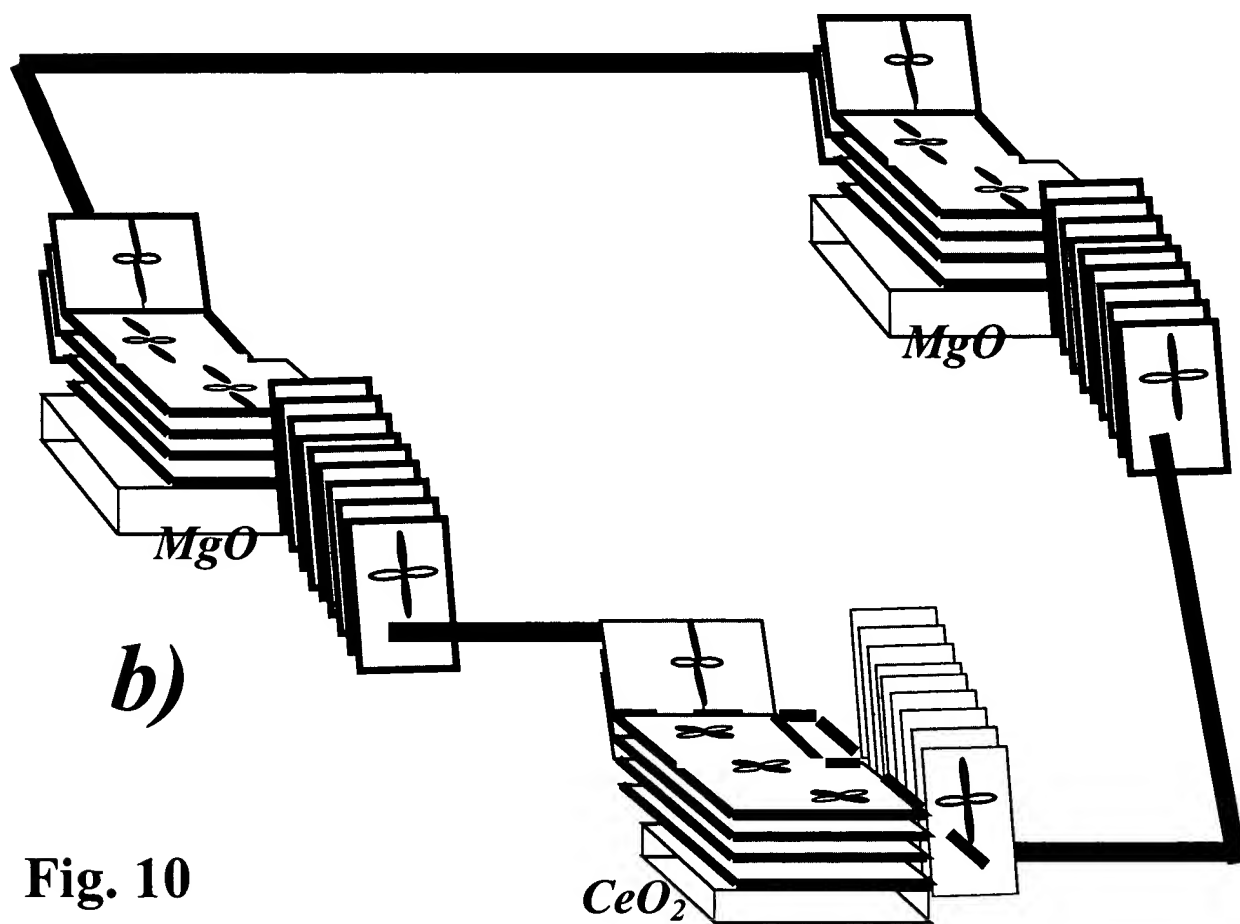
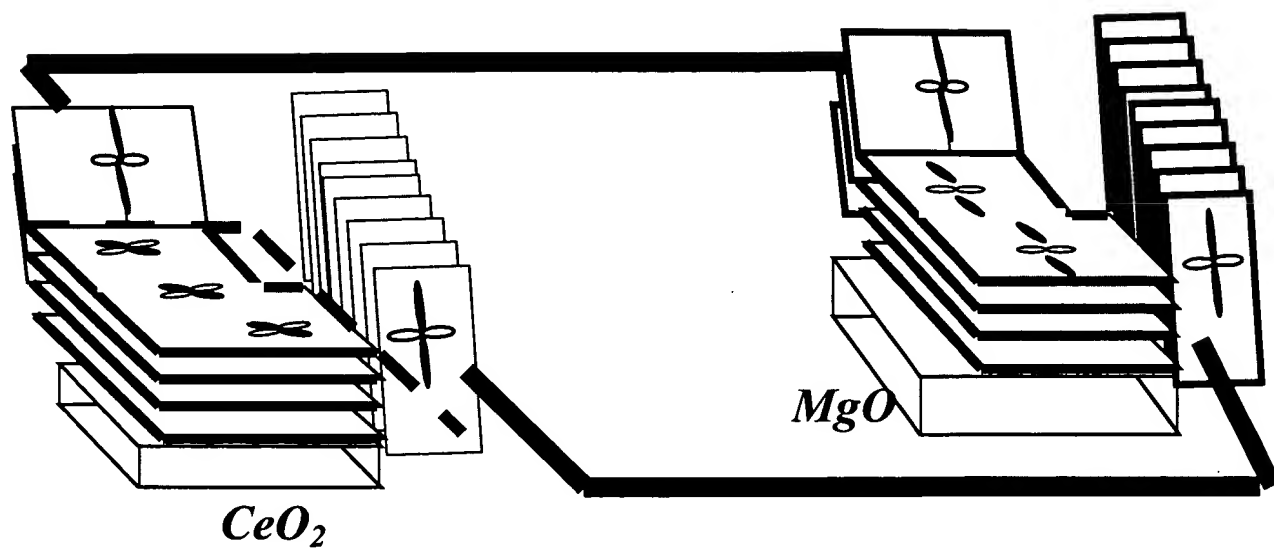
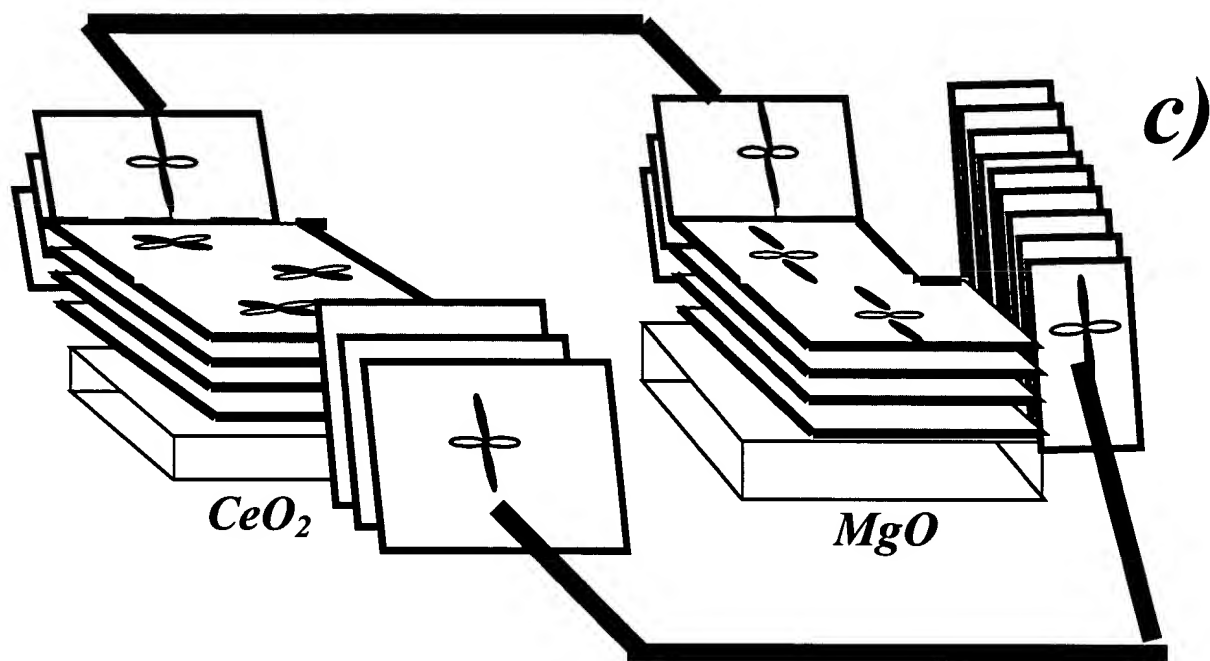


Fig. 10



**Fig. 10**



# Bi-epitaxial grain boundary junctions in $\text{YBa}_2\text{Cu}_3\text{O}_7$

K. Char, M. S. Colclough, S. M. Garrison, N. Newman, and G. Zaharchuk  
*Conductus, Inc., Sunnyvale, California 94086*

(Received 26 March 1991; accepted for publication 13 May 1991)

We have developed a new way of making grain boundary junctions in  $\text{YBa}_2\text{Cu}_3\text{O}_7$  thin films by controlling the in-plane epitaxy of the deposited film using seed and buffer layers. We produce  $45^\circ$  grain boundaries along photolithographically defined lines. The typical value of the critical current density of the junctions is  $10^3$ – $10^4$  A/cm<sup>2</sup> at 4.2 K and  $10^2$ – $10^3$  A/cm<sup>2</sup> at 77 K, while the rest of the film has a critical current density of  $1$ – $3 \times 10^6$  A/cm<sup>2</sup> at 77 K. The current-voltage characteristics of the junctions show resistively shunted junction behavior and we have used them to fabricate dc superconducting quantum interference devices (SQUIDs) which show modulation at temperatures well above 77 K. This is the first planar high  $T_c$  Josephson junction technology that appears readily extendable to high  $T_c$  integrated circuits.

Most microelectronic applications of the high  $T_c$  superconductors will rely upon microbridges such as superconductor-normal metal-superconductor (S-N-S) junctions or other weak link geometries instead of superconductor-insulator-superconductor (S-I-S) tunnel junctions. A number of weak-link structures provide reliable critical current reduction in  $\text{YBa}_2\text{Cu}_3\text{O}_7$  (YBCO) thin films; grain boundary junctions,<sup>1–3</sup> traditional edge junctions,<sup>4</sup> microbridges grown across a sharp substrate step,<sup>5</sup> and S-N-S-type junctions with Au,<sup>6</sup>  $\text{PrBa}_2\text{Cu}_3\text{O}_7$ ,<sup>7,8</sup> or  $\text{SrTi}_{1-x}\text{Nb}_x\text{O}_3$  (Ref. 9) normal layers. Of these various weak-link geometries, grain boundary junctions work well at temperatures close to  $T_c$ , have reasonably high  $I_c R_n$  products, and show behavior explained by a resistively shunted junction model with a relatively uniform current density. To date, the high angle grain boundary junctions that have been used were formed either by fusing differently oriented  $\text{SrTiO}_3$  substrates<sup>1</sup> or by patterning the randomly occurring grain boundaries in granular films.<sup>2,3</sup> Superconducting quantum interference devices (SQUIDs) made from the grain boundaries on  $\text{SrTiO}_3$  bicrystals had reasonable signal and low noise<sup>10</sup> up to temperatures very close to the  $T_c$  of the film. However, this  $\text{SrTiO}_3$  bicrystal technique has a major drawback: it cannot be readily extended to integrated circuits. On the other hand, SQUIDs made from granular films are plagued by low yield and the presence of grain boundaries in the SQUID loop itself. These lead to excessive flux noise and hysteresis in the voltage-flux response of the SQUID.

In this letter, we report for the first time the successful fabrication of high  $T_c$  weak-link Josephson junctions operating at and above 77 K that are made from grain boundary junctions whose locations are determined by conventional photolithography. This result demonstrates the feasibility of an extendable technology for fabricating high  $T_c$  Josephson devices which avoids the problems associated with the devices made from granular thin films and on bicrystal substrates. We reproducibly fabricate  $45^\circ$  grain boundaries in YBCO films by controlling their in-plane epitaxy using seed and buffer layers deposited on  $r$ -plane sapphire substrates, a method we call "bi-epitaxy." The method is quite general, and can be used on a wide variety of substrates.

Recently, we reported<sup>11</sup> the existence of two in-plane epitaxial orientations of  $c$ -axis oriented epitaxial YBCO thin films on yttria-stabilized zirconia (YSZ), resulting from the poor lattice match between YBCO and YSZ. This observation led us to realize that it would be possible to make bi-epitaxial grain boundaries on such a substrate using seed and buffer layers, or, in an alternative geometry, on a well lattice-matched substrate using poorly lattice-matched seed layers. For example, we previously reported<sup>12</sup> the growth of YBCO thin films on  $r$ -plane sapphire using buffer layers such as  $\text{SrTiO}_3$ ,  $\text{CaTiO}_3$ , YSZ, and  $\text{MgO}$ . We emphasized the importance of the in-plane epitaxy of YBCO, particularly because high-angle grain boundaries in YBCO films behave as weak links, leading to low critical current densities and high surface resistances.<sup>12,13</sup> Our efforts towards minimizing the occurrence of these high-angle grain boundaries taught us how to control them and led us to design and demonstrate a variety of  $45^\circ$  weak-link junctions. One example takes advantage of the differing epitaxial directions of two different layers,  $\text{MgO}$  and  $\text{SrTiO}_3$ , when they are deposited on an  $r$ -plane sapphire substrate. Using these two layers as a seed and a buffer layer, we have succeeded in fabricating bi-epitaxial  $45^\circ$  grain boundaries in YBCO on sapphire substrates by the following process.

Schematic views of our device structure are shown in Fig. 1. We first deposit 3–30 nm of epitaxial  $\text{MgO}$  as a seed layer on an  $r$ -plane sapphire substrate.  $\text{MgO}$  is produced by laser ablating a  $\text{Mg}$  metallic target in a 2–20 mTorr oxygen atmosphere with a substrate temperature of 300–700 °C. We then mask the  $\text{MgO}$  with conventional photoresist and remove it from, for example, half of the substrate by either Ar ion beam milling or chemical wet etching with dilute phosphoric acid. We then grow 10–100 nm of epitaxial  $\text{SrTiO}_3$  buffer layer by laser ablation on both the exposed sapphire surface and on the patterned  $\text{MgO}$  seed layer. The deposition conditions are an oxygen pressure of 100–200 mTorr and a substrate temperature of 710–760 °C. The  $\text{SrTiO}_3$  film grows in two different orientations separated by a  $45^\circ$  grain boundary. In the growth plane the epitaxial relations are  $\text{SrTiO}_3[110]//\text{Al}_2\text{O}_3[11\bar{2}0]$  and  $\text{SrTiO}_3[100]//\text{MgO}[100]//\text{Al}_2\text{O}_3[11\bar{2}0]$ , as illustrated in

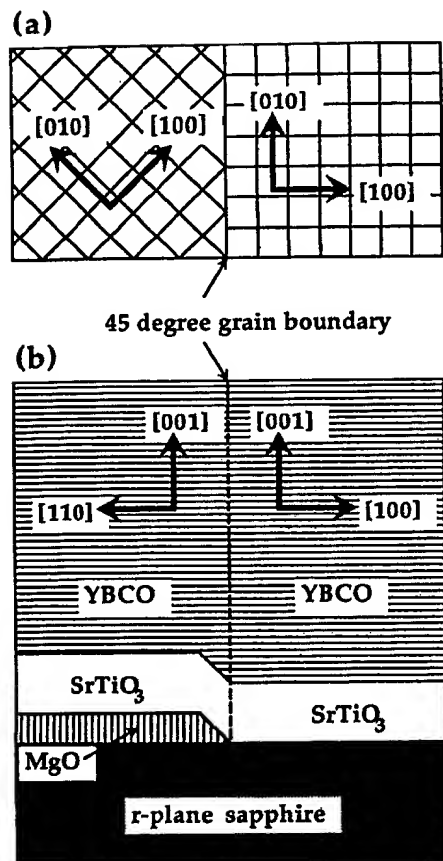


FIG. 1. Schematic view of the device structure with an MgO seed layer and a SrTiO<sub>3</sub> buffer layer on an *r*-plane sapphire substrate. (a) top view, (b) side view.

Fig. 1. We then immediately deposit YBCO, which grows epitaxially everywhere and thereby reproduces the grain boundary in the SrTiO<sub>3</sub> buffer layer. Finally the YBCO is patterned into an appropriate geometry.

The virtue of this structure is that, apart from the predefined 45° grain boundaries, there are no other high-angle grain boundaries in the YBCO film. It has been reported<sup>12</sup> that YBCO films grown on SrTiO<sub>3</sub> buffer layers on *r*-plane sapphire substrates have high critical current density and low surface resistance. In addition, the SrTiO<sub>3</sub> layer grown on the MgO buffer layer does not have any high-angle grain boundaries, as demonstrated in a  $\phi$  scan of the SrTiO<sub>3</sub> (101), although it is found<sup>13</sup> that YBCO deposited on MgO may have a number of high-angle grain boundaries. The probable explanation for this effect is that the energy needed to nucleate 45° misoriented SrTiO<sub>3</sub> grains on MgO is much higher than in the case of YBCO grown on MgO. Hence the YBCO film on SrTiO<sub>3</sub> on MgO also lacks any high-angle grain boundaries and has a high critical current density. Microbridges formed either side of the predetermined grain boundary have critical current densities of  $1\text{--}3 \times 10^6 \text{ A/cm}^2$  at 77 K. In order to show that the critical current reduction is indeed due to the grain boundary rather than simply the step at the edge, we etched only part of the MgO, reducing its thickness on one side from 20 to 10 nm, such that YBCO/SrTiO<sub>3</sub>/MgO

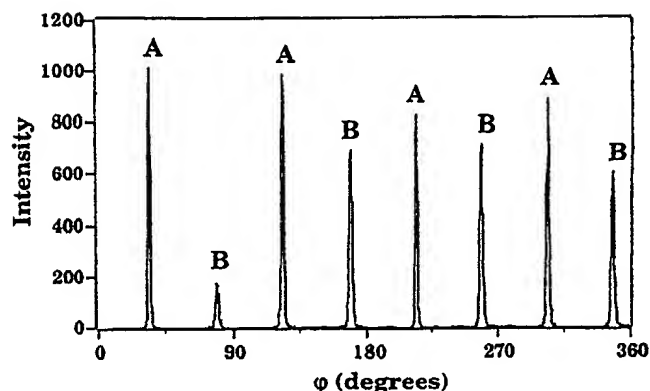


FIG. 2. X-ray  $\phi$  scan of YBCO (103) of the unpatterned structure. The peaks labeled with "A" belong to YBCO/SrTiO<sub>3</sub>/Al<sub>2</sub>O<sub>3</sub> and the peaks labeled with "B" come from YBCO/SrTiO<sub>3</sub>/MgO/Al<sub>2</sub>O<sub>3</sub>.

remained on the sapphire substrate on both sides of the step. The critical density across this step remained larger than  $10^6 \text{ A/cm}^2$  at 77 K.

A  $\phi$  scan of the YBCO (103) before the last patterning process is shown in Fig. 2. The peaks occurring 45° apart indicate that half of the YBCO is rotated 45° relative to the other half. Suitable etching experiments have shown that the peaks labeled with "A" belong to YBCO/SrTiO<sub>3</sub>/Al<sub>2</sub>O<sub>3</sub> and the peaks labeled with "B" come from YBCO/SrTiO<sub>3</sub>/MgO/Al<sub>2</sub>O<sub>3</sub>. Cross-sectional transmission electron microscope images and microdiffraction patterns show that the 45° grain boundary begins at the end of the MgO seed layer.<sup>14</sup>

As the first example of a device using multiple junctions made with our process we fabricated a square washer SQUID<sup>15</sup> as shown in the inset of Fig. 3. It was patterned across the grain boundary by photolithography and wet etched with dilute phosphoric acid. The current-voltage characteristic (*I-V*) of the SQUID at 4.2 K, which ex-

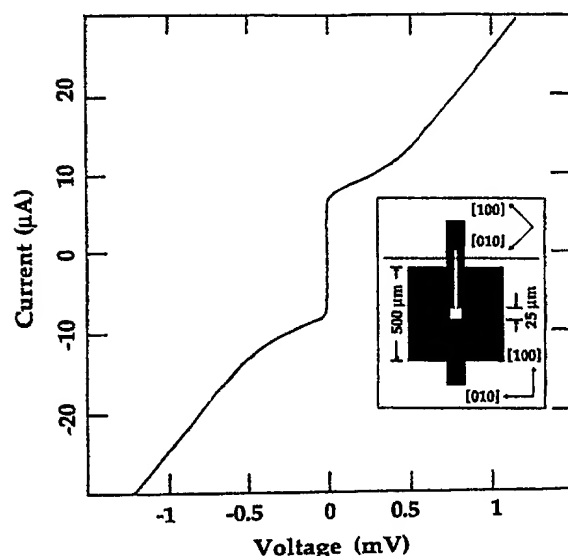


FIG. 3. Current (vertical)-voltage (horizontal) characteristics of a dc SQUID at 4.2 K. The inset shows the geometry of the SQUID.

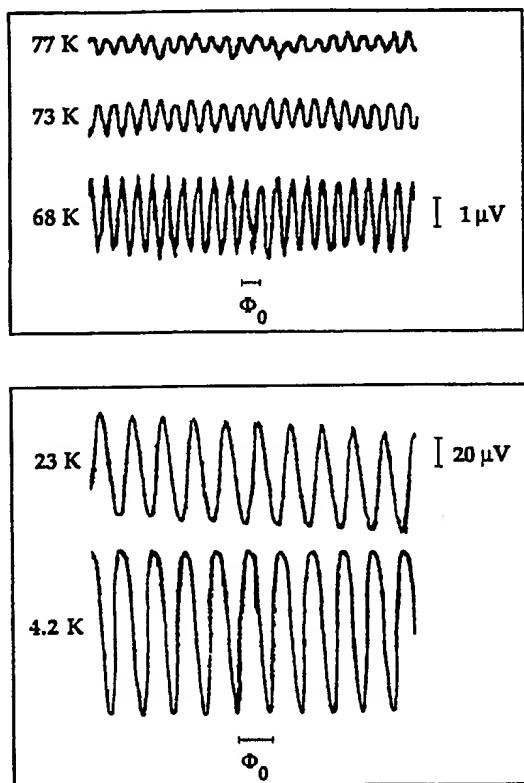


FIG. 4. Modulation voltage of the current-biased dc SQUID vs applied magnetic flux at various temperatures.

hibits resistively shunted Josephson junction behavior, is shown in Fig. 3. Each junction was  $4\text{ }\mu\text{m}$  wide and  $0.2\text{ }\mu\text{m}$  thick. The critical current of about  $10\text{ }\mu\text{A}$  at  $4.2\text{ K}$  translates to about  $10^3\text{ A/cm}^2$  critical current density across the junctions. The  $I_c R_n$  product of the junctions is about  $420\text{ }\mu\text{V}$  at  $4.2\text{ K}$ . The  $I$ - $V$ C of the SQUID at  $77\text{ K}$  shows no zero resistance part, although it is nonlinear. The small junction coupling energy  $I_c \Phi_0 / 2\pi$  compared to the thermal energy  $k_B T$  may lead to thermally activated phase slippage across the junctions, resulting in resistance at all currents.<sup>16</sup> Detailed transport properties of the junctions including the magnetic field dependence of the critical current will be reported elsewhere.<sup>17</sup>

The voltage across the current-biased dc SQUID as a function of applied field is shown for various temperatures in Fig. 4. The data were taken in a bandwidth of  $0$ – $10\text{ Hz}$  without any signal averaging. The observed period corresponds to the expected value from the geometry of the SQUID. We believe that the reduction of the modulation voltage at high temperatures is due to the decreasing critical current and the large inductance of the SQUID. We have observed dc SQUID operation at temperatures as high as  $88\text{ K}$  and have operated such a SQUID in a flux-locked loop up to  $83\text{ K}$ . The noise of this SQUID is similar to that reported in dc SQUIDs made using bicrystal substrates.<sup>10</sup> Detailed performance of the SQUID will be published elsewhere.<sup>18</sup>

A further example of small-scale integration using biepitaxial grain boundary junctions is provided by a flux

shuttle<sup>19</sup> we have fabricated. It involves two dc SQUIDs as sensors and eleven more bi-epitaxial junctions as switching elements. Our work on such integrated circuits is continuing and will be reported later.

In summary, we have reported the development of bi-epitaxial grain boundary junctions in  $\text{YBa}_2\text{Cu}_3\text{O}_7$  at multiple and predetermined locations by using only standard photolithographic techniques to control in-plane epitaxy with seed and buffer layers. The junctions have current-voltage characteristics that are well described by the resistively shunted junction model and dc SQUIDs fabricated using these junctions show modulation at temperatures as high as  $88\text{ K}$ . By increasing the critical current density of the junctions and lowering the inductance of the SQUID, the performance of the SQUIDs should improve further, especially at  $77\text{ K}$ . We believe that this technology, based on bi-epitaxial grain boundaries, can be extended to integrated circuits in the near future, and we are planning to demonstrate such circuits.

We would like to thank John Rowell, Mac Beasley, Ted Geballe, Bob Hammond, John Clarke, Aharon Kapitulnik, Randy Simon, and Roger Barton for helpful discussions on this work. We also would like to thank Jeff Rosner at Hewlett-Packard for the TEM studies.

- <sup>1</sup>D. Dimos, P. Chaudhari, J. Mannhart, and F. K. LeGoues, *Phys. Rev. Lett.* **60**, 1653 (1988).
- <sup>2</sup>R. H. Koch, W. J. Gallagher, B. Bumble, and W. Y. Lee, *Appl. Phys. Lett.* **54**, 951 (1989).
- <sup>3</sup>S. E. Russek, D. K. Lathrop, B. H. Moeckly, R. A. Buhrman, D. H. Shin, and J. Silcox, *Appl. Phys. Lett.* **57**, 1155 (1990).
- <sup>4</sup>R. B. Laibowitz, R. H. Koch, A. Gupta, G. Koren, W. J. Gallagher, V. Foglietti, B. Oh, and J. M. Viggiano, *Appl. Phys. Lett.* **56**, 686 (1990).
- <sup>5</sup>K. P. Daly, W. D. Dozier, J. F. Burch, S. B. Coons, R. Hu, C. E. Platt, and R. W. Simon, *Appl. Phys. Lett.* **58**, 543 (1991).
- <sup>6</sup>D. B. Schwartz, P. M. Mankiewich, R. E. Howard, L. D. Jackel, B. L. Straughn, E. G. Burkhardt, and A. H. Dayem, *IEEE Trans. Magn.* **25**, 1298 (1989).
- <sup>7</sup>C. T. Rogers, M. S. Hedge, B. Dutta, X. D. Wu, and T. Venkatesan, *Appl. Phys. Lett.* **55**, 2032 (1989).
- <sup>8</sup>J. Gao, W. A. M. Aarnink, G. J. Gerritsma, G. Veldhuis, and H. Rogalla, *IEEE Trans. Magn.* **27**, 3062 (1991).
- <sup>9</sup>D. K. Chin and T. Van Duzer, *Appl. Phys. Lett.* **58**, 753 (1991).
- <sup>10</sup>R. Gross, P. Chaudhari, M. Kawasaki, M. B. Ketchen, and A. Gupta, *Appl. Phys. Lett.* **57**, 727 (1990); *Physica C* **170**, 315 (1990).
- <sup>11</sup>S. M. Garrison, N. Newman, B. F. Cole, K. Char, and R. W. Barton, *Appl. Phys. Lett.* **58**, 2168 (1991).
- <sup>12</sup>K. Char, N. Newman, S. M. Garrison, R. W. Barton, R. C. Taber, S. S. Laderman, and R. D. Jacowitz, *Appl. Phys. Lett.* **57**, 409 (1990); K. Char, N. Newman, S. M. Garrison, R. W. Barton, G. Zaharchuk, S. S. Laderman, R. C. Taber, and R. D. Jacowitz, presented at Applied Superconductivity Conference, Aspen, Colorado (1990).
- <sup>13</sup>S. S. Laderman, R. C. Taber, R. D. Jacowitz, J. L. Moll, C. B. Eom, T. L. Hylton, A. F. Marshall, T. H. Geballe, and M. R. Beasley, *Phys. Rev. B* **43**, 2922 (1991).
- <sup>14</sup>S. J. Rosner (private communication).
- <sup>15</sup>M. B. Ketchen and J. M. Jaycox, *Appl. Phys. Lett.* **40**, 736 (1982).
- <sup>16</sup>R. Gross, P. Chaudhari, D. Dimos, A. Gupta, and G. Koren, *Phys. Rev. Lett.* **64**, 228 (1990).
- <sup>17</sup>P. Rosenthal, A. Barrera, M. R. Beasley, K. Char, M. S. Colclough, and G. Zaharchuk (unpublished).
- <sup>18</sup>M. S. Colclough, K. Char, G. Zaharchuk, A. H. Miklich, and J. Clarke (unpublished).
- <sup>19</sup>T. A. Fulton, R. C. Dynes, and P. W. Anderson, *Proc. IEEE* **61**, 28 (1973).

# Anomalous Periodicity of the Current-Phase Relationship of Grain-Boundary Josephson Junctions in High- $T_c$ Superconductors

E. Il'ichev, V. Zakosarenko, R.P.J. IJsselsteijn, H. E. Hoenig, V. Schultze, H.-G. Meyer  
*Department of Cryoelectronics, Institute for Physical High Technology, P.O. Box 100239, D-07702 Jena, Germany*

M. Grajcar and R. Hlubina  
*Department of Solid State Physics, Comenius University, Mlynská Dolina F2, 842 15 Bratislava, Slovakia*  
 (December 14, 2002)

The current-phase relation (CPR) for asymmetric  $45^\circ$  Josephson junctions between two  $d$ -wave superconductors has been predicted to exhibit an anomalous periodicity. We have used the single-junction interferometer to investigate the CPR for this kind of junctions in  $\text{YBa}_2\text{Cu}_3\text{O}_{7-x}$  thin films. Half-fluxon periodicity has been experimentally found, providing a novel source of evidence for the  $d$ -wave symmetry of the pairing state of the cuprates.

There is growing evidence in favor of the  $d_{x^2-y^2}$ -wave symmetry of the pairing state of the high-temperature superconductors.<sup>1</sup> An unconventional pairing state requires the existence of zeros of the order parameter in certain directions in momentum space. Thermodynamic and spectroscopic measurements do indeed suggest their existence, but by themselves they do not exclude conventional  $s$ -wave pairing with nodes.<sup>1</sup> Direct evidence for the  $d$ -wave pairing state is provided by phase-sensitive experiments, which are based on the Josephson effect.<sup>2</sup> Quite generally, the current-phase relationship (CPR) of a Josephson junction,  $I(\varphi)$ , is an odd periodic function of  $\varphi$  with a period  $2\pi$ .<sup>3</sup> Therefore  $I(\varphi)$  can be expanded in a Fourier series

$$I(\varphi) = I_1 \sin \varphi + I_2 \sin 2\varphi + \dots \quad (1)$$

In the tunnel limit we can restrict ourselves to the first two terms in Eq. (1). Since the order parameter is bound to the crystal lattice,  $I(\varphi)$  of a weak link depends on the orientation of the  $d$ -wave electrodes with respect to their boundary. The existing phase-sensitive experiments exploit possible sign changes of  $I_1$  between different geometries.<sup>2</sup> In this Letter we present a new phase-sensitive experimental test of the symmetry of the pairing state of the cuprates. Namely, in certain geometries, the  $I_1$  term should vanish by symmetry. In such cases, the CPR should exhibit an anomalous periodicity.

Let us analyze the angular dependence of  $I_{1,2}$  in a junction between two macroscopically tetragonal  $d$ -wave superconductors. As emphasized in Ref. 4, also heavily twinned orthorhombic materials such as  $\text{YBa}_2\text{Cu}_3\text{O}_{7-x}$  belong to this class, if the twin boundaries have odd symmetry. We consider first an ideally flat interface between the superconducting electrodes. Let  $\theta_1$  ( $\theta_2$ ) denote the angle between the normal to the grain boundary and the  $a$  axis in the electrode 1 (2), see Fig. 1. If we keep only the lowest-order angular harmonics, the symmetry of the problem dictates that<sup>4</sup>

$$I_1 = I_c \cos \theta_1 \cos 2\theta_2 + I_s \sin \theta_1 \sin 2\theta_2. \quad (2)$$

The coefficients  $I_c, I_s$  are functions of the barrier strength, temperature  $T$ , etc. The  $I_2$  term results from higher-order tunneling processes and we neglect its weak angular dependence. It is seen from Eq. (2) that the criterion for the observation of an anomalous CPR,  $I_1 = 0$ , is realized for an asymmetric  $45^\circ$  junction, i.e. a junction with  $\theta_1 = 45^\circ$  and  $\theta_2 = 0$ . For an interface which is not ideally flat,  $\theta_i = \theta_i(x)$  are functions of the coordinate  $x$  along the junction.  $I_1 = 0$  remains valid even in this case, if the average values  $\langle \theta_1(x) \rangle = 45^\circ$  and  $\langle \theta_2(x) \rangle = 0$ .

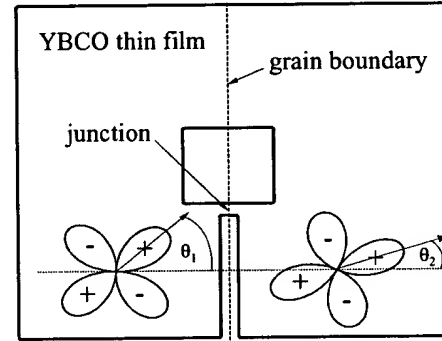


FIG. 1. Sketch of the interferometer (not in scale).

The  $I_2$  term is present also in weak links based on conventional  $s$ -wave superconductors but for all known types of weak links  $|I_2/I_1| < 1$ . For instance, for a tunnel junction  $|I_2/I_1| \ll 1$ . For a SNS junction,  $I \propto \sin \varphi/2$  at  $T = 0$ ,<sup>5</sup> and the Fourier expansion Eq. (1) leads to  $I_2/I_1 = -2/5$ . Therefore, a possible experimental observation of  $|I_2/I_1| \gg 1$  in an asymmetric  $45^\circ$  junction provides direct evidence of  $d$ -wave symmetry of the pairing state in the cuprates.

We have investigated the CPR of  $\text{YBa}_2\text{Cu}_3\text{O}_{7-x}$  thin film bicrystals with asymmetric  $45^\circ$  [001]-tilt grain boundaries<sup>6-8</sup> as sketched in Fig. 1, using a single-junction interferometer configuration in which the

Josephson junction is inserted into a superconducting loop with a small inductance  $L$ . In a stationary state without fluctuations, the phase difference  $\varphi$  across the junction is controlled by applying external magnetic flux  $\Phi_e$  penetrating the loop:  $\varphi = \varphi_e - \beta f(\varphi)$ . Here  $\varphi_e = 2\pi\Phi_e/\Phi_0$  is the external flux normalized to the flux quantum  $\Phi_0 = 2.07 \times 10^{-15} \text{ Tm}^2$ . The CPR is written as  $I(\varphi) = I_0 f(\varphi)$ , where  $I_0$  is the maximal Josephson current.  $\beta = 2\pi L I_0 / \Phi_0$  is the normalized critical current. In order to obtain the CPR for the complete phase range  $-\pi \leq \varphi \leq \pi$  the condition  $\beta < 1$  has to be fulfilled, because for  $\beta > 1$  the curve  $\varphi(\varphi_e)$  becomes multivalued and there are jumps of  $\varphi$  and a hysteresis for a sweep of  $\varphi_e$ . Following Ref. 3, we express the effective inductance of the interferometer using the derivative  $f'$  with respect to  $\varphi$  as  $L_{int} = L[1 + 1/f'(\varphi)]$ . The inductance can be probed by coupling the interferometer to a tank circuit with inductance  $L_T$ , quality factor  $Q$ , and resonance frequency  $\omega_0$ .<sup>9</sup> External flux in the interferometer is produced by a current  $I_{dc} + I_{rf}$  in the tank coil and can be expressed as  $\varphi_e = 2\pi(I_{dc} + I_{rf})M/\Phi_0 = \varphi_{dc} + \varphi_{rf}$ , where  $M^2 = k^2 L L_T$ , and  $k$  is a coupling coefficient. Taking into account the quasiparticle current in the presence of voltage  $V$  across the junction the phase difference is given by the relation  $\varphi = \varphi_{dc} + \varphi_{rf} - \beta f(\varphi) - 2\pi\tau(\varphi)V/\Phi_0$ , where  $\tau(\varphi) = L/R_J(\varphi)$  and  $R_J(\varphi)$  is the resistance of the junction. In the small-signal limit  $\varphi_{rf} \ll 1$  and in the adiabatic case  $\omega\tau \ll 1$ , keeping only the first-order terms, the effective inductance  $L_{eff}$  of the tank circuit-interferometer system reads

$$L_{eff} = L_T \left( 1 - k^2 \frac{L}{L_{int}} \right) = L_T \left( 1 - \frac{k^2 \beta f'(\varphi)}{1 + \beta f'(\varphi)} \right).$$

Thus the phase angle  $\alpha$  between the driving current and the tank voltage  $U$  at the resonant frequency of the tank circuit  $\omega_0$  is

$$\tan \alpha(\varphi) = \frac{k^2 Q \beta f'(\varphi)}{1 + \beta f'(\varphi)}. \quad (3)$$

Using the relation  $[1 + \beta f'(\varphi)]d\varphi = d\varphi_{dc}$  valid for  $\varphi_{rf} \ll 1$  and  $\omega\tau \ll 1$ , one can find the CPR from Eq. (3) by numerical integration.

The advantage of the measurement of the CPR of an asymmetric  $45^\circ$  junction with respect to the by-now standard phase-sensitive tests of pairing symmetry based on the angular dependence of  $I_1$  is twofold. First, it avoids the complications of the analysis of experiments caused by the presence of the term  $I_s$ .<sup>4</sup> Second, a flux trapped in the SQUID does not invalidate the conclusions about the ratio  $|I_2/I_1|$  and hence about the pairing symmetry, while this is not the case in standard phase-sensitive tests of the  $d$ -wave symmetry of the pairing state.<sup>10</sup>

The films of thickness 100 nm were fabricated using standard pulsed laser deposition on (001) oriented SrTiO<sub>3</sub> bicrystalline substrates with asymmetric [001] tilt misorientation angles  $45^\circ \pm 1^\circ$ . They were subsequently patterned by Ar ion-beam etching into  $4 \times 4 \text{ mm}^2$  square

washer single-junction interferometer structures (Fig. 1). The widths of the junctions were  $1 \div 2 \text{ } \mu\text{m}$ . The washer square holes had a side-length of  $50 \text{ } \mu\text{m}$ . This geometry of the interferometer gives  $L \approx 80 \text{ pH}$ . The resistance of the junction is higher than  $1 \text{ } \Omega$  and the condition for the adiabatic limit  $\omega\tau \ll 1$  is satisfied. For measurements of  $\alpha(\varphi_{dc})$ , several tank circuits with inductances  $0.2 \div 0.8 \text{ } \mu\text{H}$  and resonance frequencies  $16 \div 35 \text{ MHz}$  have been used. The unloaded quality factor of the tank circuits  $70 < Q < 150$  has been measured at various temperatures. The coupling factor  $k$  was determined from the period  $\Delta I_{dc}$  of  $\alpha(I_{dc})$  using  $M\Delta I_{dc} = \Phi_0$ . Its value varied between 0.03 and 0.09. The amplitude of  $I_{rf}$  was set to produce the flux in the interferometer lower than  $0.1\Phi_0$ .

The measurements have been performed in a gas-flow cryostat with a five-layer magnetic shielding in the temperature range  $4.2 \leq T < 90 \text{ K}$ . The experimental setup was calibrated by measuring interferometers of the same size with  $24^\circ$  and  $36^\circ$  grain boundaries. We have studied 5 samples, out of which sample No. 1 exhibited the most anomalous behavior. Samples Nos. 2,3 were less anomalous and the remaining two samples had high critical currents and their  $I(\varphi)$  was conventional. In Fig. 2 we plot the phase angle  $\alpha$  as a function of the dc current  $I_{dc}$  for samples Nos. 1,2. The data for the  $36^\circ$  junction is shown for comparison. Note that at  $T = 40 \text{ K}$  the periodicity of  $\alpha(I_{dc})$  is the same for all samples.

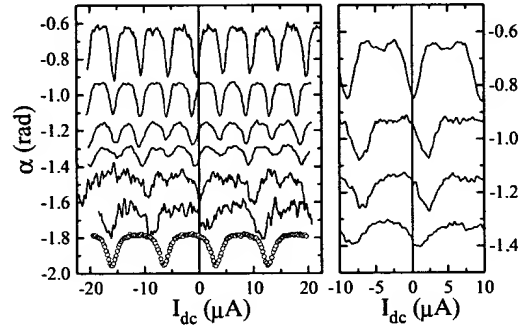


FIG. 2. Left panel: Phase angle between the driving current and the output voltage measured for the sample No. 1 at different temperatures as a function of the dc current  $I_{dc}$ . The curves are shifted along the  $y$  axis and the data for  $T = 30$  and  $40 \text{ K}$  are multiplied by factor 4 for clarity. From top to bottom, the data correspond to  $T = 4.2, 10, 15, 20, 30$  and  $40 \text{ K}$ . The data measured on  $36^\circ$  bicrystals ( $\theta_1 \approx 36^\circ, \theta_2 \approx 0$ ) at  $T = 40 \text{ K}$  in the same washer geometry are shown for comparison (open circles). Right panel: The same for the sample No. 2. From top to bottom, the data correspond to  $T = 4.2, 10, 15$  and  $20 \text{ K}$ .

We assume that the period of  $\alpha(I_{dc})$  at  $T = 40 \text{ K}$ ,  $\Delta I_{dc} = 9.6 \text{ } \mu\text{A}$ , corresponds to  $\Delta\varphi_{dc} = 2\pi$ . In order to determine the CPR we take  $\varphi_{dc} = 0$  at a maximum or minimum of  $\alpha$ . This is necessary in order to satisfy

$I(\varphi = 0) = 0$ , as required by general principles.<sup>3</sup> The experimentally observed shift of the first local extreme of  $\alpha(I_{dc})$  from  $I_{dc} = 0$  (Fig. 2) can be due to flux trapped in the interferometer washer. Most probably, this flux resides in the long junction of the interferometer. The long junction does not play an active role because the Josephson penetration depth is much shorter than its length, and external fields producing  $I_{dc}$  are smaller than its critical field. Nevertheless the long junction sets the phase difference for  $I_{dc} = 0$  at the small junction.

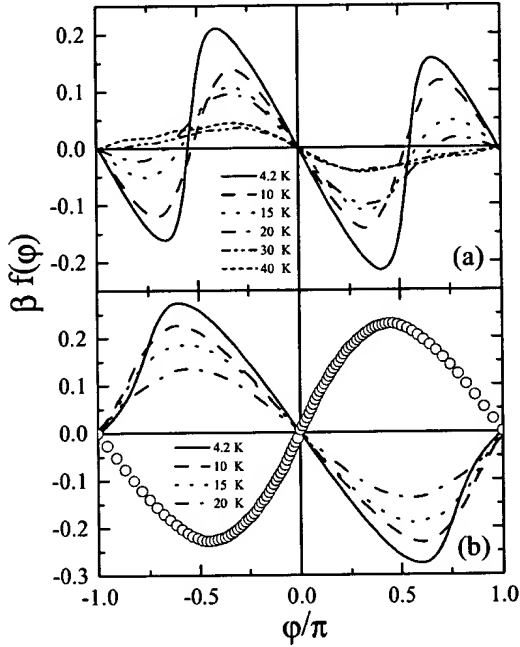


FIG. 3. a) Josephson current through the junction for the sample No. 1 as a function of the phase difference  $\varphi$ , determined from the data in Fig. 2. The statistics of  $\alpha(\varphi)$  was improved by folding the data back to the interval  $(0, \pi)$  and taking an average. The symmetry  $\alpha(\varphi) = \alpha(-\varphi)$  was assumed. b) The same for the sample No. 2. The data for the asymmetric  $36^\circ$  bicrystal at  $T = 40$  K (open circles) is also shown.

In Fig. 3, we show the CPR determined from the data in Fig. 2. For all curves we have performed a minimal necessary shift consistent with  $I(\varphi = 0) = 0$ . Thus, for the samples Nos. 1,2 we have assumed that at  $\varphi_{dc} = 0$  a minimum of  $\alpha(\varphi_{dc})$  is realized. For an interferometer with a conventional  $s$ -wave weak link (and also for the  $36^\circ$  junction), at  $\varphi_{dc} = 0$  a maximum of  $\alpha(\varphi_{dc})$  is realized. Note that the maximum (minimum) of  $\alpha(\varphi_{dc})$  at  $\varphi_{dc} = 0$  implies a diamagnetic (paramagnetic) response of the interferometer in the limit of small applied fields. In Fig. 4 we plot the coefficients  $I_1$  and  $I_2$  determined by Fourier analysis of the CPR for the sample No. 1 at various temperatures. With decreasing  $T$ ,  $|I_2|$  grows monotonically down to  $T = 4.2$  K, while the  $I_1$  component exhibits only a weak temperature dependence.

Our experimental results can be understood as follows. Deviations from ideal geometry of the asymmetric  $45^\circ$  junction,  $\langle \theta_1 \rangle = 45^\circ + \alpha_1$  and  $\langle \theta_2 \rangle = \alpha_2$ , lead to a finite value of  $I_1$ . Thus, imperfections of the junction increase its critical current. For this reason we believe that samples Nos. 2-5 contain imperfections and from now we concentrate on nearly ideal junctions (such as sample No. 1) with  $|\alpha_1|, |\alpha_2| \ll 1$ . For such junctions, the ratio  $I_2/I_1$  exhibits the following temperature dependence. For  $T \rightarrow 0$ ,  $|I_2/I_1| \gg 1$ . The region  $T \sim T_c$  can be analyzed quite generally within Ginzburg-Landau theory. Let the electrodes be described by (macroscopic) order parameters  $\Delta_{1,2} = |\Delta|e^{i\varphi_{1,2}}$ . Then the phase-dependent part of the energy of the junction is  $E = a[\Delta_1\Delta_2^* + \text{H.C.}] + b[(\Delta_1\Delta_2^*)^2 + \text{H.C.}] + \dots$  where  $a, b, \dots$  depend weakly on  $T$ .<sup>11</sup> Thus for  $T$  close to  $T_c$  we estimate  $I_1 \propto |\Delta|^2 \propto (T_c - T)$  and  $I_2 \propto |\Delta|^4 \propto (T_c - T)^2$ , leading to  $|I_2/I_1| \ll 1$ . These expectations are qualitatively consistent with the experimental data shown in Fig. 4.

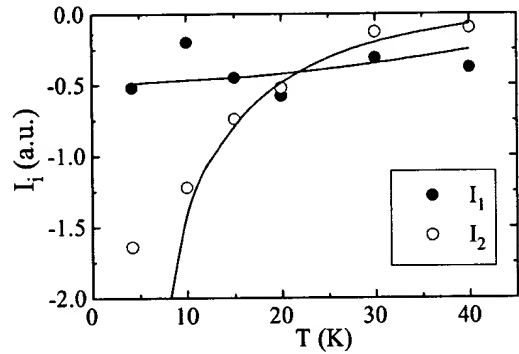


FIG. 4. Temperature dependence of the Fourier expansion coefficients  $I_{1,2}$  determined from the experimental data in Fig. 3a. Solid lines are the Fourier expansion coefficients for the numerical data in Fig. 5.

So far, our discussion was based solely on symmetry arguments. Let us attempt a more quantitative analysis of our data now. Two different microscopic pictures of asymmetric  $45^\circ$  Josephson junctions between  $d$ -wave superconductors have been considered in the literature. The first picture assumes a microscopically tetragonal material and an ideally flat interface.<sup>11-13</sup> Within this picture, there are two contributions to the Josephson current. The first is due to bulk states and in the tunnel limit it is well described by the Sigrist-Rice term  $I_c$  in Eq. (2).<sup>14</sup> The second is due to mid-gap states which develop close to the surfaces of unconventional superconductors.<sup>15</sup>  $I(\varphi)$  for the sample No. 1 calculated according to the model of Ref. 12 is shown in Fig. 5. The experimental data can be fitted by a relatively broad range of barrier heights. However, if we require the  $36^\circ$  junction to be fitted by the same (or smaller) barrier height as for the  $45^\circ$  junction, we conclude the barrier must be rather low.<sup>16</sup> The  $T$  dependence of  $I(\varphi)$  requires

a choice of  $T_c \approx 60$  K in the non-selfconsistent theory of Ref. 12. The reduction from the bulk  $T_c = 90$  K is probably due to a combined effect of surface degradation and order-parameter suppression at the sample surface. The temperature dependence of the ratio of the  $\pi$  and  $2\pi$  periodic components in  $I(\varphi)$  is seen to be in qualitative agreement with experimental data in Fig. 3a. This is explicitly demonstrated in Fig. 4 where we compare the experimentally obtained  $I_{1,2}$  with the results of the Fourier analysis of the curves in Fig. 5. The divergence of  $I_2$  as  $T \rightarrow 0$  is an artifact of the ideal junction geometry assumed in Ref. 12. If the finite roughness of the interface is taken into account, this divergence is cut off and the experimental data in Fig. 4 do indeed resemble theoretical predictions for a rough interface.<sup>13</sup> However, the nonselfconsistent theory of Ref. 12 is unable to explain the experimentally observed steep CPR close to the minima of the junction energy (see Fig. 3a). In the limit of vanishing barrier height, the theoretical CPR does have steep portions, but these are located close to the maxima of the junction energy (see also Ref. 11).

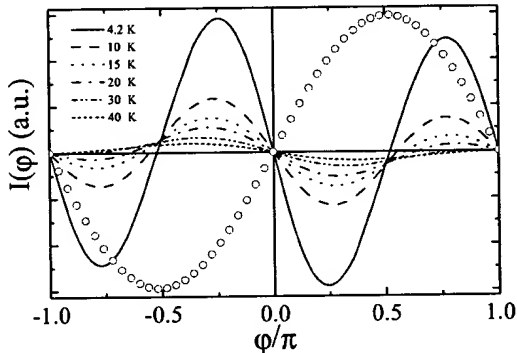


FIG. 5.  $I(\varphi)$  calculated according to Eq. (64) of Ref. 12 for a junction with  $\theta_1 = 45.5^\circ$ ,  $\theta_2 = 0$ ,  $\lambda d = 1.5$ ,  $\kappa = 0.5$ , and  $T_c = 60$  K.  $I(\varphi)$  at  $T = 40$  K for the  $36^\circ$  bicrystal (open circles) was calculated for the same parameters except for  $\theta_1 = 36^\circ$ .

In a different approach to the asymmetric  $45^\circ$  junction, one assumes a heavily twinned orthorhombic material (which is macroscopically tetragonal, however) and/or a meandering interface with  $\theta_i = \theta_i(x)$ .<sup>17,18</sup> Hence the critical current density  $j_c(x)$  is a random function with a typical amplitude  $\langle |j_c(x)| \rangle \sim j_c$ . If the average critical current along the junction  $\langle j_c \rangle \ll j_c$ , a spontaneous flux is generated in the junction, and  $|I_2/I_1| \gg 1$ .<sup>17,18</sup> In particular, for  $\langle \theta_1 \rangle = 45^\circ$  and  $\langle \theta_2 \rangle = 0$ , there is an equal amount of parts having positive and negative  $j_c$ , leading to  $\langle j_c \rangle = 0$  and  $I_1 = 0$ . Note that also within the picture of Refs. 17,18, the  $d$ -wave symmetry of the pairing state is crucial, otherwise the condition  $\langle j_c \rangle \ll j_c$  is difficult to satisfy.

Our present understanding of  $I(\varphi)$  in the asymmetric  $45^\circ$  junction is only qualitative. There is considerable experimental evidence<sup>6-8</sup> that the grain boundary junctions are at most piecewise flat. However, we cannot say whether the shape of  $I(\varphi)$  is dominated by the mid-gap states in the microscopically flat regions, or by spontaneous flux generation due to the spatial inhomogeneity of the junction. This issue requires further study.

In conclusion, we have measured the magnetic field response of a single-junction interferometer based on asymmetric  $45^\circ$  grain-boundary junctions in  $\text{YBa}_2\text{Cu}_3\text{O}_{7-x}$  thin films. Half-fluxon periodicity has been experimentally found, in agreement with theoretical predictions for  $d_{x^2-y^2}$ -wave superconductors. Hence, our results provide a novel source of evidence for the  $d$ -wave symmetry of the pairing state in the cuprates.

Financial support by the DFG (Ho 461/1-1) is gratefully acknowledged. M. G. and R. H. were supported by the Slovak Grant Agency Grant No. 1/4300/97 and the Comenius University Grant No. UK/3927/98.

- <sup>1</sup> For a review, see J. Annett, N. Goldenfeld, and A. J. Leggett, in *Physical Properties of High Temperature Superconductors*, edited by D. M. Ginsberg (World Scientific, New Jersey, 1996), Vol. V.
- <sup>2</sup> See C. C. Tsuei *et al.*, Science **271**, 329 (1996) and references therein.
- <sup>3</sup> A. Barone and G. Paterno, *Physics and Applications of the Josephson Effect*, (Wiley, New York, 1982).
- <sup>4</sup> M. B. Walker and J. Luettmmer-Strathmann, Phys. Rev. B **54**, 588 (1996).
- <sup>5</sup> I. O. Kulik and A. N. Omel'yanchuk, Fiz. Nizk. Temp. **4**, 296 (1978) [Sov. J. Low Temp. Phys. **4**, 142 (1978)].
- <sup>6</sup> J. R. Kirtley *et al.*, Phys. Rev. B **51**, 12 057 (1995).
- <sup>7</sup> H. Hilgenkamp, J. Mannhart, and B. Mayer, Phys. Rev. B **53**, 14586 (1996).
- <sup>8</sup> J. Mannhart *et al.*, Phys. Rev. Lett. **77**, 2782 (1996).
- <sup>9</sup> E.V. Il'ichev *et al.*, J. Low Temp. Phys. **106**, 503 (1997).
- <sup>10</sup> R. A. Klemm, Phys. Rev. Lett. **73**, 1871 (1994).
- <sup>11</sup> A. Huck, A. van Otterlo, and M. Sigrist, Phys. Rev. B **56**, 14 163 (1997).
- <sup>12</sup> Y. Tanaka and S. Kashiwaya, Phys. Rev. B **56**, 892 (1997).
- <sup>13</sup> Y. S. Barash, H. Burkhardt, and D. Rainer, Phys. Rev. Lett. **77**, 4070 (1996).
- <sup>14</sup> M. Sigrist and T. M. Rice, J. Phys. Soc. Jpn. **61**, 4293 (1992).
- <sup>15</sup> C. R. Hu, Phys. Rev. Lett. **72**, 1526 (1994).
- <sup>16</sup> This is consistent with the Fourier analysis of the data in Fig. 3 which finds non-negligible  $I_n$  also for  $n \geq 3$ .
- <sup>17</sup> A. J. Millis, Phys. Rev. B **49**, 15 408 (1994).
- <sup>18</sup> R. G. Mints, Phys. Rev. B **57**, R322 (1998).

IN THE UNITED STATES PATENT AND TRADEMARK OFFICE

In re application of:	)	Art Unit: 2814
Zagoskin	)	
	)	Examiner:
	)	Douglas A. Wille
Serial No. 09/452,749	)	
Filed: December 1, 1999	)	Attorney Docket:
	)	11090-003-999
	)	
For: Permanent Readout Superconducting Qubit	)	
_____	)	

**DECLARATION OF DR. ALEXANDER TZALENCHUK UNDER 37 C.F.R. § 1.132**

Assistant Commissioner for Patents  
Washington, D.C. 20231

Sir:

I, ALEXANDER TZALENCHUK, declare and state as follows:

1. I am a citizen of Russia currently residing at 244 Ashburnham Road, Ham / Richmond, Surrey, United Kingdom TW10 7SA.
2. I am familiar with the specification and claims of the above-identified patent application ("Application"), the Office Action mailed February 19, 2003, United States Patent 5,157,466 to Char *et al.* (hereinafter "Char *et al.*") and Tinkham, *Introduction to Superconductivity*, Second Edition, (hereinafter "Tinkham").
3. I am an employee of the National Physics Laboratory of the United Kingdom of Great Britain and Northern Ireland and its affiliate NPL Management Limited (herein after "NPL"). NPL is located in Teddington, Middlesex, UK, TW11 0LW, where I am employed by it as a Senior Research Scientist in its Fundamental and Wavelength Standards Team. NPL has entered into a collaborative research agreement with D-Wave Systems Inc.



(hereinafter "D-Wave"), the assignee herein, dated March 27, 2002, whereby NPL carries out certain research and measurement work for D-Wave. One product of this research and measurement work is the creation of certain intellectual property, including patent applications, all rights, title and interest to which are held by D-Wave pursuant to the terms and conditions of the aforementioned collaborative research agreement.

4. I received a B.A. in Electronics Engineering from the Chair of Crystal Physics, Faculty of Electronic Materials and Devices, Moscow Steel and Alloys Institute and a Ph.D. in Physics and Mathematics from the A.V. Shubnikov Institute of Crystallography Russian Academy of Sciences, and have been actively performing research in the field of solid state and superconducting fabrication and characterization for the past nineteen years. During that time, I have published in excess of 35 articles in the fields of solid state physics, superconducting structure fabrication, and characterization of superconducting structures and have six allowed or issued patents. My research experience encompasses work in semiconductor structures formed on bi-crystal substrates, bi-crystal substrates for high-T<sub>c</sub> superconductors, mesoscopic effects in high-T<sub>c</sub> superconductors, Josephson phenomena in high-T<sub>c</sub> bi-crystals and bi-epitaxial grain boundary Josephson junctions, and Josephson phenomena in high-T<sub>c</sub> step edge Josephson junctions, and qubits using high-T<sub>c</sub> Josephson junctions. I am a specialist in the fabrication of microstructures in high-T<sub>c</sub> superconducting devices, these include three terminal devices, SQUIDs, and qubits. I have additional expertise in the characterization of superconducting devices including instrumentation for scanning SQUID/Hall microscopy, and investigation of local magnetization and superconductivity. I have received an individual George Soros Foundation grant, on the basis of high citation index, and the Swedish Foundation for International Cooperation in Research and Higher Education, through a program to bring eminent foreign scientists and scholars to Sweden.

5. I declare that a clean Josephson junction formed using a d-wave superconducting material is defined by a current-phase relationship in which the second

harmonic makes a distinct contribution to the current-phase relationship of the clean Josephson junction.

6. I declare that the second harmonic effect on the current-phase relationship of a clean Josephson junction formed using a d-wave superconducting material is temperature dependent.

7. I declare that, in the current state of the art, the second harmonic effect on the current-phase relationship of clean Josephson junctions formed using d-wave superconducting material cannot be precisely engineered.

8. I declare that, because of the temperature dependence of the second harmonic effect and the inability to precisely engineer the second harmonic effect, it would be undesirable to form a dc SQUID using clean Josephson junctions in a d-wave superconducting material, such as  $\text{YBa}_2\text{Cu}_3\text{O}_{7-x}$  (YBCO), when the dc SQUID is intended for use in commercial SQUID magnetometers such as those described in Char *et al.*

9. I declare that Chapter 7 of Tinkham only considers conventional superconducting materials and devices made out of conventional superconducting materials.


10. I declare that, based on my experience in the field of bi-epitaxial technology, neither the bi-epitaxial technology described in Char *et al.* nor the best quality crystal structures available for bi-epitaxial Josephson junction technology were sufficiently advanced at the time of filing of the Application to prepare a clean Josephson junction such as that

described in the Application.

11. I further declare, under penalty of perjury under the laws of the United States of America, that all statements made herein of my own knowledge are true and that these statements were made with the knowledge that willful false statements and the like are

punishable by fine or imprisonment, or both, under Section 1001 or Title 18 of the United States Code.

Date: 16/04/03

  
\_\_\_\_\_  
Dr. Alexander Tzalenchuk